GINA PAOLA POLO INFANTE

Modeling and stochastic simulation to study the dynamics of *Rickettsia rickettsii* in populations of *Hydrochoerus hydrochaeris* and *Amblyomma sculptum* in the state of São Paulo, Brazil

São Paulo
2017

GINA PAOLA POLO INFANTE

Modeling and stochastic simulation to study the dynamics of *Rickettsia rickettsii* in populations of *Hydrochoerus hydrochaeris* and *Amblyomma sculptum* in the State of São Paulo, Brazil

Tese apresentada ao Programa de Pós-Graduação em Epidemiologia Experimental Aplicada às Zoonoses da Faculdade de Medicina Veterinária e Zootecnia da Universidade de São Paulo para obtenção do título de Doutor em Ciências

Departamento:
Medicina Veterinária Preventiva e Saúde Animal

Área de concentração:
Epidemiologia Experimental Aplicada às Zoonoses

Orientador: Prof. Dr. Fernando Ferreira

São Paulo
2017

DADOS INTERNACIONAIS DE CATALOGAÇÃO NA PUBLICAÇÃO

(Biblioteca Virginie Buff D'Ápice da Faculdade de Medicina Veterinária e Zootecnia da Universidade de São Paulo)

T. 3524
FMVZ

Polo Infante, Gina Paola
Modeling and stochastic simulation to study the dynamics of *Rickettsia rickettsii* in populations of *Hydrochoerus hydrochaeris* and *Amblyomma sculptum* in the State of São Paulo, Brazil. / Gina Paola Polo Infante. -- 2017.
111 p. : il.

Título traduzido: Modelagem e simulação estocástica para o estudo da dinâmica de *Rickettsia rickettsii* em populações de *Hydrochoerus hydrochaeris* e de *Amblyomma sculptum* no estado de São Paulo.

Tese (Doutorado) - Universidade de São Paulo. Faculdade de Medicina Veterinária e Zootecnia. Departamento de Medicina Veterinária Preventiva e Saúde Animal, São Paulo, 2017.

Programa de Pós-Graduação: Epidemiologia Experimental Aplicada às Zoonoses.

Área de concentração: Epidemiologia Experimental Aplicada às Zoonoses.

Orientador: Prof. Dr. Fernando Ferreira.

1. Brazilian spotted fever. 2. Stochastic modeling. 3. Computational simulations. 4. *Amblyomma sculptum*. 5. Spatial analysis. I. Título.

CERTIFICADO

Certificamos que a proposta intitulada "Capivaras, carrapatos e febre maculosa", protocolada sob o CEUA nº 5948070314, sob a responsabilidade de **Marcelo Bahia Labruna** *e equipe; Marcelo Bahia Labruna; Adriano Pinter dos Santos* - que envolve a produção, manutenção e/ou utilização de animais pertencentes ao filo Chordata, subfilo Vertebrata (exceto o homem), para fins de pesquisa científica ou ensino - está de acordo com os preceitos da Lei 11.794 de 8 de outubro de 2008, com o Decreto 6.899 de 15 de julho de 2009, bem como com as normas editadas pelo Conselho Nacional de Controle da Experimentação Animal (CONCEA), e foi **aprovada** pela Comissão de Ética no Uso de Animais da Faculdade de Medicina Veterinária e Zootecnia da Universidade de São Paulo (CEUA/FMVZ) na reunião de 27/08/2014.

We certify that the proposal "Capybaras, ticks, and Brazilian spotted fever", utilizing 8 Brazilian wild species (8 males), 80 Guinea pigs (80 males), 40 Rabbits (40 males), protocol number CEUA 5948070314, under the responsibility of **Marcelo Bahia Labruna** *and team; Marcelo Bahia Labruna; Adriano Pinter dos Santos* - which involves the production, maintenance and/or use of animals belonging to the phylum Chordata, subphylum Vertebrata (except human beings), for scientific research purposes or teaching - is in accordance with Law 11.794 of October 8, 2008, Decree 6899 of July 15, 2009, as well as with the rules issued by the National Council for Control of Animal Experimentation (CONCEA), and was **approved** by the Ethic Committee on Animal Use of the School of Veterinary Medicine and Animal Science (University of São Paulo) (CEUA/FMVZ) in the meeting of 08/27/2014.

Finalidade da Proposta: Pesquisa

Vigência da Proposta: de 07/2015 a 06/2019 Área: Medicina Veterinária Preventiva E Saúde Animal

Origem:	Animais provenientes de estabelecimentos comerciais				
Espécie:	Espécies silvestres brasileiras	sexo: Machos	idade: a	N:	8
Linhagem:	Capivara		Peso: a		
Origem:	Animais provenientes de estabelecimentos comerciais				
Espécie:	Cobaias	sexo: Machos	idade: a	N:	80
Linhagem:	Albina		Peso: a		
Origem:	Animais provenientes de estabelecimentos comerciais				
Espécie:	Coelhos	sexo: Machos	idade: a	N:	40
Linhagem:	Nova Zelândia Branco		Peso: a		

Resumo: A Febre Maculosa Brasileira (FMB), causada pela bactéria Rickettsia rickettsii, é a doença transmitida por carrapatos de maior importância médica na América Latina. No interior do estado de São Paulo, as áreas endêmicas para FMB estão associadas à presença de capivaras, hospedeiros primários para o carrapato Amblyomma cajennense, vetor de R. rickettsii nessas áreas. No entanto, há muitas outras áreas em que populações de A. cajennense são mantidas por capivaras, mas não há ocorrência de FMB. Há também áreas com A. cajennense e capivaras, em que por um determinado momento não havia endemicidade da doença; porém, com o passar dos anos, essas áreas passaram a ser endêmicas. Visando esclarecer essas lacunas da epidemiologia da doença, o presente projeto está composto por 9 subprojetos, que visam estabelecer as relações ecológicas da febre maculosa, o carrapato vetor e a capivara. Para tal, populações de capivaras, carrapatos e a fauna silvestre e doméstica associada serão estudados paralelamente por 4 anos consecutivos em 3 áreas endêmicas e 3 áreas não endêmicas para FMB no estado de São Paulo, e em duas áreas de alta diversidade no bioma Pantanal. Além disso, diversos estudos de infecção experimental de carrapatos e capivaras com o agente da FMB serão realizados para simular situações de campo. Os resultados obtidos deverão permitir um entendimento da dinâmica da infecção por R. rickettsii e ocorrência da FMB no estado. Por fim, será criado um modelo matemático sobre a circulação de R. rickettsii nas populações de carrapatos e capivaras, que deverá indicar a taxa mínima de reprodução das capivaras para que haja uma manutenção da infecção por R. rickettsii nas populações de carrapatos. Este modelo terá aplicação direta nos programas de manejo de controle de capivaras, como forma de prevenir novos casos de FMB nas áreas endêmicas, e ao mesmo tempo, impedir que áreas não endêmicas se tornem endêmicas com o passar dos anos.

Local do experimento:

São Paulo, 22 de junho de 2017

Profa. Dra. Denise Tabacchi Fantoni
Presidente da Comissão de Ética no Uso de Animais
Faculdade de Medicina Veterinária e Zootecnia da Universidade de São Paulo

Roseli da Costa Gomes
Secretaria Executiva da Comissão de Ética no Uso de Animais
Faculdade de Medicina Veterinária e Zootecnia da Universidade de São Paulo

FOLHA DE AVALIAÇÃO

Nome: POLO INFANTE, Gina Paola

Título: Modeling and stochastic simulation to study the dynamics of *Rickettsia rickettsii* in populations of *Hydrochoerus hydrochaeris* and *Amblyomma sculptum* in the State of São Paulo, Brazil.

Tese apresentada ao Programa de Pós-Graduação em Epidemiologia Experimental Aplicada às Zoonoses da Faculdade de Medicina Veterinária e Zootecnia da Universidade de São Paulo para obtenção do título de Doutor em Ciências

Data:_____/_____/_____

BANCA EXAMINADORA

Prof. Dr. :_____
Instituição:_____ Julgamento:_____

Prof. Dr. :_____
Instituição:_____ Julgamento:_____

Prof. Dr. :_____
Instituição:_____ Julgamento:_____

Prof. Dr. :_____
Instituição:_____ Julgamento:_____

Prof. Dr. :_____
Instituição:_____ Julgamento:_____

AGRADECIMENTOS

Besides my advisor, Prof. Fernando Ferreira, I would like to thank Prof. Marcelo Labruna for their immense support.

I also would like to thank the rest of my thesis committee: Prof. Roberto Kraenkel, Dr. Rodrigo Silva Pinto, and Dr. Adriano Pinter, and my doctoral qualification committee: Prof. Marcos Amaku and Prof. Francisco Chiaravalloti for their contributions to my work.

Special thanks to Néstor Calderón and Rita Garcia for being fundamental at the starting point of this whole process.

My sincere thanks also go to Prof. Dirk Brockmann from the Humboldt University of Berlin and the Robert Koch Institute, who provided me the opportunity to join his team for one year. Vielen Dank Olga, Frank, Benni, Chen-Li, Thea, Clara, Alice, Corrado, Adrian, Stephan, Niko, Peer, für dieses lustige Jahr.

I thank my anexo-mates: Ana Rita, Guilherme, Rafa, Pacho, Alex, Alejo, Tati, Juan David, for all the fun we have had in the last years. In particular, I am grateful to my great friend Antônio Rodrigues.

I also want to thank the colleagues of the Parasitology laboratory and to all fellow employees of the VPS.

I want to thank the São Paulo Research Foundation for the financial support (Grant numbers: 14/12213-1 and BEPE 16/01913-8). Also to the University of Washington (SISMID 2015) and the ICTP/Trieste for the scholarships and the courses fundamental for the development of this work.

I deeply thank my family: my parents Anita and Roque, my brother Roquito and my grandmother for motivating me and always inspiring me.

Last but not the least, I would like to thank Carlos immensely, not only for being an exemplary husband but also for being like a rescuer in my shipwrecks in the thick ocean of computational codes and mathematics in which I have sailed during these four years.

ABSTRACT

POLO, Gina. **Modeling and stochastic simulation to study the dynamics of *Rickettsia rickettsii* in populations of *Hydrochoerus hydrochaeris* and *Amblyomma sculptum* in the State of São Paulo, Brazil.** [Modelagem e simulação estocástica para o estudo da dinâmica de Rickettsia rickettsii em populações de Hydrochoerus hydrochaeris e de Amblyomma sculptum no estado de São Paulo.] 2017. 111 f. Tese (Doutor em Ciências) - Faculdade de Medicina Veterinária e Zootecnia, Universidade de São Paulo, São Paulo, 2017.

There are a huge number of pathogens with multi-component transmission cycles, involving amplifier hosts, vectors, complex pathogen life cycles and particular environmental conditions. These complex systems present challenges in terms of modeling and policy development. The deadliest tick-borne infectious disease in the world, the Brazilian Spotted Fever (BSF), is a relevant example of that. The current increase of human cases of BSF has been associated with the presence and expansion of capybaras *Hydrochoerus hydrochaeris*, amplifier host for the agent *Rickettsia rickettsii* and primary host for the tick vector *Amblyomma sculptum*. The objective of this thesis was to analyze the dynamics of the FMB with the purpose of providing bases for the planning of strategies focused on the prevention of human cases. We proposed different approaches to evaluating: *i*) the contribution of hosts and vectors in the transmission of BSF, *ii*) potential risk areas and anthropogenic parameters associated with the occurrence of human cases, *iii*) the pattern and the spatial propagation velocity of BSF, and *iv*) climatic and landscape factors that could be related to the distribution of the vector. The proposed approaches elucidated how BSF control and prevention strategies can be focused on the management of amplifier hosts populations. We found that geographical barriers generated, for example, by areas of riparian reforestation, could prevent the spatial spread of BSF, since a positive association between the occurrence of human cases and the increment of sugarcane crop was determined, as well as a higher propagation velocity of BSF in places with higher carrying capacity. This thesis was interdisciplinary and required, on one hand, expertise in biology, computational epidemiology, mathematics and statistics and on the other hand, a data-rich environment such as the Laboratory of Parasitology of the VPS/FMVZ/USP. The results of this thesis can be usefulness in the planning of public health policies related to the prevention of BSF. Furthermore, this work will open the path to further mathematical and computational studies focused on the dynamics and prevention of other vector-borne infectious diseases.

RESUMO

POLO, Gina. **Modeling and stochastic simulation to study the dynamics of *Rickettsia rickettsii* in populations of *Hydrochoerus hydrochaeris* and *Amblyomma sculptum* in the State of São Paulo, Brazil.** [Modelagem e simulação estocástica para o estudo da dinâmica de Rickettsia rickettsii em populações de Hydrochoerus hydrochaeris e de Amblyomma sculptum no estado de São Paulo.] 2017. 111 f. Tese (Doutor em Ciências) - Faculdade de Medicina Veterinária e Zootecnia, Universidade de São Paulo, São Paulo, 2017.

Existe um grande número de agentes patogênicos com ciclos de transmissão complexos, envolvendo hospedeiros amplificadores, vetores e condições ambientais particulares. Esses sistemas complexos apresentam desafios quanto a modelagem e desenvolvimento de políticas públicas. A Febre Maculosa Brasileira (FMB) é a doença transmitida por carrapatos mais letal do mundo e é um claro exemplo de um sistema complexo. O aumento atual de casos humanos de BSF tem sido associado à presença e expansão de capivaras *Hydrochoerus hydrochaeris*, hospedeiros amplificadores do agente *Rickettsia rickettsii* e hospedeiros primários do carrapato vetor *Amblyomma sculptum*. O objetivo desta tese foi analisar a dinâmica da FMB com o propósito de fornecer bases para o delineamento de estratégias de prevenção de casos em humanos. Diferentes abordagens foram propostas para avaliar: *i*) a contribuição específica de hospedeiros e vetores na transmissão da FMB, *ii*) os parâmetros antropogênicos associados com a ocorrência dos casos e potenciais áreas de risco, *iii*) o padrão e a velocidade de propagação espacial e da doença *iv*) e ,os fatores climáticos e paisagísticos que poderiam estar relacionados à distribuição do vetor. Os modelos propostos elucidaram que as estratégias de controle e prevenção da FMB podem estar focadas em práticas de manejo das populações de hospedeiros amplificadores. Uma vez que uma associação positiva entre ocorrência de casos humanos e o incremento de cultura de cana-de-açúcar foi determinada, assim como uma maior velocidade de propagação da FMB em locais com alta quantidade desta cultura, barreiras geográficas geradas, por exemplo, por zonas de reflorestamento ciliar, poderiam impedir a disseminação da FMB. Esta tese foi interdisciplinar e exigiu, por um lado, conhecimentos em biologia, epidemiologia computacional, matemática e estatística e, em contrapartida, um ambiente rico em dados biológicos como o Laboratório de Parasitologia do VPS/USP. Os resultados desta tese poderão ser utilizados na planificação de políticas de saúde pública enfocadas à prevenção da FMB. Complementarmente, este trabalho abrirá o caminho para futuros estudos matemáticos e computacionais orientados no estudo da dinâmica e prevenção de outras doenças infecciosas transmitidas por vetores.

Contents

1. Introduction **19**

2. Transmission dynamics and control of *Rickettsia rickettsii* in populations of *Hydrochoerus hydrochaeris* and *Amblyomma sculptum* **23**

2.1 Introduction . . . 23

2.2 Materials and methods . . . 25

2.3 Results and discussion . . . 29

2.4 Conclusion . . . 33

3. Basic reproduction number for the Brazilian spotted fever system **39**

3.1 Introduction . . . 39

3.2 Next generation matrix . . . 40

3.3 R_0 calculation for BSF . . . 41

3.4 Sensitivity and elasticity analysis . . . 47

3.5 Conclusion . . . 49

4. Satellite hyperspectral imagery to support tick-borne infectious diseases Surveillance **53**

4.1 Introduction . . . 53

4.2 Materials and methods . . . 55

4.3 Results . . . 58

4.4 Discussion . . . 61

4.5 Conclusion . . . 63

5. Hosts mobility and spatial spread of *Rickettsia rickettsii* **71**

5.1 Introduction . . . 71

5.2 Model . . . 73

5.3 Simulations . . . 78

5.4 Results and discussion 80

5.5 Conclusion 86

6. Current potential prediction distribution and potential response of *Amblyomma cajennense* (Fabricius, 1787) (Acari:Ixodidae) to climate and landscape changes in America **93**

6.1 Introduction 94

6.2 Materials and methods 95

6.3 Results and discussion 98

6.4 Conclusion 105

7. Conclusions **111**

List of Figures

2.1 Schematic representation of the *R. rickettsii* dynamics in populations of *H. hydrochaeris* and *A. sculptum* . . . 25

2.2 Simulations of *R. rickettsii* dynamics in populations of *H. hydrochaeris* and *A. sculptum* in different scenarios. . . . 30

2.3 Partial rank correlation coefficient (PRCC) between each parameter and average infected population after 10 years in each tick life-cycle season. . . . 31

3.1 R_0 values for the Brazilian Spotted Fever system for different fractions of infected capybaras . . . 45

3.2 Projection, sensitivity and elasticity matrices disregarding and considering infected larvae population . . . 48

4.1 Population density and Rickettsiosis occurrence in areas of transmission by *Amblyomma sculptum* in the state of São Paulo. . . . 59

4.2 Linear unmixing model result showing the pixel abundance of the endmembers selected from the state of São Paulo. . . . 60

4.3 Sugarcane crops pixel abundance difference between the 2007 - 2012 and 2000 - 2006 periods. . . . 61

4.4 Hydrography of the State of São Paulo. . . . 64

5.1 Schematic representation of the *R. rickettsii* transmission in populations of *H. hydrochaeris* and *A. sculptum*. . . . 74

5.2 Mobility model of three sub-populations. . . . 77

5.3 Study area conformed by a grid of 50×50 pixels at regular intervals of 2 km in southeastern São Paulo . . . 79

5.4 Brazilian Spotted Fever spatial propagation considering annual change of sugar cane crops . . . 82

5.5 Brazilian Spotted Fever spatial propagation considering homogeneous amount of sugarcane . . . 83

5.6 Partial rank correlation coefficient between each parameter and the average migratory population of capybaras. . . . 83

5.7 ϕ parameter depending on sugarcane amount and the distance of the barriers width. . . . 85

5.8 Spatial spread of recovered capybaras considering non-sugarcane barriers . 85

6.1 Spatial distribution of *A. cajennense* s.s., *A. sculptum*, *A. tomelliae* and *A. mixtum* 96

6.2 Current potential distribution of *A. cajennense* s.s.,*A. mixtum*, *A. sculptum* and *A. tonelliae* considering bioclimatic and landscape factors 99

6.3 Potential response of *A. cajennense* s.s.,*A. mixtum*, *A. sculptum* and *A.tonelliae* to bioclimatic conditions of 2050 and landscape changes 101

6.4 ROC curve of the different scenarios considered 102

1. Introduction

Rickettsia rickettsii is the etiological agent of the Brazilian spotted fever (BSF), the deadliest spotted fever of the world. Besides Brazil, the disease also occurs in United States, Mexico, Costa Rica, Panama, Colombia, and Argentina[1]. Between the years 1989 and 2008 in Brazil were registered 737 cases of spotted fever with laboratory confirmation, of which 80.2% were in the Southeast with a mortality rate of 31.4% [2]. Only in the state of São Paulo, there were 555 confirmed cases between the years 1985-2012, with a mortality rate of 40.5% [3]. These number has been increasing, since between 2007 and 2015, there were 1,322 reported cases just in the metropolitan region of São Paulo [3]. These numbers make the BSF, the vector-borne zoonosis that most generates human deaths in the state of São Paulo [2].

In this regard, the overall objective of this work is to understand in a deeper way the dynamics of the Brazilian spotted fever in order to provide bases for planning strategies focus on the prevention of this disease in humans. To address this, we separated our objective in four main problems: *i*) Which populations are the most important contributors to the transmission and what are the most important factors associated with the maintenance of BSF?, *ii*) what anthropogenic parameters could be associated with the occurrence of human cases and where are the risk zones of BSF?, *iii*) how does the spatial spread of this disease occurs and how could this spread be prevented?, and *iv*) what would be the potential geographic locations for the maintenance of the vector and what climatic and landscape parameters could be associated with this distribution?.

The increase in BSF human cases has been associated with the presence and expansion of capybaras *Hydrochoerus hydrochaeris*, amplifier host for the agent *Rickettsia rickettsii* and primary host for the tick vector *Amblyomma sculptum* [1]. For this reason, in a first approximation, we analyzed if the persistence of *R. rickettsii* is affected by the dynamics of the population of ticks and the density of host. We proposed a stochastic semi-discrete-time model with seasonality to evaluate the role of capybaras in the transmission dynamics of *R. rickettsii*. We identified a high risk of *R. rickettsii* dissemination generated by: *i*) the high birth rate of capybaras in endemic areas and by *ii*) the straightforward generation of new endemic areas due to the fact that a single infected capybara with just one infected tick attached is enough to trigger the disease in a non-endemic area. Subsequently, we verified the impact of potential public health interventions to prevent BSF human cases focused on the control of capybara population growth, for example by neutering. Afterwards, to quantify the potential risk of BSF, we derive an expression of the R_0 based on the next generation matrix approach, and identified the major contributors

to its changes. We noted that the elements corresponding to the number of infected attached nymphs and adult ticks produced by an infected capybara and vice versa were critical contributors to changes in the R_0.

As we had already demonstrated that capybaras were fundamental in the transmission of the disease, using satellite imagery and monitoring the variation in amplifier hosts food sources, we tested if anthropogenic factors determined the geographic spread of this disease. We identified risk areas of human rickettsiosis and hyperspectral moderate-resolution imagery was used to identify the increment and expansion of sugarcane crops. In general, a pixel abundance associated with the increment of sugarcane crops was detected in risk areas of human rickettsiosis, supporting the hypothesis of a spatial-temporal relationship between the occurrence of human rickettsiosis and sugarcane crops increment. This methodology demonstrated to be an advantage, due to the current difficulty of monitoring locally the distribution of capybaras.

Subsequently, to gain a better insight into the spatial dynamics of the *R. rickettsii* and potentially predict future epidemic outcomes, supported by the research group on Epidemiological Modeling of Infectious diseases, under supervision of the Prof. Dr. Dirk Brockmann at Robert Koch Institute and Humboldt University, we extended our previous stochastic model, joined our previous results, and considered the spatial distribution of host and ticks. We implemented a reaction-diffusion process considering bi-directional movements between base and destination locations limited by the carrying capacity of the environment (sugarcane crops). To propose a geographical control strategy, we used the Gillespie algorithm to simulate the impact of geographical barriers, generated for example by riparian reforesting, to prevent the spatial spread of BSF.

Finally, to anticipate the planning of prevention strategies in a more global way of tick-borne infectious diseases in America, we modeled the current potential distribution of the complex *A. cajennense* s.s., and the and changes in their geographical location produced by climate and landscape changes.

In this way, this thesis is comprised of five chapters corresponding to the following articles:

1. Polo G, Mera Acosta C, Labruna MB, Ferreira F. 2017. Transmission dynamics and control of Rickettsia rickettsii in populations of Hydrochoerus hydrochaeris and Amblyomma sculptum. PLoS Negl Trop Dis 11(6): e0005613.

2. Polo G, Labruna MB, Ferreira F. (To be published). Basic reproduction number for the Brazilian spotted fever system.

3. Polo G, Labruna MB, Ferreira F. 2015. Satellite Hyperspectral imagery to support

tick-borne infectious diseases surveillance. PLoS ONE 10(11): e0143736.

4. Polo G, Mera Acosta C, Labruna M, Ferreira F, Brockmann D. (To be published). Hosts mobility and spatial spread of *Rickettsia rickettsii*.

5. Polo G, Labruna MB, Ferreira F. (To be published). Current potential distribution and potential response of *Amblyomma cajennense* (Fabricius, 1787) (Acari:Ixodidae) to climate and landscape changes in America.

Our works on modeling the dynamics and the spatial spread of the Brazilian spotted fever, besides having a direct application, open a path to further mathematical and computational studies focused on the dynamics and prevention of other vector-borne infectious diseases. This project corresponds to sub-projects 8 and 9 of the thematic project "Capybaras, ticks and Brazilian Spotted Fever", under the responsibility of Prof. Marcelo Bahia Labruna and the co-Principal Investigator Prof. Fernando Ferreira, approved by the Ethic Committee on Animal Use of the School if Veterinary and Animal Science of the University of São Paulo (Protocol CEUA: 5948070314), and financed by the São Paulo Research Foundation (Grant number: 13/18046-7).

Bibliography

[1] Labruna MB. Ecology of rickettsia in South America. Annals of the New York Academy of Sciences. 2009;1166(1):156–166.

[2] São Paulo. Vigilância Epidemiológica: Agravos. Secretaria de Vigilância Epidemiológica. 2013. Url: cve.saude.sp.gov.br/

[3] Pinter A, Costa C, Holcman M, Camara M, Leite R, et al. The Brazilian Spotted Fever in the Greater São Paulo. BEPA 2016;13(151):3-47

2. Transmission dynamics and control of *Rickettsia rickettsii* in populations of *Hydrochoerus hydrochaeris* and *Amblyomma sculptum*

Abstract

Brazilian Spotted Fever (BSF), caused by the bacterium *Rickettsia rickettsii*, is the tick-borne disease that generates the largest number of human deaths in the world. In Brazil, the current increase of BSF human cases has been associated with the presence and expansion of capybaras *Hydrochoerus hydrochaeris*, which act as primary hosts for the tick *Amblyomma sculptum*, vector of the *R. rickettsii* in this area. We proposed a semi-discrete-time stochastic model to evaluate the role of capybaras in the transmission dynamics of *R. rickettsii*. Through a sensitivity analysis, we identified the parameters with significant influence on the *R. rickettsii* establishment. Afterwards, we implemented the Gillespie's algorithm to simulate the impact of potential public health interventions to prevent BSF human cases. The introduction of a single infected capybara with at least one infected attached tick is enough to trigger the disease in a non-endemic area. We found that to avoid the formation of new BSF-endemic areas, it is crucial to impede the emigration of capybaras from endemic areas by reducing their birth rate by more than 58%. Model results were corroborated by *ex-situ* data generated from field studies, and this supports our proposal to prevent BSF human cases by implementing control strategies focused on capybaras. The proposed stochastic model illustrates how strategies for the control and prevention of vector-borne infectious diseases can be focused on amplifier hosts management practices. This work provides a basis for future prevention strategies for other neglected vector-borne diseases.

2.1 Introduction

Rickettsia rickettsii is the etiological agent of the Brazilian spotted fever (BSF), the deadliest spotted fever in the world. This infection is partially pathogenic to *Amblyomma sculptum* ticks, main vectors of the *R. rickettsii* in South America[1, 2], generating a drop in the infection rate with each tick generation[3]. In addition, *A. sculptum* ticks are unable to maintain the *R. rickettsii* infection in successive generations by transovarial and transstadial transmissions[4]. Hence, the maintenance of *R. rickettsii* depends on a

constant introduction of new susceptible animals (i.e., newborn of vertebrate hosts), which act as amplifier hosts and guarantee the constant creation of new cohorts of infected ticks [4, 5, 6, 7]. This suggests that control strategies focused on vectors [8, 9] are not enough for the prevention of this tick-borne infectious disease.

In Brazil, the capybara *Hydrochoerus hydrochaeris* acts as the amplifier host of *R. rickettsii* infection [10, 11]. In southeastern Brazil, both capybaras and BSF occurrences have increased significantly over the last three decades [5, 12]. In turn, these occurrences have been spatiotemporally associated with rising production and spatial expansion of sugarcane crops, the main food source of capybaras [13]. In BSF-endemic areas, population densities of capybaras have reached numbers up to 40 times higher than those recorded in natural environments such as the Amazon and Pantanal [14]. However, the effectiveness of control strategies focused on this amplifier host and their impact on the transmission of *R. rickettsii* are unknown.

The dynamics of complex transmission cycles, such as tick-borne infectious diseases have been broadly analyzed. Hudson et al. published the first deterministic model representing the dynamics of the Louping-ill disease, an acute viral zoonosis which mainly affects sheep [15]. O'Callaghan et al. put forward tick-borne diseases dynamics considering the potential effect of a vaccination program for *Ehrlichia ruminantium* [16]. Similarly, Rosà et al. developed a model for the tick-borne encephalitis virus including the tick stages and different transmission routes [17, 18]. Despite their important role in the understanding of vector-borne diseases dynamics, unfortunately they do not include the seasonal behavior of the vector life cycle, neither the onset nor the extinction of these diseases. As it is well established, stochastic models should be used in phenomena that do not satisfy the law of large numbers such as large communities with minor outbreaks [19]. In fact, the extinction of endemic diseases can only be analyzed with stochastic models, since extinction occurs when the epidemic process deviates from the expected level [19].

In this work, we propose a discrete-state semi-discrete-time stochastic framework to evaluate the role of capybaras in the transmission dynamics of *R. rickettsii*. We identify the parameters with significant influence on the *R. rickettsii* establishment and subsequently evaluate the impact of potential public health interventions to prevent BSF in humans.

2.2 Materials and methods

Model

The *R. rickettsii* dynamics in populations of *H. hydrochaeris* and *A. sculptum* is represented in Fig 1. Our model was adjusted to a semi-discrete time dynamics in order to consider the 1-year life cycle of the tick *A. sculptum*, which is primarily controlled by the larval behavioral diapause [20]. Thus, larvae exclusively quest and feed from April to July for 110 days, nymphs from July to October for 104 days and adults particularly quest, feed and reproduce from October to March for 151 days, as shown in Fig 2.1.

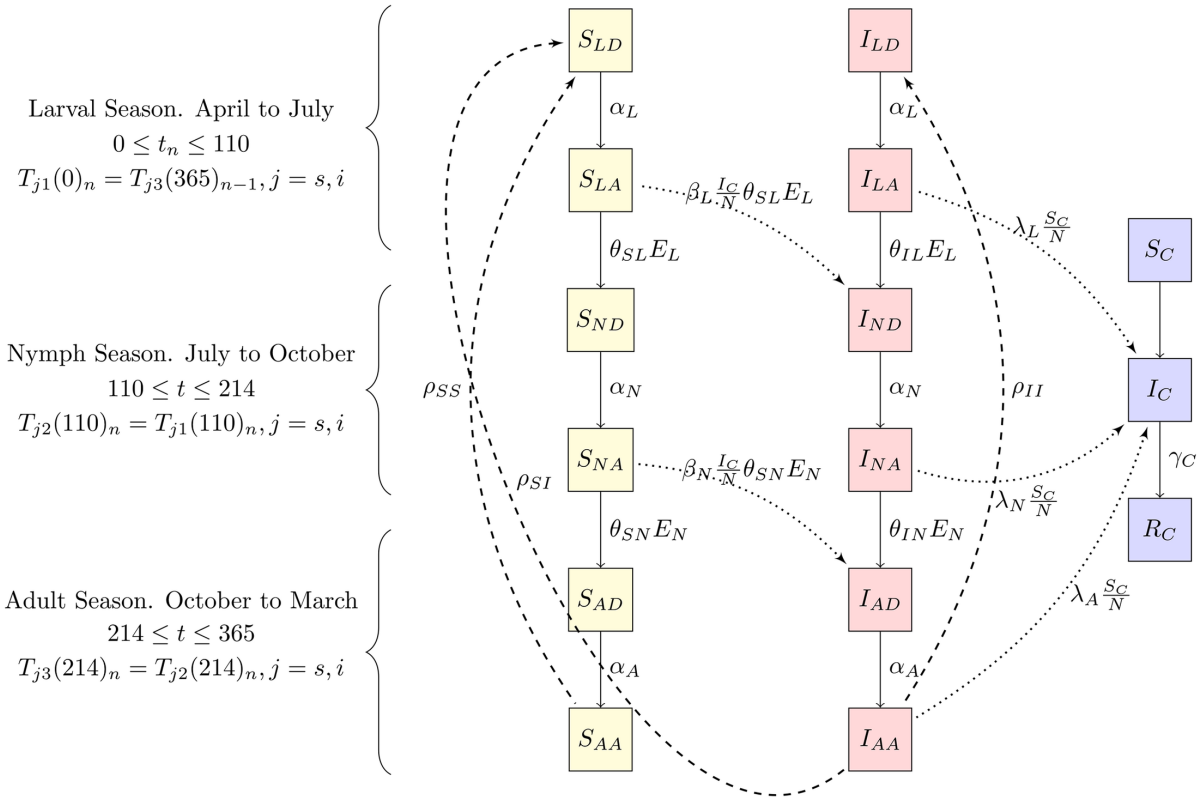

Figure 2.1 - Schematic representation of the *R. rickettsii* dynamics in populations of *H. hydrochaeris* and *A. sculptum*. Deaths, births, and migrations are not represented in the capybara population. Tick deaths are also not represented.

The tick population is classified according to the life cycle stages as larvae (L), nymphs (N) or adults (A), which could be detached from a capybara or attached to it. When a tick gets infected by an infected capybara, it remains infected until it dies. Thus, each *A. sculptum* stage is also classified according to whether it is susceptible (S) or infected (I). In this way, the population of each tick stage is represented by three indexes, where the first index denotes the infection status, the second index denotes the tick life cycle stage,

and the third index denotes detachment (D) or attachment (A).

Attached ticks at the larval and nymph stages detach at the respective rates of θ_L and θ_N. Furthermore, detached ticks at larval, nymph and adult stages can attach at rates α_L, α_N and α_A, and can die at rates δ_L, δ_N and δ_A. The production rate ρ of larvae is assumed to be proportional to the total number of adult attached ticks AA.

On the other hand, capybaras are classified as susceptible S_C, infected I_C and recovered R_C, as shown in Fig 1. They reproduce at a constant rate μ_C, die at rate δ_C and recovered at rate γ. All capybaras have the same susceptibility and there is no increased death rate of infected individuals due to disease. Susceptible capybaras can get infected by an attached larva, nymph or adult tick at a rate of λ_L, λ_N and λ_A, respectively. Once capybaras are infected, they keep the *R. rickettsii* in the bloodstream for 7 to 10 days [11], during which the infection of new susceptible larvae or nymphs that feed on it can occur at rates β_L and β_N, respectively. After this period, capybaras become immune to the disease. We do not consider a transmission rate from infected capybaras to susceptible adult ticks β_A, because of the time of *R. rickettsii* infection in ticks is greater than the time of laying. Thus, eggs can be infected only if adult ticks become infected during the larval or nymph stages [4]. Additionally, we consider a vertical transmission and hence infected adult ticks can produce infected detached larvae at rate ρ_{II}. In this way, there are 25 distinct reactions in the stochastic model which are listed in Table 1. The equivalent deterministic equations associated with the stochastic reactions are presented in the S1 File.

Time series simulations

The stochastic process detailed in Table 5.1 was simulated in the R programming language employing the Gillespie's algorithm. For each simulation we performed the number of iterations needed to get a stable performance.

We assumed a finite number of individuals distributed over a finite set of discrete states. Given an initial time t_0 and an initial population state $X(t_0)$, the Gillespie's algorithm allows us to generate the time-evolution trajectory of the state vector $X(t) \equiv (X_1(t), ..., X_N(t))$, where $X_i(t)$ is the population size of state i at time t and N is the number of states. Changes in the number of individuals in each state occur due to reactions between interacting states. The states interact through M reactions R_j, where $j = 1, \ldots, M$ denotes the jth reaction. A reaction is defined as any process that instantaneously changes the population size of at least one state [21, 22]. The time step to the next reaction was then determined as $\tau = \frac{1}{\alpha_0(x)} ln(1/r_1)$, where $\alpha_0(x) = \Sigma\alpha_j(x)$ and the index of the next reaction to execute R_j is the smallest integer j satisfying

Event	Reaction
Birth of capybara	$S_C \xrightarrow{\mu_C N} S_C + 1$
Birth of susceptible detached larvae	$S_{LD} \xrightarrow{\rho_{SS} S_{AA} + \rho_{SI} I_{AA}} S_{LD} + 1$
Birth of infected detached larvae	$I_{LD} \xrightarrow{\rho_{II} I_{AA}} I_{LD} + 1$
Engorgement of a susceptible larva	$S_{LD} \xrightarrow{\alpha_L S_{LD}} (S_{LD} - 1) + (S_{LA} + 1)$
Engorgement of an infected larva	$I_{LD} \xrightarrow{\alpha_L I_{LD}} (I_{LD} - 1) + (I_{LA} + 1)$
Transmission from an infected capybara to a susceptible larvae	$S_{LA} \xrightarrow{\beta_L \frac{I_C}{N} \theta_{SL} E_L S_{LA}} (S_{LA} - 1) + (I_{ND} + 1)$
Transmission from an infected larvae to a susceptible capybara	$S_C \xrightarrow{\lambda_L \frac{S_C}{N} I_{LA}} (S_C - 1) + (I_C + 1)$
Stage change from susceptible larvae to detached nymph	$S_{LA} \xrightarrow{\theta_{S_L} E_L S_{LA}} (S_{LA} - 1) + (S_{ND} + 1)$
Stage change from infected larvae to detached nymph	$S_{LA} \xrightarrow{\theta_{I_L} E_L I_{LA}} (S_{LA} - 1) + (S_{ND} + 1)$
Recovery rate of capybara	$I_C \xrightarrow{\gamma_C I_C} (I_C - 1) + (R_C + 1)$
Death of a susceptible capybara	$S_C \xrightarrow{\delta_C S_C} S_C - 1$
Emigration of a susceptible capybara	$S_C \xrightarrow{\epsilon_C S_C} S_C - 1$
Death of an infected capybara	$I_C \xrightarrow{\delta_C I_C} I_C - 1$
Emigration of an infected capybara	$I_C \xrightarrow{\epsilon_C I_C} I_C - 1$
Death of a recovered capybara	$R_C \xrightarrow{\delta_C R_C} R_C - 1$
Emigration of a recovered capybara	$R_C \xrightarrow{\epsilon_C R_C} R_C - 1$
Engorgement rate of a susceptible nymph	$S_{ND} \xrightarrow{\alpha_N S_{ND}} (S_{ND} - 1) + (S_{NA} + 1)$
Engorgement rate of an infected nymph	$I_{ND} \xrightarrow{\alpha_N I_{ND}} (I_{ND} - 1) + (I_{NA} + 1)$
Transmission from an infected nymph to a susceptible capybara	$S_C \xrightarrow{\lambda_N \frac{S_C}{N} I_{NA}} (S_C - 1) + (I_C + 1)$
Transmission from an infected capybara to a susceptible nymph	$S_{NA} \xrightarrow{\beta_N \frac{I_C}{N} \theta_{SN} E_N S_{NA}} (S_{NA} - 1) + (I_{AD} + 1)$
Stage change from susceptible nymph to detached adult	$S_{NA} \xrightarrow{\theta_{S_N} E_N S_{NA}} (S_{NA} - 1) + (S_{AD} + 1)$
Stage change from infected nymph to detached adult	$I_{NA} \xrightarrow{\theta_{I_N} E_N I_{NA}} (I_{NA} - 1) + (I_{AD} + 1)$
Engorgement of a susceptible adult	$S_{AD} \xrightarrow{\alpha_A S_{AD}} (S_{AD} - 1) + (S_{AA} + 1)$
Engorgement of an infected adult	$I_{AD} \xrightarrow{\alpha_A I_{AD}} (I_{AD} - 1) + (I_{AA} + 1)$
Transmission from an infected adult tick to a susceptible capybara	$S_C \xrightarrow{\lambda_A \frac{S_C}{N} I_{AA}} (S_C - 1) + (I_C + 1)$

Table 2.1 - Events and reactions of the tick-capybara-disease stochastic process

$j = \Sigma_{i=1}^{j} \alpha_i(x) > r_2 \alpha_0(x)$ [21, 22].

All parameters were estimated using previously generated data from *ex situ* field works in southeastern Brazil [4, 5, 11, 14, 23]. It is noteworthy that the natural capybara birth rate μ assumes the value of 70% of adults, 64% of females, a litter size mean of 4.2 pups, 1.23 births per female per year and a pregnancy success of 85% [14, 23]. If capybaras die at an exponential rate, then δ_C is the fraction required to die each day. The birth rate of a susceptible tick was determined assuming a female weight of 500mg [4], CEI (mg egg mass/mg engorged female × 100) of 48.4% [4],18.8 eggs/ 1 mg of eggs [24] and hatching success of 68% [4]. Likewise, the birth rate of an infected tick was determined assuming a transovarial transmission of 42.8% [4], filial infection rate of 50% [4], female weight of 372.20 mg [4], CEI of 39.55% [4], 18.8 eggs/1 mg of eggs, [24] and hatching success of 44.2% [4]. We consider a population of 20 adult female ticks per capybara and the groups of capybaras were restricted to 50 individuals [14, 23, 25]. A full list of the model's parameters used in the simulations is given in Table 2.2.

Table 2.2 - Parameters and values used in simulations

Param.	Value	Description
μ	0.005 d^{-1}	Birth rate of capybara [14, 23]
ρ_{SS}	2709 %	Susceptible larvae production per adult susceptible tick [4]
ρ_{SI}	305 %	Susceptible larvae production per adult infected tick [4]
ρ_{II}	228 %	Infected larvae production per adult infected tick [4]
E_L	10 %	Larval engorgement [4]
α_L	0.003 d^{-1}	Attached rate of a larva [4]
θ_{SL}	35 %	Stage change susceptible larvae [4]
θ_{IL}	17 %	Stage change infected larvae [4]
α_N	0.006 d^{-1}	Attached rate of a nymph [4]
E_N	40 %	Nymph engorgement [4]
θ_{SN}	60 %	Stage change susceptible nymph [4]
θ_{IN}	60 %	Stage change infected nymph [4]
α_A	0.009 d^{-1}	Attached rate of an adult[4]
E_A	70 %	Adult engorgement [4]
λ_L	9.4×10^{-5} d^{-1}	Transmission from an infected larvae to a susceptible capybara [11]
λ_N	0.046 d^{-1}	Transmission from an infected nymph to a susceptible capybara [11]
λ_A	0.046 d^{-1}	Transmission from an infected adult tick to a susceptible capybara [11]
β_L	12 %	Transmission from an infected capybara to a susceptible larvae [4, 11]
β_N	25 %	Transmission from an infected capybara to a susceptible nymph [4, 11]
$(1/\gamma)$	10 days	Capybara's infecion period [5]
γ	0.027 d^{-1}	Recovery rate of capybaras [5]
δ_C	0.002 d^{-1}	Death rate of capybaras [14]
ϵ_C	0.003 d^{-1}	Emigration rate of capybaras

Sensitivity analysis

To quantify the impact of the variation of each parameter on the output of the BSF model, we combined uncertainty through the Latin hypercube sampling (LHS) with the robust Partial rank correlation coefficient (PRCC) method [26, 27]. Initially, we obtained a random parameter distribution divided into one hundred equal probability intervals, which were then sampled. Thus, a LHS matrix was generated with one hundred rows for the number of simulations (sample size) and six columns corresponding to the number of varied parameters (α, μ_C, λ, γ_C, δ_C, ϵ_C). The parameters α and λ were varied according to the life cycle season. BSF model solutions were then simulated using each combination of parameter values through ten year simulation. One thousand model outputs were obtained and the parameter and output values were transformed into their ranks. Subsequently, we computed the PRCCs between each parameter and the average infected population size.

2.3 Results and discussion

Initially, we simulated the formation of an endemic area by the introduction of infected capybaras and infected attached ticks. For a more realistic simulation of current BSF-endemic areas of southeastern Brazil, we consider a growing population of capybaras (births greater than deaths and high emigration). We assume that this scenario corresponds with the onset of a BSF epidemic. We found that the introduction of a single infected capybara or a single infected tick is unable to trigger the disease in a non-endemic area of 50 susceptible capybaras. However, the introduction of an infected capybara with at least one infected tick attached is enough to establish a new endemic area, as shown in Fig 2 scenario A. This scenario illustrates how the fraction of infected capybaras and ticks converges to a constant from year 2 onward. In this equilibrium state, the average fraction of infected capybaras is 8.9% (95% CI= 0%-28.6%), 18.2% (95% CI= 0%-44.9%) and 17.5% (95% CI= 0%-43.9%) in the larvae, nymphs and adults season respectively. In this scenario, the average fraction of infected detached larvae is 1.25% (95% CI = 0%-7.04%), infected attached larvae 0.7% (95% CI = 0%-6.5%), infected detached nymphs 1.35% (95% CI = 0%-9.36%), infected attached nymphs 0.8% (95% CI = 0%-6.95%), infected detached adults 0.46% (95% CI = 0%-5.17%) and infected attached adults 0.54% (95% CI = 0%-5.64%). These results are consistent with previous observations in BSF-endemic areas in which the fraction of infected *A. sculptum* adults attached to horses has been reported at 0% [28] and the fraction of infected detached adults *A. sculptum* at 1% (95% CI= 0.01%-7.8 %) [28], 0.2% (95% CI= 0.01%-1.04 %) [10] and 1.28% (95% CI= 0.07%-5.59%) [29]. The fraction of infected capybaras and other tick populations remains unreported.

In scenario A, an average of 57.1% (95% CI= 22.8%-91.4%), 78.2% (95% CI= 49.6%-99.9%), and 77.2% (95% CI= 48.1%-99.9%) of capybaras became immune after a primary infection with *R. rickettsii* in the larvae, nymph and adult seasons, respectively. In practical terms, these immune capybaras include the *Rickettsia*-seropositive animals that are usually found in serosurvey studies in BSF-endemic areas. These numbers agree with previous serosurvey studies that reported 50-80% of capybaras to be seropositive for *R. rickettsii* in BSF-endemic areas [10, 30]. In this established endemic area, we observe that 563 capybaras migrated over 10 years.

Sensitivity analysis of scenario A show that the capybaras birth rate variation had the greatest impact on the average infected population size. In the nymph and adult ticks seasons, when the infection of capybaras is greater, the correlation value between the birth rate of capybaras and the average infected population is PRCC>0.6, being significant in both seasons (Fig 3). Since in BSF-endemic areas of southeastern Brazil the population of capybaras is growing[5, 12, 13, 14], theoretically, the epidemic will

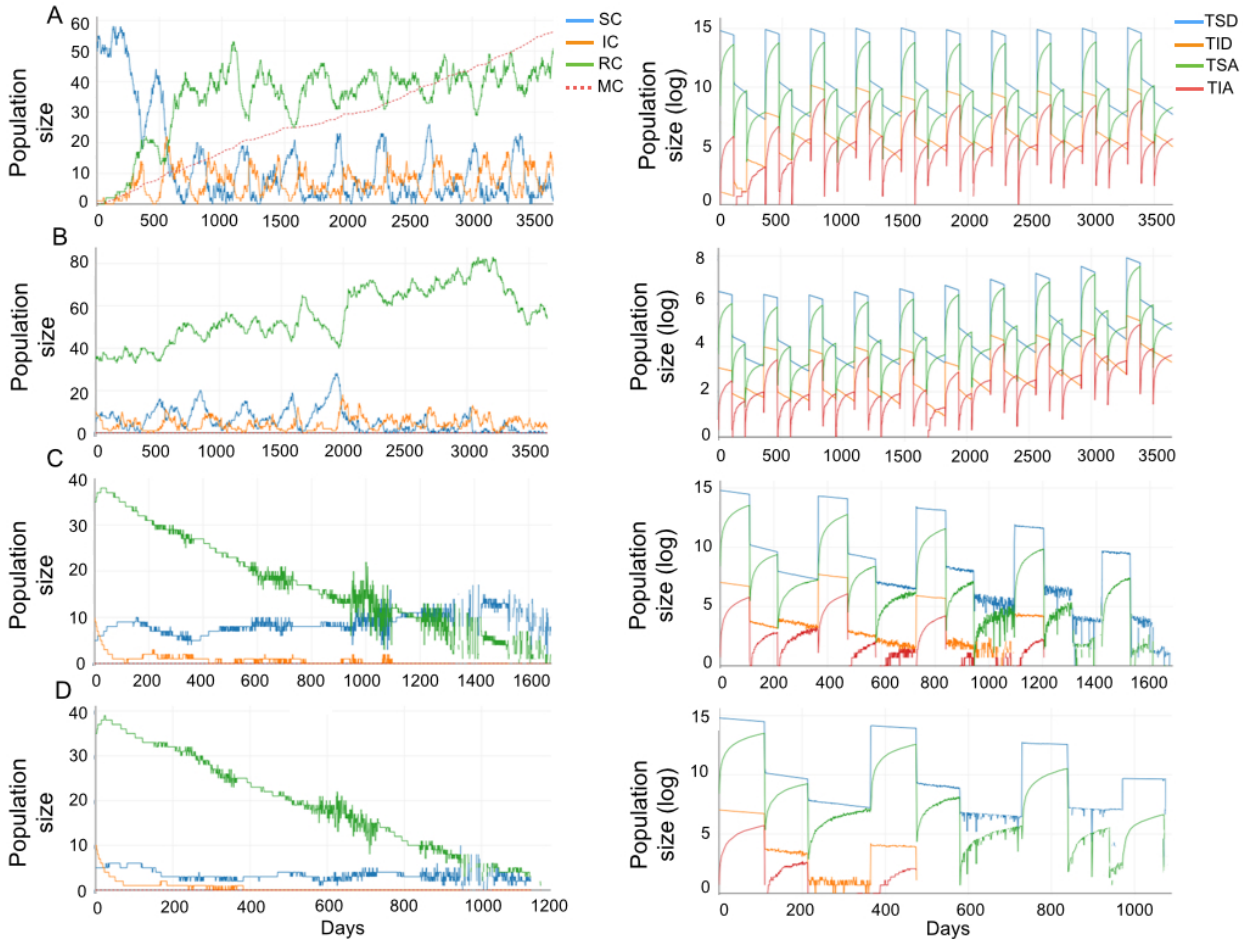

Figure 2.2 - Simulations of *R. rickettsii* dynamics in populations of *H. hydrochaeris* (left) and *A. sculptum* (right) in different scenarios. (A) Introduction of a single infected capybara with an infected attached tick. Initial values correspond with $\mu = 0.0054$, $S_C = 49$, $I_C = 1$, $R_C = 0$, $S_{AA} = 1000$ and $I_{AA} = 1$. Migratory capybaras (MC) values represent one-tenth of the real value. (B) Endemic area with a stable state of capybaras, ensuring no emigration. Initial values correspond with $\mu = 0.0021$, $S_C = 5$, $I_C = 10$, $R_C = 35$, $S_{AA} = 1000$ and $I_{AA} = 5$. (C) Endemic area with a decrease of 80% and (D) 90% in the birth rate of capybaras. Oscillations correspond with the seasonality behavior of *R. rickettsii* dynamics.

survive forever[31]. Considering $\mu = \delta_C + \epsilon$, where μ_C represents birth, δ_C death and ϵ emigration rate of capybaras, the population growth generates a high rate of emigration and consequently the spread of the disease. In this way, to better understand the effect of changes in capybara population, we investigate the host-tick-infection dynamics for different values of μ_C, under three additional scenarios: 1) an endemic area with a stable state of capybaras (births equal deaths, no emigration and no importation of the disease from outside); 2) an endemic area with a decrease of 80% and 3) 90% in the birth rate of capybaras.

Contrary to the expected behavior [32], when the population is in a stable state, the disease does not disappear. Indeed, the proportion of infected individuals remains

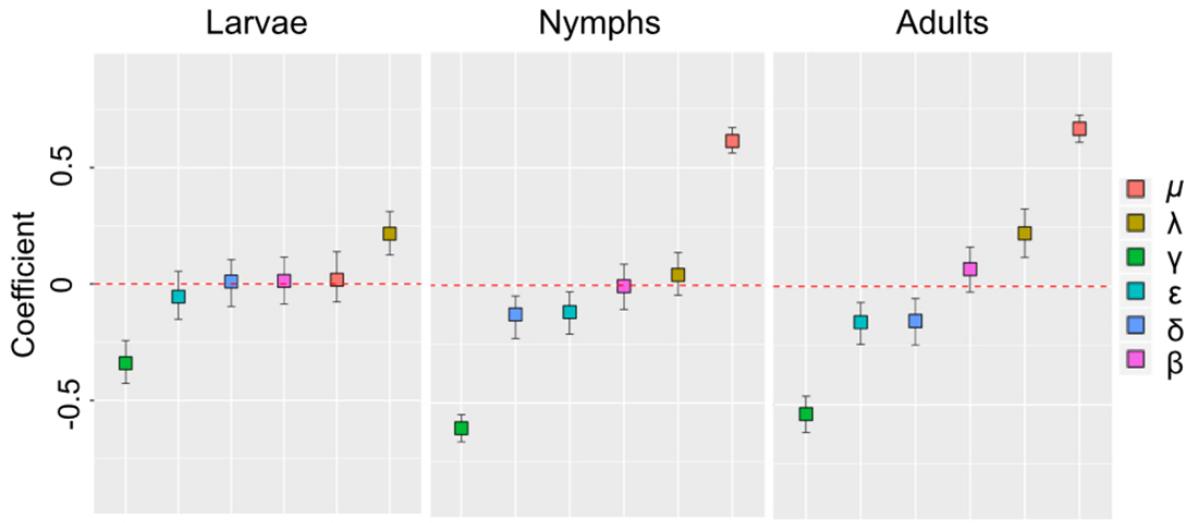

Figure 2.3 - Partial rank correlation coefficient (PRCC) between each parameter and average infected population after 10 years in each tick life-cycle season. Variations in the birth rate and in the recovery rate of capybaras have the greatest effect on the *R. rickettsii* maintenance in the nymphs and adult tick seasons. Parameters with negative PRCC will decrease the number of infected individuals as they increased.

constant over time from year 2 onward as shown in Fig 2B. In this scenario, the average fraction of infected capybaras is 4.6% (95% CI= 0.01%-19.3%), 6.3% (95% CI= 0.01%-23.1%) and 7.4% (95% CI= 0.01%-25.4%) in the larvae, nymphs and adults seasons, respectively. To ensure births equals deaths ($\mu_C = \delta_C$) and thereby guarantee no emigration ($\epsilon = 0$), it is necessary to control the capybara's birth rate in 58%. Thereby, though the disease does not disappear, this birth rate guarantees that the *R. rickettsii* will not spread from BSF-endemic areas.

Thus, for the elimination of the *R. rickettsii* from endemic areas, a decrease in the capybara's birth rate to values lower than 0.0021 is necessary. However, this can lead to a decline in capybaras population over time. When a decrease of 80% ($\mu_C = 0.0011$) in the birth rate of capybaras is considered, infected individuals tend to disappear in the fourth year along with a decrease in the total population size, as shown in Fig 2C. Otherwise, when a decrease of of 90% ($\mu_C = 0.0005$) in the birth rate of capybaras is considered, infected ticks and capybaras tend to disappear from the second year as shown in Fig 2D.

Strategies to reduce the birth rate of capybaras include the reduction of the carrying capacity, their removal, either by euthanasia or regulated hunting, and their reproductive control. As capybaras natality depends primarily on the availability of food sources, as is typically the case for rodents [33], the reduction of the carrying capacity in BSF-endemic areas is a plausible strategy to reduce their birth rate[34]. Polo et al. found a spatiotemporal relationship between the occurrence of BSF and the increment and expansion of sugarcane crops, the main food source of capybaras in southeastern Brazil

and the most important agricultural product in the region [13]. Furthermore, in this area, there is a constant availability of water sources, which allow the establishment of capybaras, as this is a semiaquatic vertebrate that depends on water sources for thermic regulation, reproduction, and predator protection [33]. Certainly, controlling these aspects is not feasible.

Additionally, because of the constant increment and abundance of vital resources offered by the environment in BSF-endemic areas of southeastern Brazil, it is important to consider that in response to the removal or elimination of recovering capybaras from theses areas, a reintroduction of susceptible animals can occur [13]. This, along with the long survival of unfed *A. sculptum* in pastures [35], and the fact that just one infected capybara with a single infected tick attached is sufficient to establish an endemic area, can cause a rapid spread of the disease and consequently an increased risk of transmission to humans.

Reproductive control of capybaras through deferentectomy and ligation of fallopian tubes was previously tested in southeastern Brazil [36]. It was observed that the reproductive management did not negatively influence individual or collective behavioral aspects, with the animals defending their territory and not migrating [36]. The sterilization of capybaras has already been authorized as a way to prevent BSF human cases in a small endemic area of southeastern Brazil [37].

Future studies encompassing field data should be performed to evaluate the role of alternative reservoirs in the dynamics of *R. rickettsii*. This is a limitation of our work since we considered BSF-endemic areas of southeastern Brazil, where capybaras are the major, though not the exclusive, hosts for either larval, nymphal or adult stages of *A. sculptum*. In most BSF-endemic areas, the only medium-to large-sized animal species is the capybara; therefore it is the only host for the *A. sculptum* adult stage, and consequently, the only suitable host species to sustain an *A. sculptum* population in the area [7, 10, 38]. However, there have been some previous reports of *A. sculptum* immature stages (larvae and nymphs) on small animals (wild mice, marsupials, birds) which usually share the same habitat with capybaras [39, 40]. Nevertheless, comparing to capybaras, the amount of larvae or nymphs that feed on these animals is minimal; i.e., while hundreds to thousands larvae and nymphs are commonly found feeding on a single capybara [41], we usually find less than 10, or exceptionally a few dozen *A. sculptum* ticks on individual small animals [39, 40, 41]. Indeed, this condition is also favored by the fact that all active stages of *A. sculptum* tend to host-quest on vegetation above 15 cm from the soil, precluding their direct contact with small mammals or ground-feeding passerine birds [20, 42].

2.4 Conclusion

This work offers an alternative for the planning of prevention strategies for tick-borne neglected infectious diseases. The planning of these type of interventions is usually performed by public entities through heuristic techniques, such as trial and error methods, without obtaining optimal results. The results of our work accurately match with data previously generated from field studies on the *R. rickettsii* dynamics in southeastern Brazil and will potentially allow the formulation of public policy to prevent BSF human cases based on the control of capybara population growth. Furthermore, this work will provide a basis for the planning of prevention programs for other neglected vector-borne infectious diseases.

Acknowledgments

The authors would like to thank Dr. Dennis Chao, Prof. Pejman Rohani and Prof. Philip O' Neill for the explanations and discussions valuable to the advancement of the model at the 7th Summer Institute in Statistics and Modeling in Infectious Diseases at the University of Washington in Seattle, Washington, USA.

Supporting information

S1 File. Equivalent deterministic equations associated with the reactions of the stochastic model for the larval, nymph and adult tick seasons.

$$
\begin{aligned}
\frac{dS_{LD}}{dt} &= \rho_{SS} S_{AA} + \rho_{SI} I_{AA} - \alpha_L S_{LD} \\
\frac{dI_{LD}}{dt} &= \rho_{II} I_{AA} - \alpha_L I_{LD} \\
\frac{dS_{LA}}{dt} &= \alpha_L S_{LD} - \beta_L \frac{I_C}{N} \theta_{SL} E_L S_{LA} - \theta_{S_L} E_L S_{LA} \\
\frac{dI_{LA}}{dt} &= \alpha_L I_{LD} - \theta_{I_L} E_L I_{LA} \\
\frac{dS_C}{dt} &= \mu_C N - \lambda_L \frac{S_C}{N} I_{LA} - \delta_C S_C - \epsilon_C S_C \\
\frac{dI_C}{dt} &= \lambda_L \frac{S_C}{N} I_{LA} - \gamma_C I_C - \delta_C I_C - \epsilon_C I_C \\
\frac{dR_C}{dt} &= \gamma_C I_C - \delta_C R_C - \epsilon_C R_C
\end{aligned}
$$

Similarly, the equivalent deterministic equations for the nymph season can be written as:

$$\begin{aligned}
\frac{dS_{ND}}{dt} &= \theta_{S_L} E_L S_{LA} - \alpha_N S_{ND} \\
\frac{dI_{ND}}{dt} &= \beta_L \frac{I_C}{N} \theta_{SL} E_L S_{LA} + \theta_{I_L} E_L I_{LA} - \alpha_N I_{ND} \\
\frac{dS_{NA}}{dt} &= \alpha_N S_{ND} - \beta_N \frac{I_C}{N} \theta_{SN} E_N S_{NA} - \theta_{S_N} E_N S_{NA} \\
\frac{dI_{NA}}{dt} &= \alpha_N I_{ND} - \theta_{I_N} E_N I_{NA} \\
\frac{dS_C}{dt} &= \mu_C N - \lambda_N \frac{S_C}{N} I_{NA} - \delta_C S_C - \epsilon_C S_C \\
\frac{dI_C}{dt} &= \lambda_N \frac{S_C}{N} I_{NA} - \gamma_C I_C - \delta_C I_C - \epsilon_C I_C \\
\frac{dR_C}{dt} &= \gamma_C I_C - \delta_C R_C - \epsilon_C R_C
\end{aligned}$$

Finally, the equivalent deterministic equations for the adult season are

$$\begin{aligned}
\frac{dS_{AD}}{dt} &= \theta_{S_N} E_N S_{NA} - \alpha_A S_{AD} \\
\frac{dI_{AD}}{dt} &= \beta_N \frac{I_C}{N} \theta_{SN} E_N S_{NA} + \theta_{I_N} E_N I_{NA} - \alpha_A I_{AD} \\
\frac{dS_{AA}}{dt} &= \alpha_A S_{AD} \\
\frac{dI_{AA}}{dt} &= \alpha_A I_{AD} \\
\frac{dS_C}{dt} &= \mu_C N - \lambda_A \frac{S_C}{N} I_{AA} - \delta_C S_C - \epsilon_C S_C \\
\frac{dI_C}{dt} &= \lambda_A \frac{S_C}{N} I_{AA} - \gamma_C I_C - \delta_C I_C - \epsilon_C I_C \\
\frac{dR_C}{dt} &= \gamma_C I_C - \delta_C R_C - \epsilon_C R_C,
\end{aligned}$$

where all parameters are detailed in Table 2.

Bibliography

[1] Nava S, Beati L, Labruna M, Caceres A, Mangold A, Guglielmone A. Reassessment of the taxonomic status of *Amblyomma cajennense* (Fabricius, 1787) with the description of three new species, *Amblyomma tonelliae* n. sp., *Amblyomma interandinum* n. sp. and *Amblyomma patinoi* n. sp., and reinstatement of *Amblyomma mixtum* Koch, 1844, and *Amblyomma sculptum* Berlese, 1888 (Ixodida: Ixodidae). Ticks and Tick-borne Diseases. 2014;(5):252–276.

[2] Martins TF, Barbieri ARM, Costa FB, Terassini FA, Camargo LMA, Peterka CRL,

et al. Geographical distribution of *Amblyomma cajennense* (sensu lato) ticks (Parasitiformes: Ixodidae) in Brazil, with description of the nymph of *A. cajennense* (sensu stricto). Parasites and Vectors. 2016;9(1):186

[3] Niebylski ML, Peacock MG, Schwan TG. Lethal effect of *Rickettsia rickettsii* on its tick vector (*Dermacentor andersoni*). Applied and Environmental Microbiology. 1999 Feb;65(2):773–778.

[4] Soares JF, Soares HS, Barbieri AM, Labruna MB. Experimental infection of the tick *Amblyomma cajennense*, Cayenne tick, with *Rickettsia rickettsii*, the agent of Rocky Mountain spotted fever. Medical and Veterinary Entomology. 2012;26(2):139–151.

[5] Labruna MB. Ecology of rickettsia in South America. Annals of the New York Academy of Sciences. 2009;1166(1):156–166.

[6] Labruna MB. Brazilian spotted fever: the role of capybaras. In: Capybara. Springer New York; 2013. p. 371–383.

[7] Krawczak FS, Agostinho WC, Polo G, Moraes-Filho J, Labruna MB. Comparative evaluation of *Amblyomma ovale* ticks infected and noninfected by *Rickettsia* sp. strain Atlantic rainforest, the agent of an emerging rickettsiosis in Brazil. Ticks and Tick-borne Diseases. 2016;7(3):502–507.

[8] Gaff H, Schaefer E. Metapopulation models in tick-borne disease transmission modeling. Adv Exp Med Bio. 2010;673:51–65.

[9] Nelson CA, Hayes CM, Markowitz MA, Flynn JJ, Graham AC, Delorey MJ, et al. The heat is on: Killing blacklegged ticks in residential washers and dryers to prevent tickborne diseases. Ticks and Tick-borne Diseases. 2016;7(5):958–963.

[10] Krawczak FS, Nieri-bastos FA, Nunes FP, Soares J, Moraes-filho J. Rickettsial infection in *Amblyomma cajennense* ticks and capybaras (*Hydrochoerus hydrochaeris*) in a Brazilian spotted fever-endemic area. Parasites and Vectors. 2014;7:1–7.

[11] Souza CE, Moraes-Filho J, Ogrzewalska M, Uchoa FC, Horta MC, Souza SSL, et al. Experimental infection of capybaras *Hydrochoerus hydrochaeris* by *Rickettsia rickettsii* and evaluation of the transmission of the infection to ticks *Amblyomma cajennense*. Veterinary Parasitology. 2009;161(1):116–121.

[12] Del Fiol F, Junqueira F, Miranda C, Maria T, Filho B. A febre maculosa no Brasil. Revista Panamericana de Salud Pública. 2010;27(10):461–466.

[13] Polo G, Labruna MB, Ferreira F. Satellite hyperspectral imagery to support tick-borne infectious diseases surveillance. PLoS ONE. 2015;p. e0119190.

[14] Ferraz K, De Barros Ferraz S, Moreira J, Couto H, Verdade L. Capybara (*Hydrochoerus hydrochaeris*) distribution in agroecosystems: a cross-scale habitat analysis. Journal of Biogeography. 2007;34(2):223–230.

[15] Hudson P, Norman R, Laurenson M, Newborn D, Gaunt M, Jones L, et al. Persistence and transmission of tick-borne viruses: *Ixodes ricinus* and louping-ill virus in red grouse populations. Parasitology. 1995;111:49–58.

[16] O'Callaghan C, Medley G, Peter T, Mahan S, Perry B. Predicting the effect of vaccination on the transmission dynamics of heartwater (*Cowdria rumination* infection). Preventive Veterinary Medicine. 1999;42:49–61.

[17] Rosa R, Pugliese A, Norman R, PJ H. Thresholds for disease persistence in models for tick- borne infections including non-viraemic transmission, extended feeding and tick aggregation. Journal Of Theoretical Biology. 2003;224:359–376.

[18] Rosa R, Pugliese. Effects of tick population dynamics and host densities on the persistence of tick-borne infections. Mathematical Biosciences. 2007;208:216–240.

[19] Anderson H, T B. Stochastic Epidemic Models and their Statistical Analysis. Lectures Notes in Statistics. Springer; 2000.

[20] Labruna M, Amaku M, Metzner J, Pinter A, Ferreira F. Larval behavioral diapause regulates life cycle of *Amblyomma cajennense* (Acari: Ixodidae) in Southeast Brazil. J Med Entomol. 2003;40:170–178.

[21] Gillespie D. A general method for numerically simulating the stochastic time evolution of coupled chemical reactions. Journal of Computational Physics. 1976;22:403–434.

[22] Pineda-Krch M. GillespieSSA: Implementing the Gillespie Stochastic Simulation Algorithm in R . Journal of Statistical Software. 2008;25:1–18.

[23] Sarango V. Manual para manejo de capibaras. Programa para la conservación y manejo sostenible del patrimonio natural y cultural de la reserva de la biosfera Yasuni. 2011;1:1–39.

[24] Labruna M, Cerqueira R, Oliveira P. Study of the weight of eggs from six Ixodid Species from Brazil. Memorias Instituto Oswaldo Cruz. 1997;92:205–207.

[25] Ojasti J. Estudio biológico del chigüire o capibara. Fondo Nacional de Investigaciones Agropecuarias; 1973.

[26] Blower S, H D. Sensitivity and uncertainty analysis of complex-models of disease transmission - an HIV model, as an example. International Statistical Review. 1994;62:229–243.

[27] Marino S, Hogue I, Ray C, DE K. A methodology for performing global uncertainty and sensitivity analysis In systems Biology. Journal of Theoretical Biology. 2008;254:178–196.

[28] Guedes E, Leite R, Pacheco R, Silveira I, MB L. Rickettsia species infecting Amblyomma ticks from an area endemic for Brazilian spotted fever in Brazil. Rev Bras Parasitol Vet. 2011;20:308–311.

[29] Guedes E, Leite R, Prata M, Pacheco R, Walker D, MB L. Detection of *Rickettsia rickettsii* in the tick *Amblyomma cajennense* in a new Brazilian spotted fever-endemic area in the state of Minas Gerais. Mem Inst Oswaldo Cruz. 2005;100:841–845.

[30] Souza C, Berger Calic S, Camargo M, Savani E, Lacerra de Souza S, Castor Lima V, et al. O papel da capivara *Hydrochaeris hydrochaeris* na cadeia epidemiologica da febre maculosa brasileira. Rev Bras Parasitol Vet. 2004;13:203–205.

[31] Britton T, House T, Lloyd A, Mollison D, Riley S, Trapman P. Five challenges for stochastic epidemic models involving global transmission. Epidemics. 2015;10:54–57

[32] Diekmann O, Heesterbeek H, Britton T. Mathematical Tools for Understanding Infectious Diseases Dynamics. Princeton University Press; 2013.

[33] Moreira J, Alvarez M, Tarifa T, Pacheco V, Taber A, Tirira D, et al. Taxonomy, Natural History and Distribution of the Capybara. In: Capybara. Springer New York; 2013. p. 3–37.

[34] Allman E, Rhodes J. Dynamic Modeling with Difference Equations. In: Mathematical Models in Biology An Introduction. Cambridge University Press; 2004. p. 371–383.

[35] Lopes C, Oliveira P, Haddad J, Domingues L, Pinheiro R, Borges L, et al. Biological parameters of ticks (*Amblyomma cajennense* Fabricius, 1787) under field and laboratory conditions in Pedro Leopoldo, State of Minas Gerais, Brazil. Brazilian Journal of Veterinary Parasitology. 2008;17:14–17.

[36] Rodrigues M. Aspectos Ecológicos e Controle Reprodutivo em uma População de Capivaras Sinantrópicas no Campus da Universidade Federal de Viçosa MG. Ph.D. Thesis. 2013;Available from: http://repositorio.ufv.br/handle/123456789/1457.

[37] Rodrigues L. MPF e prefeitura de BH fecham acordo e capivaras da Pampulha serão esterilizadas. 2017; Available from: http://agenciabrasil.ebc.com.br/geral/noticia/2017-02/ mpf-e-prefeitura-de-bh-fecham-acordo-e-capivaras-da-pampulha-serao.

[38] Labruna M, Krawczak F, Gerardi M, Binder L, Barbieri A, Paz G, et al. Isolation of Rickettsia rickettsii from the tick Amblyomma sculptum from a Brazilian spotted fever-endemic area in the Pampulha Lake region, southeastern Brazil. Vet Parasitol Reg Stud Rep. 2017;p. In press.

[39] Horta M, Labruna M, Pinter A, Linardi P, Schumaker T. Rickettsia infection in five areas of the state of São Paulo, Brazil. Memorias do Instituto Oswaldo Cruz. 2007;102:793–801.

[40] Santolin I, Luz H, Alchorne N, Pinheiro M, Melinski R, Faccini J, et al. Ticks on birds caught on the campus of the Federal Rural University of Rio de Janeiro, Brazil. Rev Bras Parasitol Vet. 2012;(21):213–218.

[41] Perez C, Almeida A, Almeida A, Carvalho V, Balestrin D, Guimarães M, et al. Ticks of genus *Amblyomma* (Acari: Ixodidae) and their relationship with hosts in endemic area for spotted fever in the State of São Paulo. Rev Bras Parasitol Vet. 2008;(17):210–217.

[42] Labruna M, Pinter A, Castro M, Castagnolli K, Garcia M, Szabo M. Some records on host questing behavior of *Amblyomma cajennense* (Acari: Ixodidae) larvae. Rev Bras Parasitol Vet. 2002;(11):91–93.

3. Basic reproduction number for the Brazilian spotted fever system

Abstract

The Brazilian Spotted Fever is an emerging and lethal disease in South America, which basic reproduction number is unknown. Endemic areas are related to the presence of capybaras *Hydrochoerus hydrochaeris*, amplifier hosts of *R. rickettsii* and primary hosts of the tick *Amblyomma sculptum*, main vector of the agent in this area. Calculating the basic reproduction number R_0 for complex infectious diseases as the*Rickettsia rickettsii* is a challenging problem because: *i*) different animal species are implicated in the transmission, *ii*) there are particular epidemiological reactions to the infectious agent at the different stages of the vector life cycle life, and *iii*) there are multiple transmission routes. We calculate the R_0 for the *R. rickettsii* system by segregating the host and ticks populations into epidemiologically different categories of individuals and constructing a next-generation matrix. Each matrix element was considered as an expected number of infected individuals of one category produced by a single infectious individual of a second category. We used field and experimental data to parameterize the next-generation matrix and obtained the final calculation of R_0. Sensitivity and elasticity analysis were performed to quantify the perturbations of each matrix element to R_0. The R_0 calculation provides insights for the design of strategic interventions for the Brazilian Spotted Fever in endemic areas of South America.

3.1 Introduction

The Basic Reproduction Number R_0 is one of the most important concepts in epidemiology of infectious diseases [1, 2, 3]. It is among the quantities most estimated for infectious diseases in outbreak situations, and provides insights when designing control interventions for established infections [3]. R_0 is defined as the average number of new cases of an infection caused by one typical infected individual, in a population consisting entirely of susceptible individuals [3, 4]. It is a threshold quantity such that if $R_0 > 1$, and outbreak can occur if the pathogen is introduced, whereas if $R_0 < 1$, it will certainly die out [3, 4]. For vector-borne diseases, the interpretation of R_0 is more complex because there are different infected categories of individuals (hosts and vectors) involved in

transmission [4].

Different expressions for R_0 have been published for tick-borne infectious diseases [5, 6, 7, 8, 9]. However, these calculations have some limitations in terms of the biological interpretation at the individual level [4]. In this work, we derive an expression of the R_0 for the Brazilian Spotted Fever system based on the next generation matrix approach [4, 10]. The next generation matrix gives the size of the next generation distributed over the different categories given in the present generation [4, 10]. An advantage of this approach is that the steps to calculate the R_0 and the matrix elements have an explicit biological basis [4]. Sensitivity and elasticity analysis were performed to quantify absolute and proportional perturbations of each matrix element to R_0. This work provides a better understanding of the Brazilian Spotted Fever dynamics and potentially will support the planning of preventive strategies in South America.

3.2 Next generation matrix

In a system divided into a finite number of discrete states, it is possible to define a matrix $\mathbf{E}$ that relates the numbers of newly infected individuals in the different categories in successive generations. This next-generation matrix term was introduced by Diekmann et al. [1], who defined R_0 as the dominant eigenvalue of $\mathbf{E}$. Assuming that the infectiousness of individuals is independent of the transmission route which the infection was acquired, we can distinguish different *categories-at-epidemiological-birth* (TEB). The term TEB refers specifically to the birth of the infection in the individual rather than the individual[2, 3]. This leads to explaining the infection process in terms of successive "generations of infected individuals", in complete analogy to demographic generations [3]. For a system with g TEB, the next-generation matrix, $\mathbf{E}$, will be a $g \times g$ matrix. For instance, a simple illustration of the next-generation matrix for a four TEB is:

$$\mathbf{E} = \begin{bmatrix} X_{00} & X_{01} & X_{02} & X_{03} \\ X_{10} & X_{11} & X_{12} & X_{13} \\ X_{20} & X_{21} & X_{22} & X_{23} \\ X_{30} & X_{31} & X_{32} & X_{33} \end{bmatrix}$$

where the matrix elements X_{ij} represents the expected number of infected individuals of category j produced by an infected individual of category i during the infectious period.

In tick-borne infectious diseases systems, there is one TEB for each tick life stage, i.e., larvae, nymphs and adults, at which infection can be acquired. In the same way, a different TEB takes into account systemic infections in vertebrate hosts. In this systems, if there is

no transmission between different TEB (X_{ij}) or even among the same TEB (X_{ii}), the matrix elements representing such transmission are zero. For instance, since co-feeding has not been reporter in any tick cycle life the transmissions larvae-larvae, nymphs-nymphs and adults-adults are zero, and naturally, by analogy the host-host transmission is also null.

3.3 R_0 calculation for BSF

The Brazilian Spotted Fever (BSF), a highly lethal zoonotic disease caused by the bacteria *Rickettsia rickettsii* and transmitted by the tick *Amblyomma sculptum* [11]. Specifically, in the transmission of this disease, the vector *A. sculptum* is incapable to maintain the infection by *R. rickettsii* in consecutive generations [12, 13]. In Brazil, the maintenance of *R. rickettsii* depends primarily on the constant introduction of susceptible capybaras *Hydrochoerus hydrochaeris* [14, 15], which act as amplifiers and guarantee a continual creation of new cohorts of infected ticks[13, 14, 15]. Accordingly, we consider that the *R. rickettsii* can be transmitted by individuals of three categories: infected capybaras (0), infected attached nymphs (1), infected attached adults (2) and infected attached larvae (3) [16]. Therefore, the element X_{00} corresponds to the transmission between Capybaras (C); elements X_{01}, X_{02} and X_{03} correspond to the Capybaras-tick transmission; elements X_{10}, X_{20} and X_{30} are associated with the transmission from tick to capybara. Hence, X_{11}, X_{13}, X_{21}, X_{22},X_{32} and X_{33} involve nonsystemic transmission between ticks (cofeeding- C_f), and the elements X_{12} and X_{31} correspond to the transstadial perpetuation (TS_P) of the disease. In addition, the element X_{23} determines the transovarial transmission (TO), that is the transmission from adult ticks to offspring. In this way, the matrix $\mathbf{E}$ can be written as:

$$\mathbf{E} = \begin{bmatrix} C \to C & C \to T_k & C \to T_k & C \to T_k \\ T_k \to C & C_f & TS_P & C_f \\ T_k \to C & C_f & C_f & TO \\ T_k \to C & TS_P & C_f & C_f \end{bmatrix}$$

We assume that the uninfected tick-capybara interaction system is in equilibrium when the disease is introduced into the system and that there are few infected individuals of the four categories at early stages. Thus,

$$\mu N = \mu S_C(t),$$

where μ is the birth rate of capybaras, N is the total population of capybaras and S_C is

the number of susceptible capybaras. Thus giving,

$$S_C = N.$$

The tick population is at equilibrium when the input rates are equal to the output rates for each stage of the tick life cycle. In our system, each tick stage is represented by three indexes, where the first index denotes susceptible (S) or infected (I); the first subindex denotes the tick life cycle stage as larvae (L), nymphs (N) or adults (A); and the third subindex denotes detachment (D) or attachment (A). In this manner, S_{LD} ticks attach to a capybara at rate α_L and develop into S_{LA}'s, which in turn can detached and become S_{ND} ticks at rate $\theta_{SL}\epsilon_L$, where θ indicates change in the life cycle stage, and ϵ express tick engorgement. Sequentially, S_{ND}'s attach at rate α_N, turn into S_{NA} ticks, which detach at rate $\theta_{SN}\epsilon_N$, develop into S_{AD}'s and attach at rate α_A becoming S_{AA} ticks. Finally, S_{AA}'s can generate new S_{LD} ticks, by transovarial transmission, at rate ρ_{SS}. Thus,

$$\begin{aligned}
\rho_{SS}S_{AA}(t) &= \alpha_L S_{LD}(t) \\
\alpha_L S_{LD}(t) &= (\theta_{S_L}\epsilon_L)S_{LA}(t) \\
(\theta_{S_L}\epsilon_L)S_{LA}(t) &= \alpha_N S_{ND}(t) \\
\alpha_N S_{ND}(t) &= (\theta_{S_N}\epsilon_N)S_{NA}(t) \\
(\theta_{S_N}\epsilon_N)S_{NA}(t) &= \alpha_A S_{AD}(t) \\
\alpha_A S_{AD}(t) &= \rho_{SS}S_{AA}(t)
\end{aligned}$$

Thereby:

$$\begin{aligned}
S_{LD}(t) &= \frac{\alpha_A}{\alpha_L}S_{AD}(t) \\
S_{LA}(t) &= \frac{\rho_{SS}}{\theta_{SL}\epsilon_L}S_{AA}(t) \\
S_{ND}(t) &= \frac{\alpha_L}{\alpha_N}S_{LD}(t) \\
S_{NA}(t) &= \frac{\theta_{SL}\epsilon_L}{\theta_{SN}\epsilon_N}S_{LA}(t) \\
S_{AD}(t) &= \frac{\alpha_N}{\alpha_A}S_{ND}(t) \\
S_{AA}(t) &= \frac{\theta_{SN}\epsilon_N}{\rho_{SS}}S_{NA}(t)
\end{aligned}$$

In a first approach, we do not considered larvae population in the next-generation matrix. Thus, let infected capybaras be of category 0, infected attached nymphs be of category 1 and infected attached adult ticks be of category 2. $\{X_{ij}; i, j = 0, 1, 2\}$ is the number of infected individuals of category j produced by an infected individual of category i.

An infected capybara can infect attached susceptible nymphs. It must first infect

susceptible larvae attached to it, which in turn detach and develop into infected detached nymphs at rate $\beta_L \frac{IC}{N} \theta_{SL} \epsilon_L$, which in turn attach at rate α_N. Thus the number of infected attached nymphs produced by an infected capybara, is:

$$E[X_{01}] = \beta_L \frac{IC}{N} \theta_{SL} \epsilon_L S_{LA} \alpha_N$$

Analogously, an infected capybara produces infected attached adult ticks when it infects susceptible nymphs attached to it at rate $\beta_N \frac{IC}{N} \theta_{SN} \epsilon_N$, which then attach at rate α_A. Thus:

$$E[X_{02}] = \beta_N \frac{IC}{N} \theta_{SN} \epsilon_N S_{NA} \alpha_A$$

An infected capybara can not produce another infected capybara. In this way:

$$E[X_{00}] = 0$$

An infected attached nymph, while feeding, can infect capybaras at rate λ_N. Since $(\frac{S_C}{N}) \approx 1$ at the initial stages of infection, the number of capybaras produced by an infected nymph is:

$$E[X_{10}] = \lambda_N I_{NA}$$

Additionally, an infected attached nymph grows into an infected attached adult if it detaches and develops into an infected adult at rate $\theta_{IN} \epsilon_N$, which later attach to a capybara at rate α_A. Hence, the number of infected attached adults originated by an infected attached nymph is:

$$E[X_{12}] = \theta_{IN} \epsilon_N I_{NA} \alpha_A$$

As cofeeding transmission has not been reported in *Amblyomma sculptum* ticks, an infected attached nymph can not produce another infected nymph:

$$E[X_{11}] = 0$$

Similarly, an infected attached adult tick generates an infected capybara if it attaches to a susceptible capaybara and infects it at rate λ_A. Since $(\frac{S_C}{N}) \approx 1$ at the initial stages, thus:

$$E[X_{20}] = \lambda_A I_{AA}$$

Due to the absence of cofeeding, infected adult ticks can not produce infected nymphs

neither another infected attached adult. Thus,

$$E[X_{21}] = 0$$
$$E[X_{22}] = 0$$

Let $\mathbf{E_1} = \{m_{ij}\}_{i,j=0}^{2}$ be the expectation matrix:

$$\begin{bmatrix} 0 & \beta_L \frac{IC}{N} \theta_{SL} \epsilon_L S_{LA} \alpha_N & \beta_N \frac{IC}{N} \theta_{SN} \epsilon_N S_{NA} \alpha_A \\ \lambda_N I_{NA} & 0 & \theta_{IN} \epsilon_N I_{NA} \alpha_A \\ \lambda_A I_{AA} & 0 & 0 \end{bmatrix}$$

Thus, the eigenvalues are obtain from the characteristic equation $det(\mathbf{E_1} - \zeta I_{n3}) = 0$, where naturally, it is assumed that the eigenvalues are ζ, and I_{n3} is 3×3 unitary matrix. Let the characteristic polynomial of $\mathbf{E_1}$ be $f(\zeta)$:

$$f(\zeta) = \zeta^3 - \zeta\xi_1 - \xi_0 = 0$$

where,

$$\xi_1 = \beta_L \frac{IC}{N} \theta_{SL} \epsilon_L S_{LA} \alpha_N \lambda_N I_{NA} + \beta_N \frac{IC}{N} \theta_{SN} \epsilon_N S_{NA} \alpha_A \lambda_A I_{AA}$$

and,

$$\xi_0 = \beta_L \frac{IC}{N} \theta_{SL} \epsilon_L S_{LA} \alpha_N \theta_{IN} \epsilon_N I_{NA} \alpha_A \lambda_A I_{AA}.$$

The resultant expression for R_0 is given by the dominant eigenvalue of the matrix $\mathbf{M_1}$:

$$R_0 = \frac{\sqrt[3]{\frac{2}{3}}\xi_1}{\sqrt[3]{\sqrt{3}\sqrt{27\xi_0^2 - 4\xi_1^3} + 9\xi_0}} + \frac{\sqrt[3]{\sqrt{3}\sqrt{27\xi_0^2 - 4\xi_1^3} + 9\xi_0}}{\sqrt[3]{2}3^{2/3}} \tag{3.1}$$

The other two eigenvalues contained imaginary values and therefore were not considered.

In the context of tick-borne infectious diseases, the next-generation matrix gives the size of the next generation distributed over the different categories given in the present generation. Thus, if the generation grow in size, this translates as an increase in infected numbers for all categories [1, 2, 4]. R_0 values obtained from this calculation are shown in Figure 3.1A. All parameters were obtained from a previously published work of the transmission dynamics of the Brazilian Spotted Fever [16].

In a second approach, considering larvae population, let infected capybaras be of category 0, infected attached nymphs be of category 1, infected attached adult ticks be

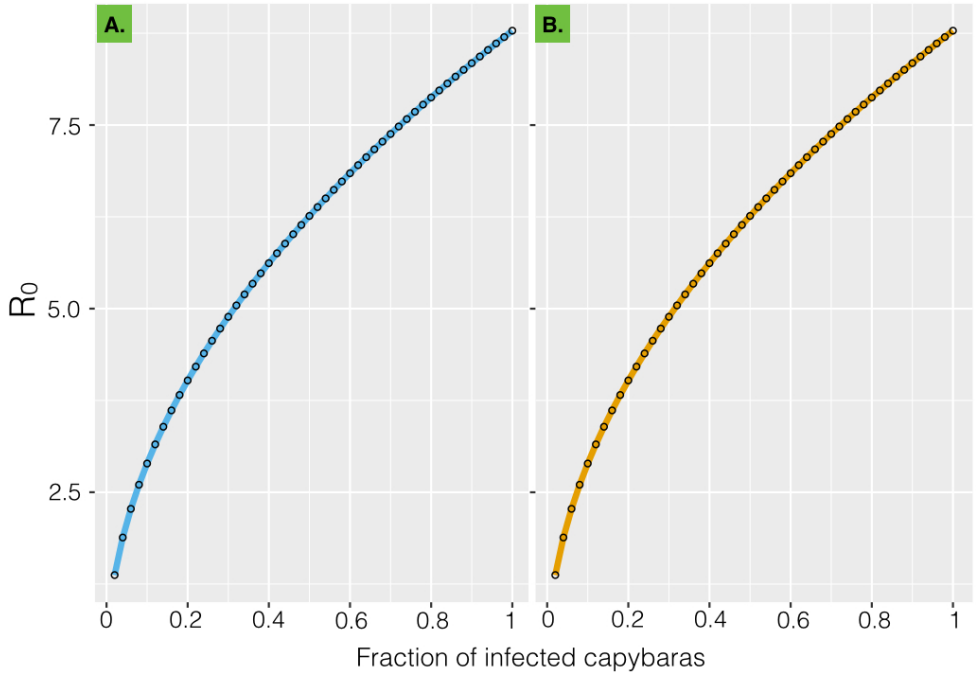

Figure 3.1 - R_0 values for the Brazilian Spotted Fever system for different fractions of infected capybaras, disregarding (A) and considering (B) infected attached larvae population. As observed, in both cases R_0 is very close. This demonstrates a low impact of the larval population on the maintenance of the disease.

of category 2 and infected attached larvae be of category 3. Thus, $\{X_{ij}; i, j = 0, 1, 2, 3\}$. An infected attached larvae, while feeding, can infect capybaras at rate λ_L. Since $\frac{S_C}{N} \approx 1$ at initial stages. Thus,

$$E[X_{30}] = \lambda_L I_{LA}$$

Additionally, an infected attached larvae generates an infected attached nymph if satisfactorily detach at rate $\theta_{IL}\epsilon_L$ and develop into an infected nymph, which in turn attach to a capybara at rate α_N. Hence,

$$E[X_{31}] = \theta_{IL}\epsilon_L I_{ND}\alpha_N$$

An infected attached larvae can not generate infected attached adults or other infected attached larvae:

$$E[X_{32}] = 0$$
$$E[X_{33}] = 0$$

Infected attached larvae can only be generated by adult infected attached ticks by transovarial transmission. They lay eggs that develop into detached larvae at rate ρ_{II}, which

in turn attach at rate α_L. The ρ_{II} rate considers a transovarial transmission of 42.8%, filial infection rate of 50%, female weight of 372.20 mg, CEI (mg egg mass/mg engorged female $\times$ 100) of 39.55%, 18.8 eggs/1 mg of eggs, and hatching success of 44.2%. Thus,

$$E[X_{23}] = \rho_{II} I_{AA} \alpha_L$$

Infected capybaras and infected attached nymphs can not generate infected attached larvae. Hence,

$$E[X_{03}] = 0$$
$$E[X_{13}] = 0$$

Thus, now let $\mathbf{E} = \{m_{ij}\}_{i,j=0}^{2}$ be the expectation matrix:

$$\begin{bmatrix} 0 & \beta_{L_\eta}\theta_{SL}\epsilon_L S_{LA}\alpha_N & \beta_{N_\eta}\theta_{SN}\epsilon_N S_{NA}\alpha_A & 0 \\ \lambda_N I_{NA} & 0 & \theta_{IN}\epsilon_N I_{NA}\alpha_A & 0 \\ \lambda_A I_{AA} & 0 & 0 & \rho_{II} I_{AA}\alpha_L \\ \lambda_L I_{LA} & \theta_{IL}\epsilon_L I_{ND}\alpha_N & 0 & 0 \end{bmatrix}$$

where $\beta_L\eta = \beta_L * \frac{IC}{N}$ and $\beta_N\eta = \beta_N * \frac{IC}{N}$. The eigenvalues are obtain from $\mathbf{E} - \zeta I_{n4} = 0$. Then, in this second approach, the characteristic polynomial of $\mathbf{E}$ is given by:

$$f'(\zeta) = \zeta^4 + \zeta^2\xi_2' - \zeta\xi_1' - \xi_0'$$

where,

$$\begin{aligned} \xi_2' &= \beta_L \frac{IC}{N}\theta_{SL}\epsilon_L S_{LA}\alpha_N\lambda_N I_{NA} \\ &\quad + \beta_N \frac{IC}{N}\theta_{SN}\epsilon_N S_{NA}\alpha_A\lambda_A I_{AA} \\ \xi_1' &= \beta_L \frac{IC}{N}\theta_{SL}\epsilon_L S_{LA}\alpha_N\theta_{IN}\epsilon_N I_{NA}\alpha_A\lambda_A I_{AA} \\ &\quad + \beta_N \frac{IC}{N}\theta_{SN}\epsilon_N S_{NA}\alpha_A\rho_{II} I_{AA}\alpha_L\lambda_L I_{LA} \\ &\quad + \theta_{IN}\epsilon_N I_{NA}\alpha_A\rho_{II} I_{AA}\alpha_L\theta_{IL}\epsilon_L I_{ND}\alpha_N \end{aligned}$$

and,

$$\xi_0' = \beta_L \frac{IC}{N} \theta_{SL} \epsilon_L S_{LA} \alpha_N \theta_{IN} \epsilon_N I_{NA} \alpha_A \rho_{II} I_{AA} \alpha_L \lambda_L I_{LA} + \beta_N \frac{IC}{N} \theta_{SN} \epsilon_N S_{NA} \alpha_A \lambda_N I_{NA} \rho_{II} I_{AA} \alpha_L \theta_{IL} \epsilon_L I_{ND} \alpha_N$$

The resultant expression for R_0 is also given by the dominant eigenvalue of the new matrix $\mathbf{E}$. R_0 values obtained from this second approach for different fractions of infected capybaras are shown in Figure 3.1B. As observed, in both cases R_0 is very close, which demonstrates a low impact of the matrix elements $E[X_{23}]$, $E[X_{30}]$ and $E[X_{31}]$ in the maintenance of the disease. These matrix elements corresponds to the transovarial transmission from adult ticks, the transmission of the disease from infected attached larvae to capybaras and the transstadial perpetuation of the disease from infected larvae to attached nymphs, respectively.

3.4 Sensitivity and elasticity analysis

Sensitivity and elasticity analyses were performed to quantify absolute and proportional perturbations of each matrix element to the R_0, calculated by obtaining the dominant eigenvalue in each of the approaches. Sensitivity and elasticity analyses are powerful tools to systematically quantify how projection results depend on individual parameters[10]. These calculations were performed using the R statistical package "popbio" [17]. This package consists on a R translation of the Matlab code for the analysis of projection matrix models described in Matrix Population Models by Caswell, 2001 [10].

To evaluated the effects of absolute perturbations, we calculated the sensitivity of the R_0 to changes in the projection matrix elements $E[X_{ij}]$ for the two previous approaches, which respectively disregard and consider infected attached larvae populations. Considering that R_0 is a function of $E[X_{ij}]$, we define the sensitivity of R_0 to changes in $E[X_{ij}]$ as:

$$\mathbf{S} = \frac{\partial R_0}{\partial_{E[X_{ij}]}}$$

The sensitivity gives the effect on R_0 of changes in any entry of $\mathbf{E}$, including those that may be regarded as fixed at zero [10]. As shown in Figure 3.2, in both approaches, it can be noted that R_0 is more sensitive to changes in the matrix elements $E[X_{01}]$, $E[X_{02}]$ and $E[X_{12}]$, which correspond to the number of infected attached nymphs and adults generated by an infected capybara, and with the number of infected adult ticks produced by an infected attached nymph. Additionally although cofeeding was considered 0, if the matrix elements $E[X_{11}]$ and $E[X_{22}]$ and $E[X_{22}]$, change by a small amount $\delta_{E[X_{ij}]}$, the

resulting change in R_0 would be approximately $0.40\delta_{E[X_{11}]}$, 0.15 $\delta_{E[X_{22}]}$, and 0.15 $\delta_{E[X_{32}]}$, respectively. This information may be interesting for future studies concerned with this kind of transmission.

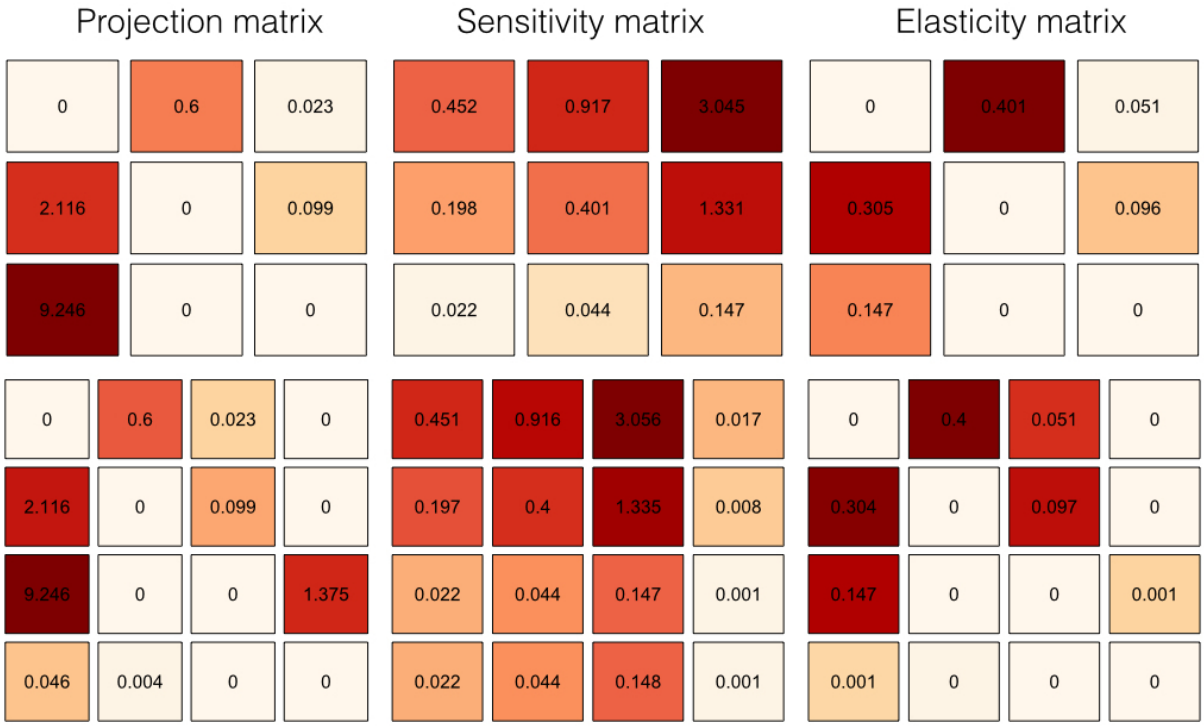

Figure 3.2 - Projection, sensitivity and elasticity matrices disregarding (top) and considering (bottom) infected larvae population.

Additionally, to evaluate the proportional response of R_0 to proportional perturbations, we performed an elasticity analysis. We estimated the elasticity of R_0 with respect to $E[X_{ij}]$ defined as:

$$\mathbf{T} = \frac{E[X_{ij}]}{R_0} \frac{\partial R_0}{\partial_{E[X_{ij}]}}$$

The elasticities of R_0 with respect to $E[X_{ij}]$ are interpreted as the contributions of each $E[X_{ij}]$ to R_0. For projection matrices, this has led to their interpretation as the relative contribution to population growth from the respective transition in the life cycle [18]. If a matrix entry is 0, the corresponding element elasticity is 0. This relies o the demonstration that the elasticities of R_0 with respect to $E[X_{ij}]$ always sum 1 [18]. Thus,

$$\sum_{ij} e_{ij} = \sum_{ij} \frac{E[X_{ij}]}{R_0} \frac{\partial R_0}{\partial_{E[X_{ij}]}} = 1$$

Hence, e_{ij} can be interpreted as the proportional contribution of $E[X_{ij}]$ to R_0.

Figure 3.2 shows the elasticities of R_0 to changes in the element matrix of our two

approximations. The elasticities of the three matrix elements $E[X_{01}]$, $E[X_{10}]$ and $E[X_{20}]$ sum approximately 85.3%. Accordingly, the elements corresponding to the number of infected attached nymphs produced by an infected capybara and with the number of infected capybaras produced by infected attached nymphs and adult ticks are the major contributors to changes in the R_0 in the Brazilian Spotted Fever System.

3.5 Conclusion

We derive an expression of the R_0 for the Brazilian Spotted Fever system on the basis of the next generation matrix approach. Through sensitivity and elasticity analysis, it was noted that the elements corresponding to the number of infected attached nymphs and adult ticks produced by an infected capybara and vice versa, and the number of infected adult ticks produced by an infected attached nymphs were the major contributors to changes in the R_0 in the Brazilian Spotted Fever system. This results provide a better understanding of the Brazilian Spotted Fever dynamics and potentially will support the planning of preventive strategies for this disease in South America.

Acknowledgments

The authors would like to thank São Paulo Research Foundation (FAPESP) for the financial support. Grants: 2016/01913-8 and 2014/12213-1 to GP, and 2013/18046-7 to MBL. We also thank Coordenação de Aperfeiçoamento de Pessoal de Nível Superior-CAPES/PROEX 2327/2015.

Bibliography

[1] Diekmann O, Heesterbeek J, Metz J. On the definition and computation of the basic reproduction ratio R0 in models for infectious diseases in heterogeneous populations. J. Math. Biol.1990.28:365–82.

[2] Diekmann O, Heesterbeek J. Mathematical Epidemiology of Infectious Diseases: Model Analysis and Interpretation. Wiley, New York. 2000.

[3] Diekmann O, Heesterbeek J, Britton T. Mathematical Tools for Understanding Infectious Disease Dynamics. Princeton University Press. 2013.

[4] Hartemink N, Randolph S, Davis S, Heesterbeek J. The basic reproduction number for complex disease systems: defining R(0) for tick-borne infections. The American

Naturalist. 2008.171(6):743-54.

[5] Randolph, S. E. Ticks are not insects: consequences of contrasting vector biology for transmission potential. Parasitology Today.1998. 14:186–192.

[6] Randolph S, Miklisova D, Lysy J, Rogers D, Labuda M. Incidence from coincidence: patterns of tick infestations on rodents facilitate transmission of tick-borne encephalitis virus. Parasitology.1999. 118:177–186.

[7] Caraco T, Glavanakov S, Chen G, Flaherty J, Ohsumi T, Szymanski B. Stage-structured infection transmission and a spatial epidemic: a model for Lyme disease. American Naturalist. 2002. 160:348–359.

[8] Norman R, Bowers R, Begon M, Hudson P. Persistence of tick-borne virus in the presence of multiple host species: tick reservoirs and parasite mediated competition Journal of Theoretical Biology. 1999. 200:111–118.

[9] Foppa I. The basic reproductive number of tick-borne encephalitis virus. Journal of Mathematical Biology. 2005. 51:616–628.

[10] Caswell H. Matrix Population Models: Construction, Analysis and Interpretation. Second Edition Sinauer Assoc., Inc. Publishers. Sunderland, Massachusetts. 2001.

[11] Nava S, Beati L, Labruna M, Caceres A, Mangold A, Guglielmone A. Reassessment of the taxonomic status of *Amblyomma cajennense* (Fabricius, 1787) with the description of three new species, *Amblyomma tonelliae* n. sp., *Amblyomma interandinum* n. sp. and *Amblyomma patinoi* n. sp., and reinstatement of *Amblyomma mixtum* Koch, 1844, and *Amblyomma sculptum* Berlese, 1888 (Ixodida: Ixodidae). Ticks and Tick-borne Diseases. 2014;(5):252–276.

[12] Niebylski ML, Peacock MG, Schwan TG. Lethal effect of *Rickettsia rickettsii* on its tick vector (Dermacentor andersoni) Applied and Environmental Microbiology. 1999 Feb;65(2):773–778.

[13] Soares JF, Soares HS, Barbieri AM, Labruna MB. Experimental infection of the tick *Amblyomma cajennense*, Cayenne tick, with *Rickettsia rickettsii*, the agent of Rocky Mountain spotted fever. Medical and Veterinary Entomology. 2012;26(2):139–151.

[14] Krawczak FS, Nieri-bastos FA, Nunes FP, Soares J, Moraes-filho J. Rickettsial infection in *Amblyomma cajennense* ticks and capybaras (*Hydrochoerus hydrochaeris*) in a Brazilian spotted fever-endemic area. Parasites and Vectors.2014;7:1–7.

[15] Souza CE, Moraes-Filho J, Ogrzewalska M, Uchoa FC, Horta MC, Souza SSL, et al. Experimental infection of capybaras *Hydrochoerus hydrochaeris* by *Rickettsia rickettsii* and evaluation of the transmission of the infection to ticks *Amblyomma cajennense* Veterinary Parasitology. 2009;161(1):116–121.

[16] Polo G, Mera Acosta C, Labruna M, Ferreira F. Transmission dynamics and control of *Rickettsia rickettsii* in populations of *Hydrochoerus hydrochaeris* and *Amblyomma sculptum* PLoS Neglected Tropical Diseases. 2017. 11(6):e0005613

[17] Stubben C, Milligan B. Estimating and Analyzing Demographic Models Using the popbio Package in R Journal of Statistical Software. 2007. 22:11.

[18] de Kroon H, Plaisier A, van Groenendael J, Caswell H. Elasticity: the relative contribution of demographic parameters to population growth rate. Ecology. 1986. 67:1427-1431.

4. Satellite hyperspectral imagery to support tick-borne infectious diseases surveillance

Abstract

This study proposed the use of satellite hyperspectral imagery to support tick-borne infectious diseases surveillance based on monitoring the variation in amplifier hosts food sources. To verify this strategy, we used the data of the human rickettsiosis occurrences in southeastern Brazil, region in which the emergence of this disease is associated with the rising capybara population. Spatio-temporal analysis based on Monte Carlo simulations was used to identify risk areas of human rickettsiosis and hyperspectral moderate-resolution imagery was used to identify the increment and expansion of sugarcane crops, main food source of capybaras. In general, a pixel abundance associated with increment of sugarcane crops was detected in risk areas of human rickettsiosis. Thus, the hypothesis that there is a spatio-temporal relationship between the occurrence of human rickettsiosis and the sugarcane crops increment was verified. Therefore, due to the difficulty of monitoring locally the distribution of infectious agents, vectors and animal host's, satellite hyperspectral imagery can be used as a complementary tool for the surveillance of tick-borne infectious diseases and potentially of other vector-borne diseases.

4.1 Introduction

Active disease surveillance, which involves searching for evidence of disease through routine and monitoring in endemic areas, could help prevent an outbreak, or slow transmission at an earlier stage of an epidemic [1]. Recently, due to the spatial expansion of emerging vector-borne diseases and the difficulty to monitor locally the presence of infectious agents, their vectors and their hosts, epidemiologists are adopting new remote sensing techniques to predict vector habitats based on the identification, characterization and management of environmental variables such as temperature, humidity and land cover type [1, 2]. Based on this strategy, satellite imagery such as those from Advanced Spaceborne Thermal Emission and Reflection Radiometer (ASTER), Landsat, Moderate Resolution Imaging Spectroradiometer (MODIS), and Advanced Very High Resolution Radiometer (AVHRR), have been used to propose preventive strategies for mosquito-borne diseases [3, 4, 5, 6, 7]. Ticks are obligatory parasites of vertebrate hosts and

depending on their hosts for movement over large distances. Consequently, tick-borne infectious diseases can be spread over geographical areas by the movement of tick hosts carrying either infected ticks or transmitting diseases to susceptible ticks in neighboring locations. In this paper we proposed the use of satellite imagery to support tick-borne infectious diseases surveillance based on the expansion of amplifier host's food sources.

Rickettsia rickettsii is the etiological agent of the most severe form of rickettsiosis, referred to as Brazilian spotted fever (BSF) in Brazil. The disease also occurs in the United States, Mexico, Costa Rica, Panama, Colombia, and Argentina. In South America, the tick *Amblyomma sculptum* is the main vector, but other tick species, such as *Rhipicephalus sanguineus* and *Amblyomma aureolatum*, are also involved in more restricted areas [8]. *R. rickettsii* is partially pathogenic to ticks so the infection rate drops in the tick population with each tick generation [9]. Furthermore, less than 50% of *A. sculptum* maintain transovarial and transestadial infections and are unable to keep the infection by *R. rickettsii* efficiently in successive generations [10]. Thus the participation of amplifier hosts for the maintenance of the bacteria becomes essential to guarantee a constant development of new generations of infected ticks [9, 11]. In South America, it was recently found that the capybara *Hydrochoerus hydrochaeris* acts as the amplifier host of *R. rickettsii* infection for the tick *A. sculptum*. [12, 13]. Once infected, the capybara keeps the *R. rickettsii* in the bloodstream for 7 to 10 days, when the infection of susceptible ticks that feed on it may occur [13], generating new cohorts of infected ticks. In addition capybaras are prolific, producing a mean of six pups per female per year [14], generating a constant introduction of susceptible animals. In North America, where *Dermacentor* spp. ticks are main vectors of *R. rickettsii*, several small rodent species such *Microtus pennsylvanicus*, *Microtus pinetorum*, *Peromyscus leucopus* and *Sigmodon hispidus* can also maintained the *R. rickettsii* infection between ticks [15].

In Brazil, there may be a causal relationship between the rising capybara population and the re-emergence of the disease, since both capybara populations and the number of BSF occurrences have increased significantly over the last three decades [1, 16]. Between the years 1989 and 2008, there were recorded 737 cases of Brazilian spotted fever with laboratory confirmation, of which 80.2% were in the southeastern region with a lethality of 31.4% [16]. In the state of São Paulo, southeastern Brazil, there were 555 confirmed cases between the years 1985 - 2012, with a lethality of 40.5% [17]. Additionally, in endemic areas for BSF in the state of São Paulo, population densities of capybaras have reached numbers up to 40 times higher than those recorded in natural environments such as the Amazon and Pantanal [18]. In this region, the constant availability of water resources (S1 Fig.)4.4, is essential for establishment of capybara populations, since this is a semiaquatic vertebrate species that depends on water source for thermic regulation, reproduction (capybaras mate only in water), and predator protection [19]. On the other hand, the

increase of capybara populations in these areas should depend primarily on availability of food sources, as typically known for rodents such as capybaras [19]. Sugar cane is well known as one of the most appreciated food by capybaras, and the economic impact of capybara on damage to sugarcane crops is a reality in the state of São Paulo [20]. In the state of São Paulo, sugar cane is indeed the most common farming [21, 22]. Because sugar cane farming occurs throughout the year, regardless of season, it represents the main food source for capybaras in many areas [18]. Thereby, the increase in the availability of food sources, near watercourses, increases the habitat carrying capacity for capybaras, resulting in population growth of susceptible animals. The carrying capacity represents the maximum number of individuals that the environment can sustain indefinitely given the availability of vital resources (i.e. water, food, habitat) [23]. This in turn could modulate the transmission of diseases carried by these animals.

Among *A. sculptum* populations that are sustained by capybara hosts, it has been proposed that the maintenance of *R. rickettsii* depends primarily on a constant introduction of susceptible animals (i.e., newborn capybaras), which will act as amplifier hosts and will guarantee the constant creation of new cohorts of infected ticks [8, 11, 10]. Hence, the approach adopted in this paper is based on the premise that the expansion of cultivated sugarcane areas would translate into an increase of the population density of capybaras (i.e., higher reproduction index), and consequently on the higher exposure of humans to *R. rickettsii*-infected ticks (i.e., higher number of BSF cases). In this way, to support the BSF surveillance, we suggest a methodology based on the spatio-temporal monitoring of the increment and expansion of sugarcane crops, main food source for capybaras in the state of São Paulo, southeastern Brazil.

4.2 Materials and methods

Study area

To verify if is possible to anticipate the occurrence of tick-borne infectious diseases using the satellite hyperspectral methodology proposed, which is based on monitoring the variation in amplifier hosts food sources, we used the data of the BSF occurrences in the state of São Paulo, southeastern Brazil, region in which the emergence of this disease is associated with the rising capybara population. This study area located at coordinates 19°44' S to 24°28' S 44 °05' W to 53°31' W, covering an area of 248 808 km^2. With 43,663,669 inhabitants and 625 territorial divisions, São Paulo is the most populous state of Brazil. The topography is characterized largely as a plateau (90%), with altitudes that vary from 300 m to 900 m. The region has a tropical climate, with a hot and humid

summer (October to February) and dry winter (June to August).

Brazilian spotted fever occurrence

Data collection

The occurrence of Brazilian spotted fever in the state of São Paulo from 2000 to 2012 were obtained from the web site of the São Paulo State Center of Epidemiological Surveillance [24]. We considered only the BSF cases that occurred in areas of transmission by *A. sculptum*, as previously determined [25]. The human population of each São Paulo territorial division was obtained from the website of the Brazilian Institute of Geography and Statistics [26].

Retrospective Spatial analysis

A retrospective high rate spatio-temporal statistic based on a discrete Poisson distribution, implemented in a software SaTScan, was used for the identification of spatial clusters and risk areas for BSF occurrence. This method produced a set of clusters, the relative risk in the different clusters, and a corresponding $p-$value for each cluster based on Monte-Carlo simulations.

The statistic uses a circular window of variable radius that moves across the map. For each circle a likelihood ratio statistic is computed based on the number of observed and expected cases within and outside the circle and compared with the likelihood, L_0 [27]. We used a likelihood function under the alternative hypothesis assuming Poisson distributed cases proportional to:

$$\left(\frac{\gamma}{E(\gamma)}\right)^{\gamma}\left(\frac{N-\gamma}{N-E(\gamma)}\right)^{N-\gamma} I() \tag{4.1}$$

where γ and $E(\gamma)$ represent the observed and expected number of cases in a circle and $N-\gamma$ and $N-E(\gamma)$ the observed and expected number of cases outside the circle. N is the total number of cases. The indicator function $I()$ is equal to 1 if the observed number of cases within the circle is larger than the expected number of cases given the null hypothesis and 0 otherwise [27]. The circles with the highest likelihood ratio values are identified as potential clusters. An associated p-value, based on 999 Monte Carlo simulations, was computed and used to evaluate whether the cases are randomly distributed in space or otherwise. We included only primary clusters, as long as their corresponding p-values

were less than 0.05.

Hyperspectral / multitemporal analysis

Satellite imagery obtaining

To detect increment and expansion of sugarcane crops we used time series from the Enhanced Vegetation Index (EVI) for the entire state of São Paulo from 2000 to 2012. The EVI imagery were obtained from the Moderate Resolution Imaging Spectroradiometer (MODIS) sensor on board the Terra satellite of the National Aeronautics and Space Administration (NASA) [28]. The gathered images from MODIS, including 176 spectral bands with 250m (red, near-infrared), 500m (mid-infrared) and 1000m (thermal infrared) spatial resolutions. The vegetation spectrum typically absorbs in the red and blue wavelengths, reflects in the green wavelength, strongly reflects in the near infrared wavelength, and displays strong absorption features in wavelengths where atmospheric water is present[29, 30]. These hyperspectral images spans the time period from 2000 to 2012 in 16 day increments. To prepare the images for the analysis, we created a mask to disregard screen brightness values equal to 0 and 255 to rule out specific areas, such as water, in our analyses. All procedures using satellite images were executed using the software ENVI 5.2.

Principal component analysis

The principal component analysis was used to transform the original hyperspectral image data, highly correlated, into a new set of uncorrelated variables called principal components. By rotating the coordinate system to align with orthogonal dimensions of uncorrelated variance, any location-specific pixel time series P_{xt} contained in a N image time series can be represented as a linear combination of temporal patterns, F, and their location-specific components, C, as:

$$P_{xt} = \sum_{i=1}^{N} C_{ix} F_{it} \tag{4.2}$$

where C_{ix} is the spatial Principal Component (PC), F_{it} is the corresponding temporal Empirical Orthogonal Function (EOF) and i is the dimension [31, 32, 33, 34, 35]. The EOF's are the eigenvectors of the covariance matrix that represent uncorrelated temporal patterns of variability within the data [31]. Thus, the principal components can be

determined by computing the eigenvectors and eigenvalues of the covariance matrix.

Linear spectral unmixing analysis

The relative abundance of sugarcane crops was depicted in the hyperspectral imagery based on the endmembers spectral characteristics, using linear spectral unmixing. Endmembers are a collection of constituent spectra corresponding to distinct ground substances [36]. Each location-specific (x) pixel P_{xt} in an N image time series can be represented as a linear combination of D' temporal endmembers, E_{it}, and a residual component, ε, as:

$$P_{xt} = \sum_{i=1}^{D'} f_{ix} E_{it} + \varepsilon \tag{4.3}$$

where the pixel-specific fractions f_{ix} may represent either the areal fraction of the pixel exhibiting the temporal pattern of the corresponding endmember, or more generally, the Euclidean proximity of that pixel to the corresponding endmember in the temporal feature space. In a temporal unmixing model, each pixel is the linear combination of different temporal endmembers and corresponding fractions [31]. The result is a set of fraction maps representing the spatial distribution of different endmember abundances so, the pixel values indicate the fraction of the pixel that contains the endmember material corresponding to that image.

4.3 Results

The distribution of BSF cases in areas of transmission by *A. sculptum* and the São Paulo population density are shown in Fig. 4.1. In São Paulo, from 2000 to 2012 there were reported 386 cases of BSF with an incidence of 0.4 year^{-1} for each 100 000 persons. The retrospective space-time analysis scanning for clusters with high rates using the discrete Poisson model and 999 Monte Carlo simulations detected four spatio-temporal clusters ($p<0.05$) demarcated in two periods: 2000 to 2006 and 2007 to 2012 as shown in Fig. 4.1. Because of these two temporal clusters found, all following analysis will be presented considering these two periods. Respectively, the number of cases were 178 and 208. The relative risk of the spatial cluster concerning the first period was 8.54 and the relative risk of the three spatial clusters concerning the second period were 1.64, 3.44 and 9.39 as is also shown in Fig. 4.1.

Using principal component analysis, we quantify the spectral dimensionality of the global composite and render the mixing space to select the endmembers. The eigenvalues

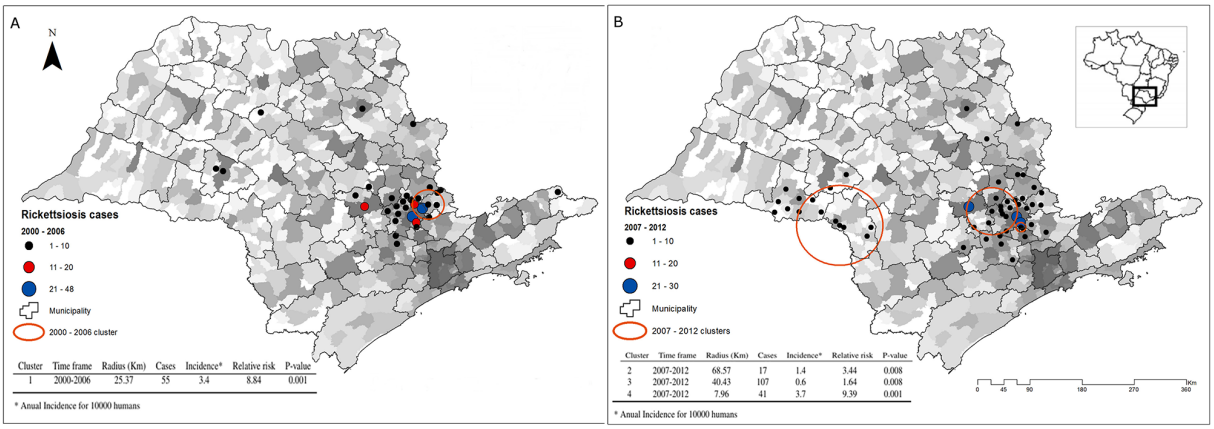

Figure 4.1 - Population density and Rickettsiosis occurrence in areas of transmission by *Amblyomma sculptum* in the state of São Paulo. High population density is represented with a higher gray tone and low population density with a lower gray tone. (A) Cases reported and cluster detected from 2000 to 2006. (B) Cases reported and clusters detected from 2007 to 2012. (Polo et al., 2015)

that derive the amount of variation accounted by each principal component within the feature space, show that nearly 95% of the information within this feature space was found in the first six principal components (66.3% in channel 1, 11.9% in channel 2, 6.3% in channel 3, 4.4% in channel 4, 3.4% in channel 5, 2.4% in channel 6) and for this reason the following analysis considers only the first six principal components. After rendering the mixing space from the six low order principal components we identify three endmembers corresponding to Atlantic vegetation, sugarcane crops and substrates. Substrates includes rock, sediment, soil and non-photosynthetic vegetation and in the case of São Paulo some rivers are also detected as substrates due to the high contamination of water sources. The first four principal components have an annual or biannual frequency change that represents the main vegetation phenology changes over the area. In contrast, the other principal components exhibit poorly expressed annual frequency variability because the corresponding phases stem from noise or substrate, or only represent phenology in small areas. S2 Fig. is shown the spectral reflectance information for each endmember selected through the study period. It is shown that the Atlantic vegetation is characterized by an annual cycle, the crop-vegetation by a biannual cycle and the substrate by a poorly annual frequency variability.

Fig. 4.2 represents the pixel abundance of the endmembers selected from the state of São Paulo, using the linear unmixing model. The linear unmixing model yields per pixel endmember fractions which can be interpreted as quantitative estimates of the areal abundance of the specific endmembers (Atlantic vegetation, sugarcane crops and substrates) contributing to the mixed pixel. Thus, in Fig. 4.2 each pixel obtain information of the single mixing fraction that minimize the summed square of the mismatch for all bands using the least square solution. In general, the biannual cycle endmember abundance

consistent with sugarcane crops, represented in red, is detected in the cluster areas for rickettsiosis occurrence in both periods. S3 Fig. is shown the error map correspondent for each period obtain from the Root Mean Square (RMS) difference between the observed and modeled mixtures. The RMS was used to quantify model misfit and the effects of endmember variability. The RSM mean value for the pixels was 0.318. Black colors indicate that the endmembers chosen for the analysis are well characterized and correspond with the most surface of the state of São Paulo and white colors represent misfit values. Low RMS misfit supports the statistical validity of the linear mixing model but does not guarantee accurate or physically meaningful results. Thus, we verify and confirm the geographical pattern of the sugarcane endmember obtained from joint principal component and linear spectral unmixing analysis with the information of the distribution and expansion of sugarcane crops from previous studies from the state of São Paulo [21, 22] and from the Canasat-Area Project of the Brazilian National Institute for Space Research [37], which mapping the sugarcane distribution of the state of São Paulo once a year using remote sensing imagery acquired by the Landsat, CBERS and Resourcesat-I satellites [37].

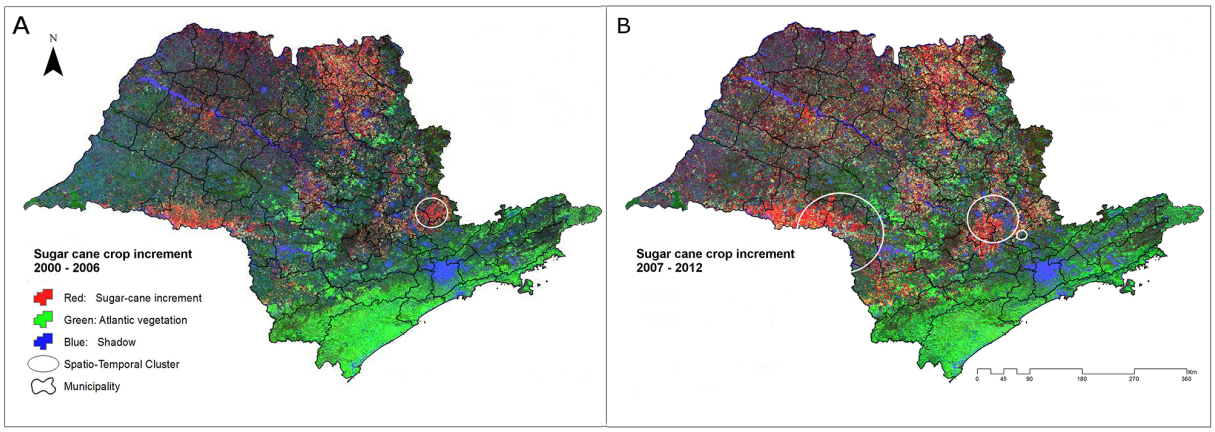

Figure 4.2 - Linear unmixing model result showing the pixel abundance of the endmembers selected from the state of São Paulo. (A) 2000 - 2006. (B) 2007 - 2012. Atlantic vegetation is represented in green, sugarcane crops in red and substrates in the blue channel.

To verify if the increment of the sugarcane crops was associated with the presence of BSF, the pixel abundance mean values were compared in the four risk areas for BSF occurrence between both periods. Fig. 4.3 shows the sugarcane crops pixel abundance difference between the 2007 - 2012 and 2000 - 2006 periods. To confirm this difference, the sugarcane crops pixel abundance mean values of the clusters was compared between the 2000 - 2006 and the 2007 - 2012 periods. It was found that the sugarcane crops pixel abundance mean (124.37) of the three clusters detected from 2007 to 2012 was higher than the pixel abundance mean (88.16) of this zones from 2000 to 2006 ($p < 0.05$). The sugarcane crops pixel abundance mean (136.81) of the cluster detected from 2000 to 2006 was higher than the sugarcane crops pixel abundance mean (120.13) of this zone from

2007 to 2012, nevertheless this difference was not statistically significant. Consistently, the sugarcane crops pixel abundance mean was 1.4 times higher in the risk zones for BSF occurrence. This indicate that the increment and expansion of sugarcane crops coincide with BSF risk areas. Nevertheless, the reduction of the sugarcane crops not necessarily corresponds with the disappearance of a BSF risk zones.

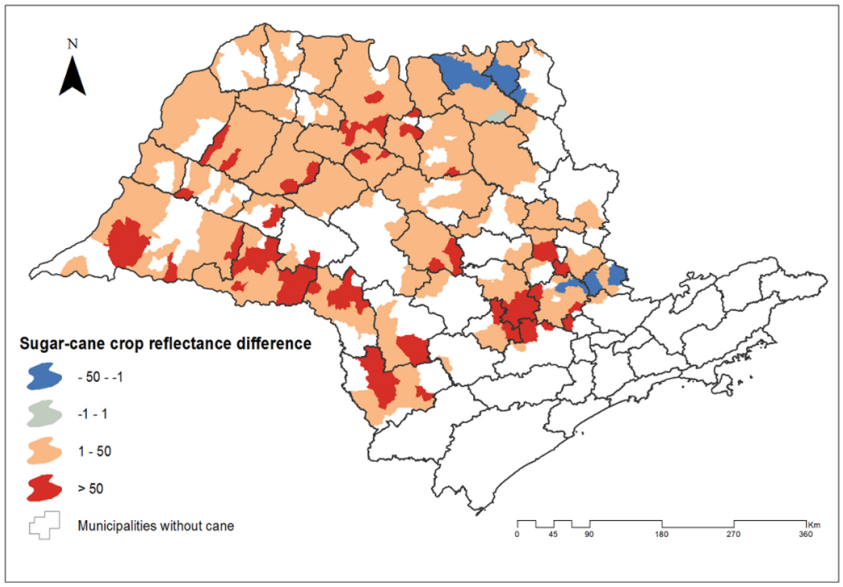

Figure 4.3 - Sugarcane crops pixel abundance difference between the 2007 - 2012 and 2000 - 2006 periods. Negative (blue) values indicate that the pixel abundance was higher at 2000 - 2006 period and positive (red) values indicate that the pixel abundance value was higher at the 2007 - 2012 period.

4.4 Discussion

Spatial epidemiology aims to investigate the spatial distribution of diseases in order to identify risk areas, determine ecological risk factors for disease transmission and strategically guide disease control actions [38, 39]. In our study, four significant high-risk regions for BSF were identified by the spatio-temporal scan statistic approach for two delimited time periods: 2000 to 2006 and 2007 to 2012. The circular scan statistic used in this study has been proved to be useful for many studies [40, 41, 42, 43]. Gaudart et al (2005) compared the oblique decision tree model, a complex statistical technique with the Kulldorff's SaTScan cluster technique, which was used in this study. They produced similar results using both methods in a village in West Africa to identify malaria risk clusters [43]. The circular isotopic technique of the Kulldorff's SaTScan makes it a useful tool to detect clusters but has limitations when detecting irregular shaped clusters due to its fixed scan window [44, 45].

The suitability of an area for vector-borne disease transmission depends on environmental variables such as temperature, humidity and land cover type. Because these factors can be monitored using remote sensing, it is possible to construct models that predict regions and periods favorable for the presence of the vectors, their hosts and the diseases carried by these. In addition to satellite-derived climate variables, many recent epidemiological studies have made use of the link between vegetation amount and vector populations via the application of normalized difference vegetation index (NDVI) imagery [46]. Due to the essential involvement of the capybaras in the BSF transmission, we used the MODIS enhanced vegetation index (EVI), which offers improvements over the NDVI, to identify sugarcane crops increment and subsequently link this increment with the occurrence of BSF, since we rely on the premisse that higher food availability increases capybara reproduction index, and consequently, higher number of *R. rickettsii*-infected ticks [8, 11, 10]. Many remote sensing approaches have been developed to identify cropping practices, such as crop type and cropping intensity, across large spatial and temporal scales [47, 48, 49, 50]. Studies have used mainly Landsat data to assess crop type and cropping intensity. However, the accuracy of the Landsat method depends on several different factors such Landsat image availability for the appropriate time period during crop growth cycles [51]. The low temporal resolution of Landsat and its susceptibility to missing values, and the coverage required to assess crop type and cropping intensity is not assured in most agricultural regions, particularly in the tropics where there are often periods of intense cloud covering [52]. High-temporal resolution data from MODIS are of great relevance for modeling the transmission of vector-borne disease since they fill these gaps and allow an assessment of vector and disease distribution and their potential spread.

Studies have been conducted with remote sensing to identify landscapes linked to a higher risk of emerging vector-borne diseases [53, 54]. These studies showed that many factors influence the distribution of ticks and tick-borne diseases, including changes in human activities, biotopes, animal abundance and animal distribution. Therefore, to identify populations, regions or periods at risk for tick-borne diseases, forecasting models must account for many parameters [55]. We demonstrated that areas of BSF occurrence matched significantly with the areas of increment of sugarcane crops, main food source for capybaras, amplifier host for *R. rickettsii*. In the state of São Paulo, this single parameter remains constant throughout the year and because of this we do not considered other external factors. In the United States a reduction in the biodiversity due to deforestation and forest fragmentation lead to an increase in the density of white-tailed deer and white-footed mouse and their attendant ticks, leading to the emergence of Lyme disease over the last several decades [4, 6, 56, 57, 58].

Our study shows that it is possible to detect high-risk areas for BSF through hyper-

spectral satellite imagery. We suggest that such analyses will be beneficial by enabling surveillance strategies to be focused on the highest risk regions for BSF. However, several factors need to be considered for these technologies to be routinely adopted for public health management such as, the availability of resources for gathering, processing, and modeling geospatial data, training of personnel on the proper interpretation of results and the continuous availability of remote sensing data in a timely manner [1]. We believe the method could have similar benefits if applied to other vector-borne data collected from other regions and could thus help to improve national surveillance networks for human rickettsiosis.

While our data suggest that the increment in sugarcane crops, observed in Brazil in recent decades had a spatio-temporal relationship with to the occurrence of BSF, our study cannot rule out that other factors that are correlated with the risk of *R rickettsii* infection are also causal for the observed association. Indeed this ecological study does not provide individual-level analysis.

4.5 Conclusion

Our initial hypothesis, that there is a relationship between the sugarcane crops increment and the occurrence of BSF, was objectively reinforced in this paper. In this way, in order to anticipate the occurrence of BSF in the state of São Paulo, we suggest a methodology based on the monitoring of the increment and expansion of sugarcane crops, main food source for the *R. rickettsii* amplifier host. Thus, when facing difficulty in monitoring locally the presence of *R. rickettsii*, their vectors or their hosts, the remote sensing could help to associate the presence of the disease with environmental changes. The methodology proposed can guide epidemiological surveillance programs in hotspot areas.

Acknowledgments

The authors would like to thank Carlos Mera Acosta from Institute of Physics of University of São Paulo for the explanations and the discussions fundamental for the development of the article. The authors also would like to thank Prof. Christopher Small from Lamont-Doherty Earth Observatory of Columbia University since the satellite imagery methodology here described was developed based on his lectures at the University of São Paulo. Finally, we thank Prof. Marcos Amaku and Prof. Francisco Chiaravalotti for their suggested changes to improve the article.

Supporting information

S1 Fig

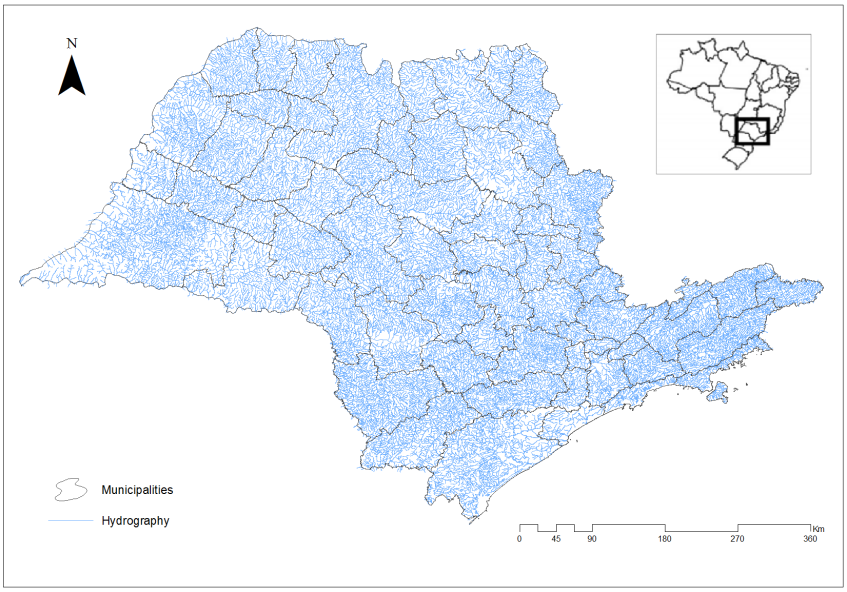

Figure 4.4 - Hydrography of the State of São Paulo. The uniform distribution of water sources is evident throughout the state.

Bibliography

[1] Kalluri S, Gilruth P, Rogers D, Szczur M. Surveillance of Arthropod Vector-Borne Infectious Diseases Using Remote Sensing Techniques: A Review. PLoS Pathogens. 2007 Oct;3(10):e116.

[2] Garni R, Tran A, Guis H, Baldet T, Benallal K, Boubidi S, et al. Remote sensing, land cover changes, and vector-borne diseases: use of high spatial resolution satellite imagery to map the risk of occurrence of cutaneous leishmaniasis in Ghardaia, Algeria. Infection, genetics and evolution : Journal of Molecular Epidemiology and Evolutionary Genetics in Infectious Diseases. 2014 Dec;28:725–734.

[3] Beck LR, Rodriguez MH, Dister SW, Rodriguez AD, Washino RK, Roberts DR, et al. Assessment of a remote sensing-based model for predicting malaria transmission risk in villages of Chiapas, Mexico. The American Journal of Tropical Medicine and Hygiene. 1997 Jan;56(1):99–106.

[4] Estrada-Peña A. Increasing habitat suitability in the United States for the tick that transmits Lyme disease: a remote sensing approach. Environmental Health Perspectives. 2002 Jul;110(7):635–640.

[5] Liu H, Weng Q. Enhancing temporal resolution of satellite imagery for public health studies: A case study of West Nile Virus outbreak in Los Angeles in 2007. Remote Sensing of Environment. 2012 Feb;117(0):57–71.

[6] Allan BF, Keesing F, Ostfeld RS. Effect of Forest Fragmentation on Lyme Disease Risk. Conservation Biology. 2003;17(1):267–272.

[7] Winters AM, Eisen RJ, Lozano-Fuentes S, Moore CG, Pape WJ, Eisen L. Predictive spatial models for risk of West Nile virus exposure in eastern and western Colorado. The American Journal of Tropical Medicine and Hygiene. 2008 Oct;79(4):581–590.

[8] Labruna MB. Ecology of rickettsia in South America. Annals of the New York Academy of Sciences. 2009;1166(1):156–166.

[9] Niebylski ML, Peacock MG, Schwan TG. Lethal Effect of Rickettsia rickettsii on Its Tick Vector (Dermacentor andersoni). Applied and Environmental Microbiology. 1999 Feb;65(2):773–778.

[10] Soares JF, Soares HS, Barbieri AM, Labruna MB. Experimental infection of the tick Amblyomma cajennense, Cayenne tick, with Rickettsia rickettsii, the agent of Rocky Mountain spotted fever. Medical and Veterinary Entomology. 2012;26(2):139–151.

[11] Labruna MB. Brazilian spotted fever: the role of capybaras. In: Capybara. Springer New York; 2013. p. 371–383.

[12] Krawczak FS, Nieri-bastos FA, Nunes FP, Soares JaF, Moraes-filho J. Rickettsial infection in Amblyomma cajennense ticks and capybaras (Hydrochoerus hydrochaeris) in a Brazilian spotted fever-endemic area. Parasites & Vectors. 2014;7:1–7.

[13] Souza CE, Moraes-Filho J, Ogrzewalska M, Uchoa FC, Horta MC, Souza SSL, et al. Experimental infection of capybaras Hydrochoerus hydrochaeris by Rickettsia rickettsii and evaluation of the transmission of the infection to ticks Amblyomma cajennense. Veterinary Parasitology. 2009;161(1):116–121.

[14] Ojasti J. Estudio biológico del chigüire o capibara. Fondo Nacional de Investigaciones Agropecuarias; 1973.

[15] Burgdorfer W. Ecological and epidemiological considerations of Rocky Mountain spotted fever and scrub typhus. Biology of Rickettsial Diseases. 1988;1:33–50.

[16] Del Fiol F, Junqueira F, Miranda C, Maria T, Filho B. A febre maculosa no Brasil. Revista Panamericana de Salud Pública. 2010;27(10):461–466.

[17] Sao-Paulo. Distribuição dos casos confirmados de febre maculosa, segundo municipio de infecção no Estado de São Paulo, 1998 2013. Centro de Vigilância Epidemiológica. Secretaria da Saúde do Estado de São Paulo; 2013.

[18] Ferraz K, De Barros Ferraz S, Moreira J, Couto H, Verdade L. Capybara (Hydrochoerus hydrochaeris) distribution in agroecosystems: a cross-scale habitat analysis. Journal of Biogeography. 2007;34(2):223–230.

[19] Moreira J, Alvarez M, Tarifa T, Pacheco V, Taber A, Tirira D, et al. Taxonomy, Natural History and Distribution of the Capybara. In: Capybara. Springer New York; 2013. p. 3–37.

[20] Felix G, Almeida P, Piovezan U, Garcia R, Lima K, Naas I, et al. Feeding behavior and crop damage caused by capybaras (Hydrochoerus hydrochaeris) in an agricultural landscape. Brazilian Journal of Biology. 2014;74(4):779–786.

[21] Rudorff BFT, de Aguiar DA, da Silva WF, Sugawara LM, Adami M, Moreira MA. Studies on the rapid expansion of sugarcane for ethanol production in Sao Paulo state (Brazil) using Landsat data. Remote Sensing. 2010;2:1057–1076.

[22] Vicente LE, Gomesdaniel D, Victoria DDC, Garçon EAM, Bolf EL, Andrade RG, et al. Séries temporais de NDVI do sensor SPOT Vegetation e algoritmo SAM aplicados ao mapeamento de cana-de-açúcar. Pesquisa Agropecuaria Brasileira. 2012;47(1):1337–1345.

[23] Allman E, Rhodes J. Dynamic Modeling with Difference Equations. In: Mathematical Models in Biology An Introduction. Cambridge University Press; 2004. p. 371–383.

[24] CVE-SES. Centro de Vigilância Epidemiológica. Distribuição dos casos confirmados de Febre Maculosa Brasileira, segundo município de infecção no Estado de São Paulo, 1998 - 2012 . http://wwwcvesaudespgovbr/htm/zoo/fmlpihtm. 2013;.

[25] Pinter A, Franca A, Souza C, Sabbo C, Mendes E, Pereira F, et al. Febre Maculosa Brasileira. BEPA Suplemento. 2011;8:19–24.

[26] IBGE. Brazilian Institute of Geography and Statistics. Censo 2010. Estado de São Paulo. http://downloadsibgegovbr/. 2010;.

[27] Kulldorff M. A spatial scan statistic. Communications in Statistics - Theory and Methods. 1997 Jan;26(6):1481–1496.

[28] NASA. National Aeronautics and Space Administration. Moderate Resolution Imaging Spectroradiometer. http://modisgsfcnasagov/. 2014;.

[29] Thenkabail P, Smith R, De Pauw E. Hyperspectral Vegetation Indices and Their Relationships with Agricultural Crop Characteristics. Remote Sensing of Environment. 2000;71(2):158—-182.

[30] Thenkabail P, Lyon J, Huete A. In: Hyperspectral Remote Sensing of Vegetation. Taylor and Francis Group; 2012. .

[31] Small C. Spatiotemporal dimensionality and Time-Space characterization of multitemporal imagery. Remote Sensing of Environment. 2012 Sep;124:793–809.

[32] Rodarmel C, Shan J. Principal Component Analysis for Hyperspectral Image Classification. Surveying and Land Information Systems. 2002;62(2):115–000.

[33] Green A, Berman M, Switzer P, Craig MD. A transformation for ordering multispectral data in terms of image quality with implications for noise removal. IEEE Transactions on Geoscience and Remote Sensing. 1988;26(1):65–74.

[34] Lee JB, Woodyatt AS, Berman M. Enhancement of high spectral resolution remote-sensing data by a noise-adjusted principal components transform. Geoscience and Remote Sensing, IEEE Transactions on. 1990;28(3):295–304.

[35] Singh A, Harrison A. Standardized principal components. International Journal of Remote Sensing. 1985 Jun;6(6):883–896.

[36] Keshava N, Mustard JF. Spectral unmixing. Signal Processing Magazine, IEEE. 2002;19(1):44–57.

[37] INPE. Instituto de Pesquisas Espaciais. CanaSat: monitoramento da cana-de-açúcar. http://wwwdsrinpebr/laf/canasat/en/). 2013;.

[38] Polo G, Acosta CM, Dias RA. Spatial accessibility to vaccination sites in a campaign against rabies in São Paulo city, Brazil. Preventive Veterinary Medicine. 2013;.

[39] Polo G, Acosta CM, Ferreira F, Dias RA. Location-Allocation and Accessibility Models for Improving the Spatial Planning of Public Health Services. PLoS ONE. 2015 Mar;10(3):e0119190.

[40] Cousens S, Smith PG, Ward H, Everington D, Knight RS, Zeidler M, et al. Geographical distribution of variant Creutzfeldt-Jakob disease in Great Britain, 1994-2000. Lancet. 2001;357(9261):1002–1007.

[41] Fèvre EM, Coleman PG, Odiit M, Magona JW, Welburn SC, Woolhouse MEJ. The origins of a new Trypanosoma brucei rhodesiense sleeping sickness outbreak in eastern Uganda. Lancet. 2001;358(9282):625–628.

[42] Mostashari F, Kulldorff M, Hartman JJ, Miller JR, Kulasekera V. Dead bird clusters as an early warning system for West Nile virus activity. Emerging Infectious Diseases. 2003;9(6):641–646.

[43] Gaudart J, Poudiougou B, Ranque S, Doumbo O. Oblique decision trees for spatial pattern detection: optimal algorithm and application to malaria risk. BMC Medical Research Methodology. 2005;5(1):22.

[44] Aamodt G, Samuelsen SO, Skrondal A. A simulation study of three methods for detecting disease clusters. International Journal of Health Geographics. 2006;5:15.

[45] Patil GP, Taillie C. Geographic and Network Surveillance via Scan Statistics for Critical Area Detection. Statistical Science. 2003;p. 457–465.

[46] Tatem AJ, Noor AM, Hay SI. Defining approaches to settlement mapping for public health management in Kenya using medium spatial resolution satellite imagery. Remote Sensing of Environment. 2004 Oct;93(1-2):42–52.

[47] Jain M, Mondal P, DeFries RS, Small C, Galford GL. Mapping cropping intensity of smallholder farms: A comparison of methods using multiple sensors. Remote Sensing of Environment. 2013 Jul;134(0):210–223.

[48] Biradar CM, Xiao X. Quantifying the area and spatial distribution of double- and triple-cropping croplands in India with multi-temporal MODIS imagery in 2005. International Journal of Remote Sensing. 2011 Feb;32(2):367–386.

[49] Quarmby N, Townshend J, Settle J, White K, Milnes M, Hindle T, et al. Linear mixture modeling applied to AVHRR data for crop area estimation. International Journal of Remote Sensing. 1992 Feb;13(3):415–425.

[50] Xiao X, Boles S, Liu J, Zhuang D, Frolking S, Li C, et al. Mapping paddy rice agriculture in southern China using multi-temporal MODIS images. Remote Sensing of Environment. 2005 Apr;95(4):480–492.

[51] Martínez-Casasnovas JA, Martín-Montero A, Auxiliadora Casterad M. Mapping multi-year cropping patterns in small irrigation districts from time-series analysis of Landsat TM images. European Journal of Agronomy. 2005 Sep;23(2):159–169.

[52] Fang H, Wu B, Liu H, Huang X. Using NOAA AVHRR and Landsat TM to estimate rice area year-by-year. International Journal of Remote Sensing. 1998 Jan;19(3):521–525.

[53] James M, Bowman A, Forbes K, Lewis F, J M, Gilbert L. 37. Environmental determinants of Ixodes ricinus ticks and the incidence of Borrelia burgdorferi sensu lato, the agent of Lyme borreliosis, in Scotland. Parasitology. 2013;140:237—246.

[54] Wolfe N, Daszak P, Kilpatrick M, Burke D. Bushmeat Hunting, Deforestation, and Prediction of Zoonotic Disease. Emerging Infectious Diseases. 2005;11(12):1822–1827.

[55] Lambin E, Tran A, Vanwambeke S, Linard C, Soti V. Pathogenic landscapes: Interactions between land, people, disease vectors, and their animal hosts. International Journal of Health Geographics. 2010;9(1):54.

[56] Glass G, Amerasinghe F, Morgan J, Scott T. Predicting Ixodes scapularis abundance on white-tailed deer using geographic information systems. The American Journal of Tropical Medicince and Hygiene. 1994 Nov;51(5):538–544.

[57] Wood C, Lafferty K. Biodiversity and disease: a synthesis of ecological perspectives on Lyme disease transmission. Trends in Ecology and Evolution. 2013;28:239–247.

[58] Simon JA, Marrotte RR, Desrosiers N, Fiset J, Gaitan J, Gonzalez A, et al. Climate change and habitat fragmentation drive the occurrence of Borrelia burgdorferi, the agent of Lyme disease, at the northeastern limit of its distribution. Evolutionary Applications. 2014;7(7):750–764.

5. Hosts mobility and spatial spread of *Rickettsia rickettsii*

Abstract

There are a huge number of pathogens with multi-component transmission cycles, involving amplifier hosts, vectors or complex pathogen life cycles. These complex systems present challenges in terms of modeling and policy development. The deadliest tick-borne infectious disease in the world, the Brazilian Spotted Fever (BSF), is a relevant example of that. The current increase of human cases of BSF has been associated with the presence and expansion of the capybara *Hydrochoerus hydrochaeris*, amplifier host for the agent *Rickettsia rickettsii* and primary host for the tick vector *Amblyomma sculptum*. We modeled the spatial distribution of capybaras and ticks to gain a better insight into the spatial spread of the *R. rickettsii* and potentially predict future epidemic outcomes. We implemented a reaction-diffusion process in which individuals were divided into classes denoting their state with respect to the disease (SIR). The model considered bidirectional movements between base and destination locations limited by the carrying capacity of the environment. We used the Gillespie algorithm to stochastically solve the proposed model and simulate the impact of potential interventions to impede the spatial spread of the disease. Mobility of capybaras and their attached ticks was significantly influenced by the birth rate of capybaras and therefore, disease propagation velocity was higher in places with higher carrying capacity. Some geographical barriers, generated for example by riparian reforesting, can impede the spatial spread of BSF. The results of this work will allow the formulation of public actions focused on the prevention of BSF human cases.

5.1 Introduction

Stochastic epidemic models have been used to guide control policies for tick-borne infectious diseases [1, 2, 3]. These models typically assumed that vector and host populations are homogeneous, disregarding the movement of infected individuals and the consequent spatial spread of these infectious diseases [4]. Nonetheless, reaction-diffusion equations can be used to incorporate the spatial movement of individuals into stochastic epidemic models and predict the spatial advance of a disease [5, 6, 7, 8, 9, 10, 11, 12, 13, 14]. In this approach a reaction-diffusion framework is considered and therefore, individuals are di-

vided into a set of subgroups, each of which has its own stochastic dynamics described by a differential equation system, and adjacent subgroups are coupled by individual random movements with constant velocity [15, 16].

A remarkable example of a spatial spread system dependent on amplifier hosts is the Brazilian Spotted Fever (BSF), a highly lethal zoonotic disease caused by the bacteria *Rickettsia rickettsii* and transmitted by the tick *Amblyomma sculptum* [17]. Specifically, in the transmission of this disease, the vector *A. sculptum* is unable to maintain the infection by *R. rickettsii* in successive generations [18]. In Brazil, the maintenance of *R. rickettsii* depends primarily on the constant introduction of susceptible capybaras *Hydrochoerus hydrochaeris* [19, 20], which act as amplifiers and guarantee the constant creation of new cohorts of infected ticks[21, 18, 22]. Additionally, since ticks are limited in their mobility, *R. rickettsii* can spread over geographical areas by the movement of infected capybaras carrying either infected ticks from endemic areas or by transmitting the disease directly to susceptible ticks in neighboring regions. Currently, in endemic BSF areas, population densities of capybaras have reached numbers up to 40 times higher than those recorded in natural environments such as the Amazon and Pantanal [23] and thus, the risk of humans infection have increased significantly over the last three decades [21, 24].

In southeastern Brazil, genetic analyses have confirmed a rapid spatial expansion of capybaras with evidence of secondary contacts between phylogroups [25]. In this region, the formation of capybaras subgroups and their migration occurs chiefly when they leave in search of food [26, 25, 27]. However, young capybaras can also migrate after the occurrence of agonistic behaviors[28, 27] and in the beginning of the sexual maturity [29]. The maximum and mean dispersal distances of capybaras have been reported in 5600 m and 3366 m, respectively [30, 31]. Moreover, it has been found that the home range of capybara groups differs in the different countries of South America. For instance, it covers from 6 to 16 ha in Venezuela [32], 11.3 to 27.6 ha in Argentina [33], 56 ha in Colombia [34] although up to 183 ha in Paraguay [35] or even from 196 ha [36] to 200 ha in Brazil [37]. The average abundance index of the groups of capybaras in southeastern Brazil has been reported in 50.55 individuals [38].

The infection by *R. rickettsii* among different populations of capybaras and ticks in a homogeneous space was previously modeled [3]. In this preceding approach, two main risk factors for the *R. rickettsii* dissemination were identified: the current high birth rate of capybaras in endemic areas and the straightforward generation of new endemic areas due to the fact that a single infected capybara with just one infected tick attached are enough to trigger the disease in a non-endemic area. However, the risk of dissemination may be greater if it is considered: *i*) the current increase of the carrying capacity, determined by the abundance of sugarcane crops, main food source of capybaras in São Paulo [39], *ii*) the ubiquitous distribution of the vector *A. sculptum* in the state of São Paulo [40, 41, 17]

and *iii*) the large number of rivers in the region, through which capybaras can migrate [39].

This work aims to model a reaction-diffusion system that considers the spatial structure of capybaras to gain a better insight into the spatial diffusion of the *R. rickettsii* in São Paulo. We calculated the BSF propagation and verified if the model described the reported spatial-temporal spread of BSF in São Paulo. In addition, we create different scenarios to evaluate the effectiveness of preventing the capybaras exodus to control the spatial spread of the *R. rickettsii* and consequently prevent BSF human cases. This work contributes to the development of forthcoming mathematical and computational studies focused on the dynamics and prevention of vector-borne infectious diseases.

5.2 Model

Non-spatial transmission dynamics

Figure 5.1 schematically summarizes the BSF transmission dynamics for each capybara subgroup. In this diagram, individuals are represented by X^k, where k is the kind of animal (capybara C or tick T) and X stands for the infectious state (susceptible S, infected I, and recovered R). In this way, capybaras were classified in three populations as susceptible (S^C), infected (I^C) and recovered (R^C), as represented in Fig. 5.1. Hence, the total capybara population is given by $N^C = S^C + I^C + R^C$. In order to consider the seasonal one-year generation pattern of the tick *A. sculptum*, the model was adjusted to a semi-discrete time dynamics [42]. Ticks (T) were divided according to the stage of the life cycle as larvae, nymphs and adults, which were indexed as $T = 1, 2, 3$, respectively. They can be detached (D) from a capybara or attached (A) to it. Additionally, when a tick gets infected by an infected capybara, it remains infected until it dies. Thus, each *A. sculptum* stage was also classified according to whether it is susceptible (S) or infected (I). Thereby, we represented all stages of the tick life-cycle as S^{TA}, S^{TD}, I^{TA} and I^{TD}.

As also represented in Fig. 5.1, S^C's can be infected by an attached tick at rate λ. All capybaras have the same susceptibility and there is no increased death rate δ_C of infected individuals due to disease. Once capybaras are infected, they keep the *R. rickettsii* in the bloodstream for 7 to 10 days [20], during which the infection of new susceptible ticks that feed on it can occur at rate β. After this period, capybaras recovered at rate γ and become immune to the disease. As capybaras natality depends primarily on the availability of food sources, as is typically the case of rodents [44], in the proposed model the birth rate μ of the capybara population was determined by the amount of sugarcane in the region

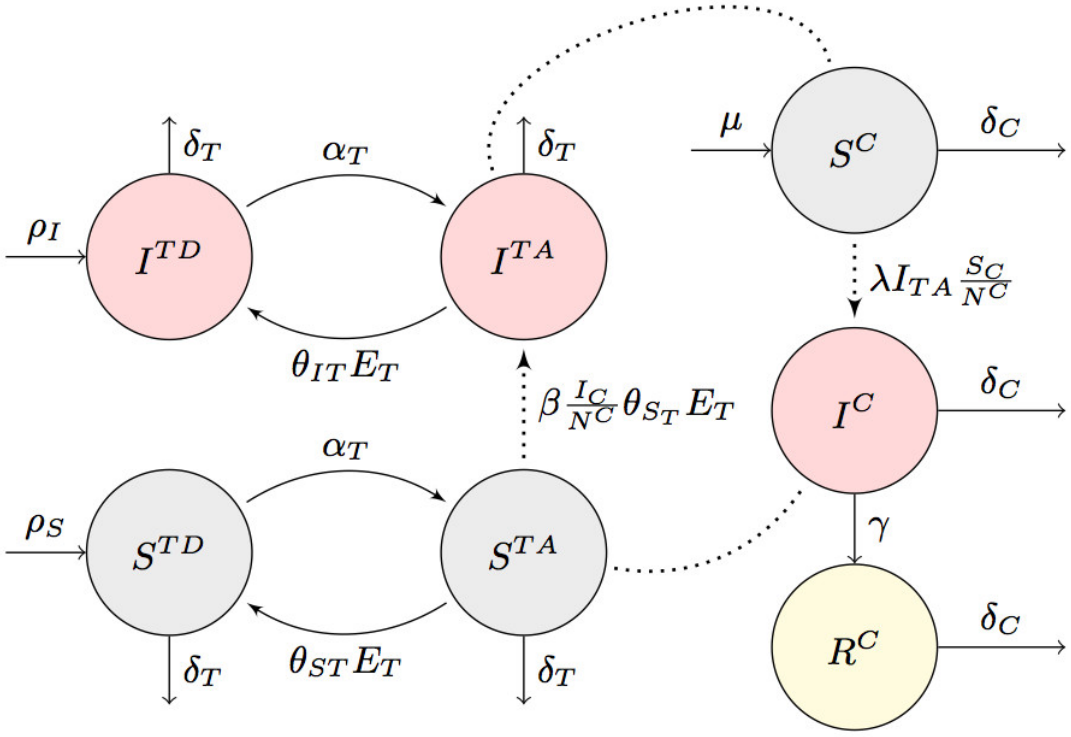

Figure 5.1 - Schematic representation of the *R. rickettsii* transmission in populations of *H. hydrochaeris* and *A. sculptum*. T = larvae, nymph or adult ticks.

obeying the function:

$$\mu_C = (v(1 - e^{(-yc[i,j])}) + z) \times N^C, \tag{5.1}$$

where c is the amount in hectares (ha) of sugarcane at position $[i, j]$, e is the Euler's number and $v = 0.0059$, $y = 0.02$ and $z = 0.0011$ are coefficients determined to adjust the function to a natural capybara birth rate $\mu_C \approx 0.005d^{-1}$, in areas with an average amount of sugar cane. The total number of capybars, N^C was restricted to 50 individuals [38, 23, 45, 43]. This parameter was calculated assuming 70% of adults, 64% of females, a litter size mean of 4.2 pups, 1.23 births per female per year and a pregnancy success of 85% [3, 46, 44, 47]. Also, a birth rate close to zero was considered in areas without sugarcane, and a maximum birth rate, $\mu_C = 0.0073d^{-1}$, was considered in areas with a maximum amount of sugarcane, as described below. This latter value considers the maximum litter size of capybaras reported in 6.1 pups [48, 49].

Moreover, ticks can attach at rate α_T, a proportion of them engorges E_T, detach at rate θ_T and die at rate δ_T. The production rate ρ of T was assumed to be proportional to the total number of susceptible and infected attached ticks of the previous generation $(T-1)$. The values of all taxes involved in the system reactions describing the non-spatial transmission dynamics are specified in Table 5.1.

This system of reactions can also be described by a coupled differential equation system,

Table 5.1 - Events and reactions of the tick-capybara-disease stochastic process

Event	Reaction	Parameter value
Birth of capybara	$S_C \xrightarrow{\mu_C N} S_C + 1$	$\mu = 0.005d^{-1}$ [23, 43]
Birth of a susceptible detached larvae	$S_{LD} \xrightarrow{\rho_{SS}S_{AA}+\rho_{SI}I_{AA}} S_{LD} + 1$	$\rho_{SS} = 2709; \rho_{SI} = 305$ [18]
Birth of infected detached larvae	$I_{LD} \xrightarrow{\rho_{II}I_{AA}} I_{LD} + 1$	$\rho_{II} = 228$ [18]
Engorgement of a susceptible larva	$S_{LD} \xrightarrow{\alpha_L S_{LD}} (S_{LD} - 1) + (S_{LA} + 1)$	$\alpha_L = 0.003d^{-1}$ [18]
Engorgement of an infected larva	$I_{LD} \xrightarrow{\alpha_L I_{LD}} (I_{LD} - 1) + (I_{LA} + 1)$	$\alpha_L = 0.003d^{-1}$ [18]
Transmission from IC to susceptible larvae	$S_{LA} \xrightarrow{\beta_L \frac{I_C}{N}\theta_{SL}E_L S_{LA}} (S_{LA} - 1) + (I_{ND} + 1)$	$\beta_L = 0.12; \theta_{SL} = 0.35; EL = 0.10$ [18, 20]
Transmission from infected larvae to SC	$S_C \xrightarrow{\lambda_L \frac{S_C}{N} I_{LA}} (S_C - 1) + (I_C + 1)$	$\lambda_L = 9.4 \times 10^{-5}d^{-1}$ [20]
Change from susceptible larvae to detached nymph	$S_{LA} \xrightarrow{\theta_{S_L}E_L S_{LA}} (S_{LA} - 1) + (S_{ND} + 1)$	$\theta_{SL} = 0.35; EL = 0.10$ [18]
Change from infected larvae to detached nymph	$S_{LA} \xrightarrow{\theta_{I_L}E_L I_{LA}} (S_{LA} - 1) + (S_{ND} + 1)$	$\theta_{IL} = 0.17; EL = 0.10$ [18]
Recovery rate of capybara	$I_C \xrightarrow{\gamma_C I_C} (I_C - 1) + (R_C + 1)$	$\gamma = 0.027d^{-1}$ [21]
Death of a susceptible capybara	$S_C \xrightarrow{\delta_C S_C} S_C - 1$	$\delta_C = 0.002d^{-1}$ [23]
Death of an infected capybara	$I_C \xrightarrow{\delta_C I_C} I_C - 1$	$\delta_C = 0.002d^{-1}$ [23]
Death of a recovered capybara	$R_C \xrightarrow{\delta_C R_C} R_C - 1$	$\delta_C = 0.002d^{-1}$ [23]
Engorgement rate of a susceptible nymph	$S_{ND} \xrightarrow{\alpha_N S_{ND}} (S_{ND} - 1) + (S_{NA} + 1)$	$\alpha_N = 0.006d^{-1}$ [18]
Engorgement rate of an infected nymph	$I_{ND} \xrightarrow{\alpha_N I_{ND}} (I_{ND} - 1) + (I_{NA} + 1)$	$\alpha_N = 0.006d^{-1}$ [18]
Transmission from infected nymph to SC	$S_C \xrightarrow{\lambda_N \frac{S_C}{N} I_{NA}} (S_C - 1) + (I_C + 1)$	$\lambda_N = 0.046d^{-1}$ [20]
Transmission from IC to susceptible nymph	$S_{NA} \xrightarrow{\beta_N \frac{I_C}{N}\theta_{SN}E_N S_{NA}} (S_{NA} - 1) + (I_{AD} + 1)$	$\beta_N = 25; \theta_{SN} = 0.60; EN = 0.40$[18, 20]
Change from susceptible nymph to detached adult	$S_{NA} \xrightarrow{\theta_{S_N}E_N S_{NA}} (S_{NA} - 1) + (S_{AD} + 1)$	$\theta_{SN} = 0.60$ [18]
Change from infected nymph to detached adult	$I_{NA} \xrightarrow{\theta_{I_N}E_N I_{NA}} (I_{NA} - 1) + (I_{AD} + 1)$	$\theta_{IN} = 0.60$ [18]
Engorgement of a susceptible adult	$S_{AD} \xrightarrow{\alpha_A S_{AD}} (S_{AD} - 1) + (S_{AA} + 1)$	$\alpha_A = 0.009d^{-1}$ [18]
Engorgement of an infected adult	$I_{AD} \xrightarrow{\alpha_A I_{AD}} (I_{AD} - 1) + (I_{AA} + 1)$	$\alpha_A = 0.009d^{-1}$ [18]
Transmission from infected adult to a SC	$S_C \xrightarrow{\lambda_A \frac{S_C}{N} I_{AA}} (S_C - 1) + (I_C + 1)$	$\lambda_A = 0.046d^{-1}$ [20]

For ticks:

$$\begin{aligned}
\dot{S}^{TD} &= \rho_S S^{(T-1)A} + \theta_{ST}E_T - \alpha_T S^{TD} - \delta_T, \\
\dot{I}^{TD} &= \rho_I I^{(T-1)A} + \theta_{IT}E_T - \alpha_T I^{TD} - \delta_T, \\
\dot{S}^{TA} &= \alpha_T S^{TD} - \beta\frac{I^C}{N^C}\theta_S E_T S^{TA} - \theta_S E_T S^{TA} - \delta_T, \\
\dot{I}^{TA} &= \alpha_T I^{TD} + \beta\frac{I^C}{N^C}\theta_S E_T S^{TA} - \theta_{I_T} E_T I^{TA} - \delta_T,
\end{aligned} \tag{5.2}$$

For capybaras:

$$\begin{aligned}
\dot{S}^C &= \mu_C N^C - \lambda\frac{S^C}{N^C}I^{TA} - \delta_C S^C \\
\dot{I}^C &= \lambda\frac{S^C}{N^C}I^{TA} - \gamma I^C - \delta_C I^C, \\
\dot{R}^C &= \gamma I^C - \delta_C R^C,
\end{aligned} \tag{5.3}$$

which has been previously studied [3] not only for the stationary state, but also for the

effect of rates changes.

Spatial spread

Capybaras are territorial animals typically distributed on groups in delimited areas [34, 37, 36, 32, 33, 35]. This was included in our description by considering capybaras subgroups of N_{ij}^C animals, in a grid at regular intervals l of 2 km, at positions $x_{ij} = (il, jl)$.As in the non-spatial dynamics, capybaras and ticks have the same classification and stages. We rely on the assumption that infected individuals transmit the disease only to susceptible individuals at their current location and no other processes occur at the same time. Consequently, the dispersal dynamics is governed by a Markov process,

$$X_{ij}^k \underset{\phi_{ij,nm}^k}{\overset{\phi_{nm,ij}^k}{\rightleftharpoons}} X_{nm}^k. \tag{5.4}$$

where individuals of type k have a unique mobility rate ϕ_{nm}^k that determines their travel between locations ij and nm. This allows to generalize the non-spatial coupled differential equation system describing the *R. rickettsii* dynamics,

$$\begin{aligned}
\partial_t S_{ij}^C &= \mu_C N_{ij}^C - \lambda_{ij} \frac{S_{ij}^C}{N_{ij}^C} I_{ij}^{TA} - \delta_C S_{ij}^C \\
&\quad + \sum_{nm} (\phi_{ij,nm} S_{nm}^C - \phi_{nm,ij} S_{ij}^C), \\
\partial_t I_{ij}^C &= \lambda_{ij} \frac{S_{ij}^C}{N_{ij}^C} I_{ij}^{TA} - \gamma I_{ij}^C - \delta_C I_{ij}^C \\
&\quad + \sum_{nm} (\phi_{ij,nm} I_{nm}^C - \phi_{nm,ij}) I_{ij}^C), \\
\partial_t R_{ij}^C &= \gamma I_{ij}^C - \delta_C R_{ij}^C \\
&\quad + \sum_{nm} (\phi_{ij,nm} R_{nm}^C - \phi_{nm,ij} R_{ij}^C).
\end{aligned} \tag{5.5}$$

where S_{ij}^C, I_{ij}^C and R_{ij}^C are the number of susceptible, infected and recovered capybaras located in the subgroup ij. N_{ij}^C is the total number of capybaras at ij, given by $N_{ij}^C = \sum_{ij} = S_{ij}^C + I_{ij}^C + R_{ij}^C$. Here, the differential equations for ticks are not represented, since we assume that susceptible and infected attached ticks are carried by capybaras and are diffused in this way. The tight connection of our discrete model to spatially continuous

reaction-diffusion systems is trivial for our case, in which the travel rates associated with the mobility between neighboring subgroups in a grid in which population are placed at regular intervals l can be written as:

$$w_{ij,nm} = \phi_{ij,i-1j}\delta_{nm,i-1j} + \phi_{ij,i+1j}\delta_{nm,i+1j} + \phi_{ij,ij-1}\delta_{nm,ij-1} + \phi_{ij,ij+1}\delta_{nm,ij+1}, \tag{5.6}$$

where $\delta_{nm,ij}$ is the Kronecker delta, which is 0 if $nm \neq ij$ and 1 if $nm = ij$. Equation 5.6 yields,

$$\partial_t I = \lambda_{IS} - \gamma I - \delta I + D\partial_x^2 I, \quad \partial_t S = -\lambda_{IS} - \delta S + D\partial_x^2 S$$

where $I(x,t) = I_{ij}/N_{ij}$, $S(x,t) = S_{ij}/N_{ij}$ and $D = l^2\phi$. Thus, $N_{ij}/N_{nm} = w_{ij}/w_{nm}$ and thereby the number of capybaras and attached ticks in the subgroups is conserved $\boldsymbol{M} = \sum_{nm} N_{nm}$. Figure 5.2 shows a graphic representation of our reaction-diffusion system considering three subgroups of ticks and capybaras.

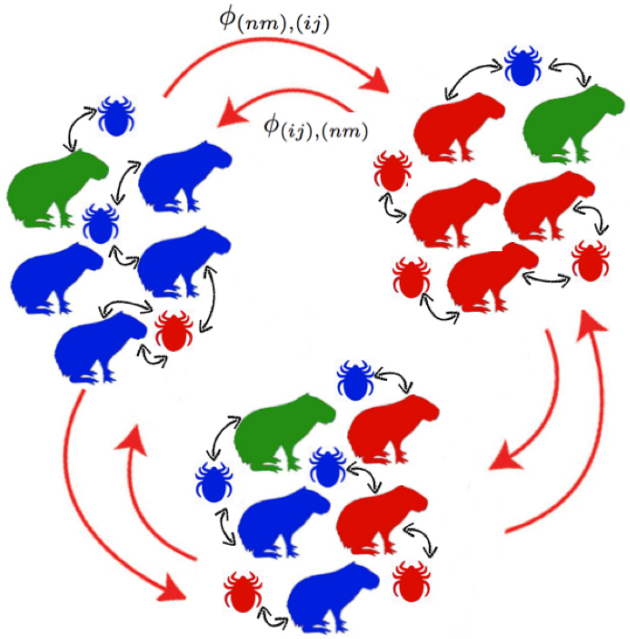

Figure 5.2 - Mobility model of three sub-populations. Arrows represent capybaras travel randomly between different locations governed by the set of transition rates $\phi_{(ij),(nm)}$ and $\phi_{(nm),(ij)}$.

For sufficiently localized initial conditions these systems can exhibit traveling waves with constant velocity v:

$$v = 2\sqrt{\lambda D(1-\gamma/\lambda)} \sim \sqrt{\phi}. \tag{5.7}$$

Considering annual changes in the carrying capacity, it is expected that this velocity will not remain constant, since it can not be assumed that susceptible, infectious, and recovered capybaras diffuse at equal rate ϕ. Indeed, a spatial-temporal relationship be-

tween occurrence of human rickettsiosis and sugarcane crops increment has been verified by satellite hyperspectral imagery in São Paulo [39]. For this reason, we considered that the movement of capybaras depends on the spatial distribution and amount of sugarcane crops, as it is their main food source in this region. In this way, the probability associated with the migration site depended on the carrying capacity determined by the amount of sugarcane of the neighbors,

$$\phi_{ij,nm} = p\frac{g}{e^{-bc_{nm}}} + q, \tag{5.8}$$

where c_{nm} is the amount (ha) of sugarcane in the population at the position (ln, lm) and the other characters are coefficients determined to adjust the function to the annual change in the carrying capacity throughout the study area according to the geographical pattern of the sugarcane, as explained below. We obtained this annual geographical pattern from 2005 to 2015 for each municipality from the Canasat-Area Project of the Brazilian National Institute for Space Research, which maps the sugarcane distribution of the state of São Paulo once a year using remote sensing imagery by the Landsat, CBERS and Resourcesat-I satellites [50].

5.3 Simulations

The proposed reaction-diffusion system was implemented in the R language using the Gillespie algorithm [51, 52]. All parameters were estimated using data generated from *ex situ* field works in southeastern Brazil. A full list of the model's reactions and parameters used in the simulations is given in Table 5.1.

Target area

To showcase our approach, we considered a study area of 10 000 km^2 at southeastern state of São Paulo, which was divided into subregions of 4 km^2 (area of a capybara subgroup). This division was included in the simulations by considering a grid of 50 × 50 pixels at regular intervals of 2 km, as shown in Figure 5.3. This area was selected because it has been identified as the most important area for the occurrence of human cases of BSF in the state of São Paulo [39], as it is shown in Figure 5.3A. In fact, this zone corresponds with three out of four spatial-temporal hotspot risk areas previously found through a retrospective space-time analysis [39]. This area is also critical because there is an increment of the availability of sugarcane crops, which increases the carrying capacity of the region [39], the vector *A. sculptum* is ubiquitous [53, 40, 41, 17] and there is a constant availability of water sources, which generates a propitious environment for the establishment of capybaras groups, their ticks and consequently for *R. rickettsii*.

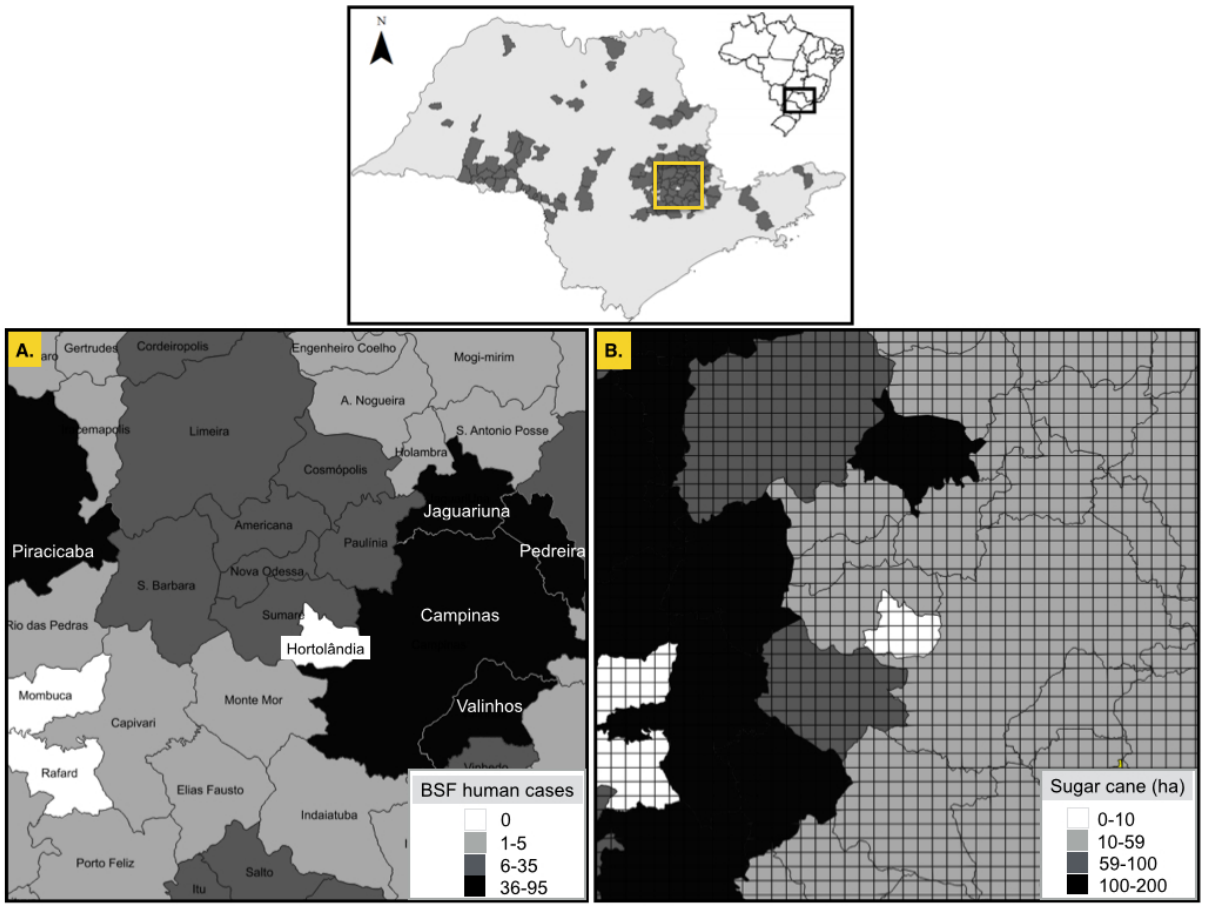

Figure 5.3 - The square in the top figure represents the study area conformed by a grid of 50×50 pixels at regular intervals of 2 km in southeastern São Paulo. Grey polygons represent municipalities with human BSF. **A.** Spatial distribution of cumulative human cases of BSF from 1985 to 2015 and **B.** Sugar cane amount in the study area in the year 2015.

To verify if our model describes the observed spatial-temporal spread of the BSF in the state of São Paulo, we obtained the information of the human cases from 1985 to 2016 from the website of the São Paulo State Center of Epidemiological Surveillance (CVE/SES-SP)[54]. We considered only BSF human cases from areas of transmission by *A. sculptum*, as previously determined [53]. Hence, we excluded BSF cases from the metropolitan area of São Paulo and from the São Paulo coast, where the implicated vectors have completely different ecological traits, in which capybaras play no role. The human cases of BSF are reported for each municipality and each year. Fig 5.3A shows the spatial distribution of the cumulative human cases of BSF from 1985 to 2016.

Subsequently, we also determined the average of sugarcane coverage of each municipality for each pixel by taking the total amount (ha) of sugarcane divided by the total number of pixels in a given municipality. For instance in Fig 5.3B, it is shown the sugarcane amount (ha) of 2015. We found that in São Paulo, the current average of sugarcane

coverage in a pixel of 4km^2 is about 59 ha and the maximum average of sugarcane coverage is 200 ha.To determine the impact of the amount of sugarcane on the propagation velocity of the BSF, we considered different scenarios with homogeneous sugarcane amount (10ha, 59ha, 100ha and 200ha). To identify a strategy to regulate disease propagation, we simulated different scenarios considering natural barriers with different widths (from 300 m to 4 km) assuming different migration distances.

Groups of capybaras were restricted to 50 individuals [38, 23, 45, 43] in all simulations. We also considered that each initially established subgroup should be localized in a spatial region with sugarcane. Accordingly, we also consider susceptible capybaras subgroups ($N = 50$) around each initial central area considered. We considered two initial central areas with a growing capybara population from where it was reported by public health entities that the disease has spread since 2005 [54]. In this areas the number of individuals considered corresponds with previous results obtained for endemic areas[3]: $S^C = 5$, $I^C = 10$, $R^C = 35$, $S^{AA} = 1000$ and $I^{AA} = 5$.

Uncertainty and sensitivity analysis

To quantify the impact of the parameters variation α, μ_C, λ, γ, δ_C and ϕ on the abundance of susceptible, infected and recovered migratory capybaras and infected nymphs derived from the reaction-diffusion model, we combined uncertainty through the Latin hypercube sampling (LHS) with the robust Partial rank correlation coefficient (PRCC) method [55, 56]. The LHS procedure was implemented by dividing the range of values for a given parameter into equally one hundred intervals. As parameters ranges are unreported, the LHS was sorted from a set of uniform distributions [56] (5.1). Starting from this, model outputs were obtained of all possible combination of parameters and the parameter and output values were transformed into their ranks. PRCC were calculated between each of the input variables (α, μ_C, λ, γ_C, δ_C, ϕ) and the amount of susceptible, infected and recovered migratory capybaras.

5.4 Results and discussion

The main application of our reaction-diffusion system for the spread of the BSF is the design of control strategies to prevent, or at least minimize the spread of this disease to humans. To address this problem, we verify if our model can describe the observed spatial-temporal spread of the BSF in the state of São Paulo by simulating the Markov stochastic process describing the *R. rickettsii* infection among *H. hydrochaeris* and *A. sculptum*. In this way, we start by calculating the annual Euclidean distance traveled by

the disease using the real data of human cases of BSF.

After reports of the disease between 1920 and 1940, in which the lethality reached 80% in the states of São Paulo and Minas Gerais, BSF only re-emerged in 1985 in the municipality of Pedreira. In 1986, BSF was reported in Jaguariuna, traveling a distance of 15.4 km yr^{-1}. Although the disease spread again in São Paulo at this time, detection and reporting of the disease began to be effective years later [57]. The Brazilian Information System for Notifiable Diseases (SINAN) was created in 1993 and it was not until then that new cases were reported again in Jaguariuna. From 1993 to 1995 the disease reached the municipality of Campinas (10.8 km yr^{-1}) and in 1996 reached Limeira (18.5 km yr^{-1}). Considering only the largest distances of each year, from Campinas, the disease reached Monte Alegre do Sul in 1997 (23.1 km yr^{-1}), Santo Antônio da Posse in 1998 (10.94 km yr^{-1}) and Piracicaba in 2002 (11.9 km yr^{-1}). After 8 years, in 2003, it reached the region of Ipeuna located at 90.40 km (11.3 km yr^{-1}) and Oriente (43.55 km yr^{-1}). In 2004, it reached the northwestern region of the state in Rio Preto (22.7 km yr^{-1}) and after 10 years in 2005, it reached the western region in Marília (33.5 km yr^{-1}) and the northern in Mococa (15.92 km yr^{-1}). In 2007, it reached Cândido Mota (31.25 km yr^{-1}) and Cruzalia (34.25 km yr^{-1}), and in 2008 Maracaí (31.67 km yr^{-1}). In 2009 the disease reached the northern border in Guaíra (22.84 km yr^{-1}), in 2010 the eastern border in Silveiras (16.34 km yr^{-1}) and in 2011 the western border of the state (31.15 km yr^{-1}). In 2012 human cases occurred in Rancharia (25.7 km yr^{-1}) in 2013 in Iepê (24.8 km yr^{-1}) and in 2014 traveled the longest distance to the municipality of Fernandôpolis at 461.9 km (24.31 km yr^{-1}). Here, we consider only the cases from 2005 to 2015 due to the fact that this year, the satellite monitoring of sugarcane started in the state of São Paulo [58]. Notwithstanding, Fig. 5.4 shows the change in the amount of BSF human cases from 2005 to 2016.

The migration rate $\phi_{ij,nm}$ of Equation 5.8 was adjusted in order to reproduce the reported spread of the disease from two initial endemic central areas with growing capybaras populations, in which cases were reported in 2005. Furthermore, $\phi_{ij,nm}$ must consider that the probability to migrate to a neighboring area with higher amount of sugarcane is higher. The pair of initial areas are represented in the first panel of Fig. 5.4. Consequently, based on Equation 5.7, we calculated the rate of migration ϕ by simulating different values of p,g,h and q to reproduce the propagation velocity in the studied region considering the average of sugarcane coverage. When the distribution of the sugarcane is considered, in the proposed reaction-diffusion system, we find that for $p = 0.0014$, $g = 0.2$, $h = 0.01$ and $q = 0.0054$, infected individuals appear in the same municipalities where the reported cases occurred, as shown in Fig. 5.4. We also found that migration and infections are null in areas without sugarcane, as in the central region of Hortolândia. In these sugarcane-free areas, no cases have been reported either, coinciding with the projections of our

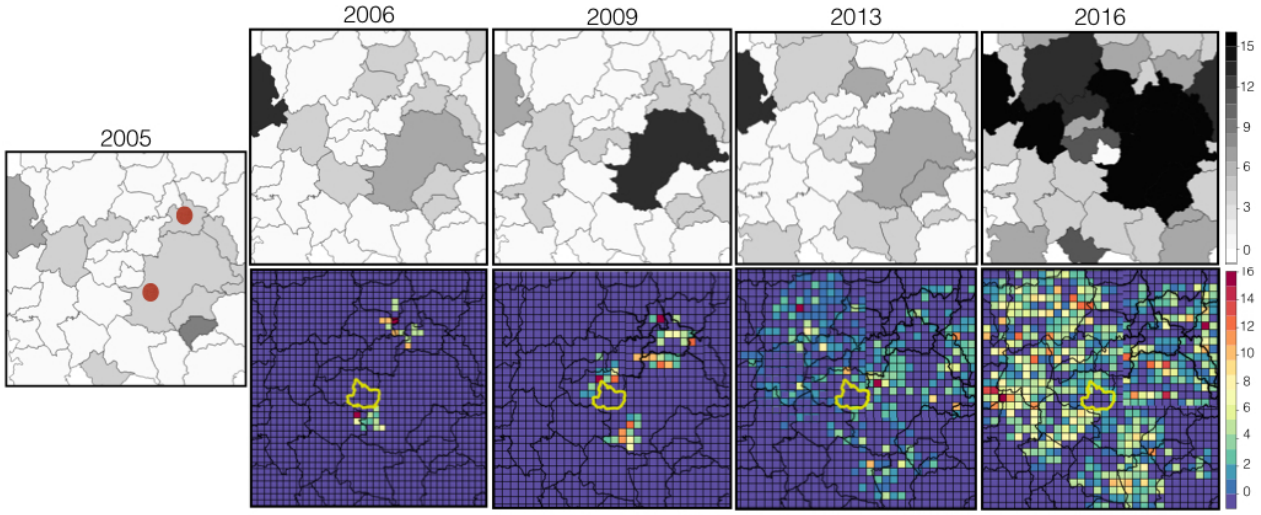

Figure 5.4 - Brazilian Spotted Fever spatial propagation considering annual change of sugar cane crops. Red dots represent the two central areas considered. The one located more to the north is located in the municipality of Jaguariuna and the other in Campinas. Yellow polygon represents the municipality of Hortolândia, which reported no cases or sugar cane crops, nor migration of infected individuals in the proposed model.

reaction-diffusion model.

Using the found migration rate, we determined the impact of the quantity of sugarcane on the propagation velocity of the disease by considering four different scenarios with homogeneous sugar cane amount: 10 ha, 59 ha, 100 ha and 200 ha. We find that the propagation velocity increases as the carrying capacity becomes greater. Figure 5.5A shows a quantity of sugarcane of 10 ha in which the propagation velocity of the disease is 6 km yr^{-1}. In Figure 5.5B we plotted a homogeneous amount of 59 ha in which the spread of velocity is 10 km/yr^{-1}. This propagation velocity is very close to the velocity of propagation obtained from Equation 5.7 ($\approx$ 11.6 km/yr^{-1}), considering $\phi = \mu - \delta$. A homogeneous amount of 100 ha provokes a propagation velocity of the disease of 16 km yr^{-1} and a homogeneous quantity of 200 ha generates a propagation velocity of 26 km yr^{-1} as also shown in Figure 5.5D. In these scenarios, the migration of infected individuals is symmetrical due to the homogeneous distribution of the sugarcane.

Sensitivity analysis shows that the uncertainties in estimating the values of the birth rate of capybaras are the most critical in affecting the prediction of the number of migratory susceptible, infected and recovered capybaras (Figure 5.6). In fact, in the specific case of infected capybaras, the unique factor that significantly and positively impacted their migration was their birth rate (PRCC = 0.94; 99% CI = 0.91 - 0.97). This positive value in the PRCC of the birth rate implies that when the value of this input variable increases, the future number of migratory capybaras will also increase. Furthermore, the future number of infected migratory capybaras decreases significantly as the recovery (PRCC = -0.87; 99% CI = -0.95 - -0.82) and death (PRCC = -0.41; 99% CI = -0.64 -

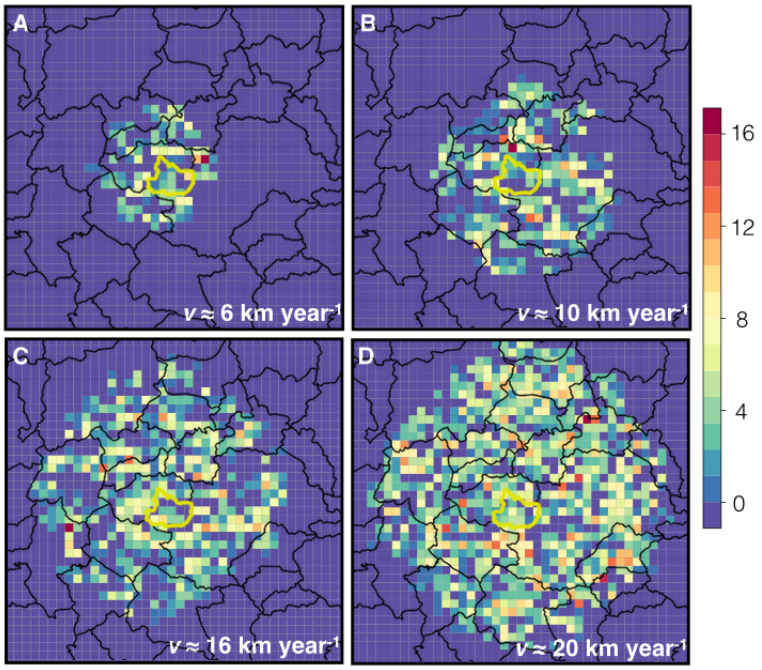

Figure 5.5 - Brazilian Spotted Fever spatial propagation considering homogeneous amount of sugarcane. (A) 10 ha, (B) 59 ha, (C) 100 ha and (D) 200 ha. In these scenarios, the migration of infected individuals is symmetrical due to the homogeneous distribution of the sugarcane.

-0.18) rates increase, as also shown in Figure 5.6. Migration rate of capybaras (ϕ) only impact significantly the number of susceptible migratory capybaras (PRCC = 0.48; 99% CI = 0.28 - 0.73).

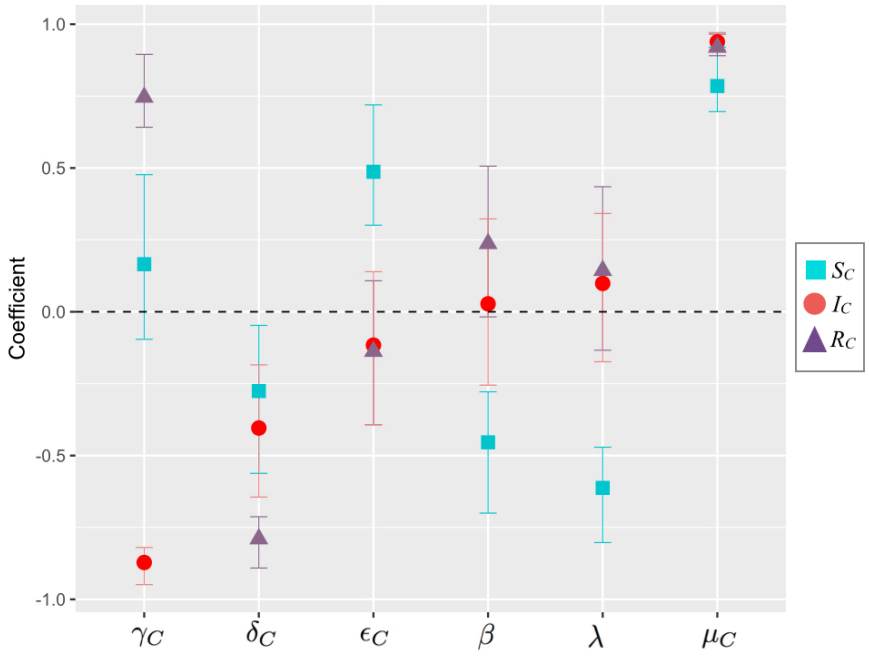

Figure 5.6 - Partial rank correlation coefficient between each parameter and the average migratory population of capybaras.

As capybaras natality depends primarily on the availability of food sources, the interruption of their access to food sources is a plausible strategy to reduce their birth rate. Because of this, we evaluated if the employment of riparian reforesting might work as a strategy to block the access of capybaras to food sources (sugarcane crops), thereby decreasing their birth rate, and consequently preventing the spread of the diseases to humans. Since capybaras do not tend to move more than 500 meters from water bodies while foraging [59, 60, 61], riparian reforesting up to 500 meters around water resources could be an alternative to interrupting their access to sugarcane crops, reducing their supply of food, and consequently their birth rate. However, the distance of riparian reforestating should be greater since capybaras dispersal distances up to 5600 m [30, 31] and home ranges up to 200 ha have been reported in South America [37]. In areas with established groups of capybaras, riparian forested areas in the early stages are at risk in terms of plant survival due to the trampling of young plants of woody species; therefore, damage control management practices are required [62]. Thus, riparian reforestation could be undertaken as a preventive strategy in areas where groups of capybaras have not yet established. Positively, riparian forests provide positive ecological impacts, such as biodiversity conservation, regularization of hydrological cycles, water and soil conservation, sediment retention, carbon fixation and pollutant filtering [63, 64, 65]. To solve our hypothesis that riparian (foodless areas) barriers can serve to mitigate the impact of amplifier hosts in the spatial propagation and transmission of BSF to humans, two factors were determined, the maximum amount of sugarcane of these barriers and the width thereof. To response this, we assumed that $\phi_{ij,nm}$ is also a function of the width of the barrier as shown in Figure 5.7 and written as:

$$\phi_{ij,nm} = \left(p\frac{g}{e^{-c[i,j]h}} + q\right)\left(\frac{1 - e^{-d[i,j]b}}{f} + 1\right) \tag{5.9}$$

where $c[i, j]$ and $d[i, j]$ are the amount of sugarcane and the distance of the barrier width at coordinates i, j. p, g, h and q are the same that in 5.8, and $b = 0.001$ and $f = 53.6$.

There are no data on the migratory behavior of capybaras in foodless regions, which means that the maximum distance that these amplifier hosts can migrate in regions deprived of food is unknown. Therefore, we assumed three different maximum migration distances (2km, 4km and 6km) [32, 30, 31]. This allow us to estimate the critical distance that the barrier must have in order to avoid the migration of infected individuals. We considered populations of ticks and capybaras surrounded by non-sugarcane barriers from 300 m to 4 km. In these scenarios, regardless of the amount of cane where they were, migration of individuals was interrupted from a barrier width of 4km and therefore the spread of the disease was also intercepted. The disease was able to cross barriers of less

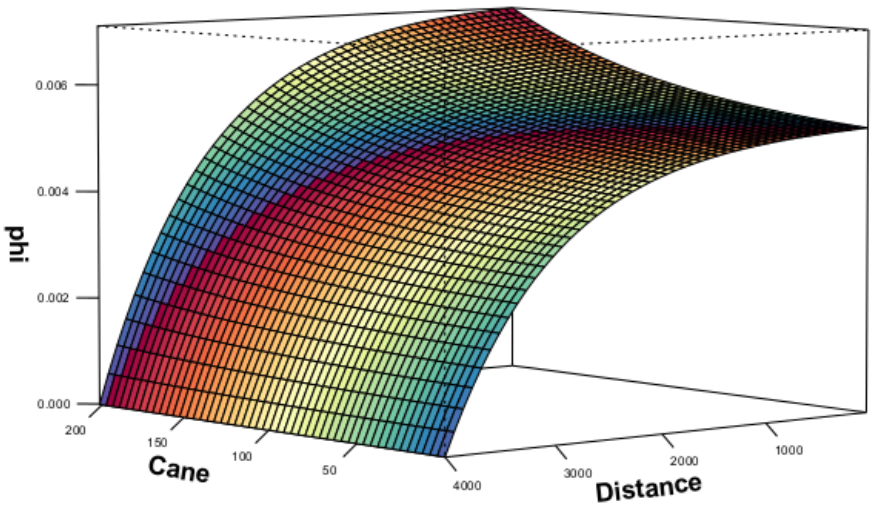

Figure 5.7 - ϕ parameter depending on sugarcane amount and the distance of the barriers width.

than 2 km in the first year of simulation, barriers of 3km in the second year (Figure 5.8) and barriers of 3.5 km in the third year. Additionally, it was verified that the spatial movement of capybaras obeys the distribution of the sugarcane as shown in Figure 5.8.

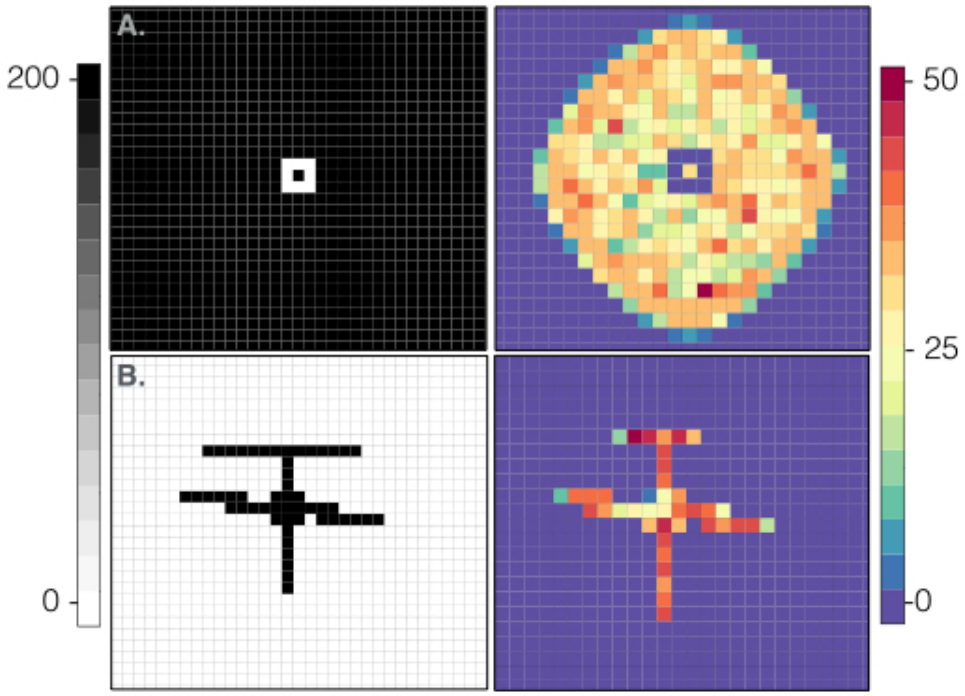

Figure 5.8 - A. Design of a non-sugarcane barrier of 3 km around a central point (left). Spatial spread of recovered capybaras after a 5-year simulation considering the barrier on the left (right). B. Design of a sugarcane corridor of 200 ha within a foodless area (left). Spatial distribution of recovered capybaras after 3-year simulations.

5.5 Conclusion

We developed a reaction-diffusion system for the spread of an infectious disease by considering the spatial structure and migration of amplifier hosts. Our results indicate that as we vary the amount of food sources, the velocity at which the disease advances is roughly proportional to the carrying capacity, hence proportional to the local risk of zoonotic infection. Since our model considered a reasonably realistic spatial structure of capybaras and ticks and allowed to represent accurately the spatial dynamics of the Brazilian Spotted Fever in the state of São Paulo, it can allow the formulation of public actions focused on the prevention of this diseases and potentially other vector-borne diseases. The results of the sensitivity analysis can be used to focus prevention strategies on the birth rate of capybaras, as this analysis identified that this parameter (do to their estimation uncertainty) is the most important in the prediction of infected migratory capybaras. Some geographical barriers, generated for example by riparian reforesting, can generate positive ecological impacts and can impede the spread of BSF to humans.

Acknowledgments

We thank the financial support by the Fundação de Amparo à Pesquisa do Estado de São Paulo - FAPESP; grant Numbers 16/01913-8 (GP. Research Internships Abroad - BEPE), 14/12213-1 (GP. Doctoral fellowship) and 13/18046-7 (MBL. Thematic project.).

Bibliography

[1] P. Hancock, R. Brackley, and S. Palmer, "Modelling the effect of temperature variation on the seasonal dynamics of ixodes ricinus tick populations.," **International Journal for Parasitology**, vol. 41, pp. 513–522, 2011.

[2] L. Ferreri, M. Giacobini, P. Bajardi, L. Bertolotti, L. Bolzoni, V. Tagliapietre, A. Rizzoli, and R. Rosa, "Pattern of tick aggre- gation on mice: larger than expected distribution tail enhances the spread of tick-borne pathogens," **Plos Computational Biology**, vol. 10, p. e1003931, 2014.

[3] G. Polo, C. Mera Acosta, M. Labruna, and F. Ferreira, "Transmission dynamic and control of *Rickettsia rickettsii* in populations of *Hydrochoerus hydrochaeris* and

Amblyomma sculptum," **Plos Neglected Tropical Diseases**, vol. 11, p. e0005613, 2017.

[4] T. Hollingsworth, J. Pulliam, S. Funk, J. Truscott, V. Isham, and A. Lloyd, "Seven challenges for modelling indirect transmission: Vector-borne diseases, macroparasites and neglected tropical diseases," **Epidemics**, vol. 10, pp. 16–20, 2015.

[5] J. Murray, E. Stanley, and D. Brown, "On the spatial spread of rabies among foxes," **Proceedings of the Royal Society, London, Series B**, vol. 229, pp. 111–150, 1986.

[6] F. Van den Bosch, R. Hengeveld, and M. JA, "Analysing the velocity of animal range expansion.," **Journal of Biogeography**, vol. 19, pp. 135–150, 1992.

[7] R. Wilson and V. Capasso, "Analysis of a reaction-diffusion system modeling man-environment-man epidemics," **Journal on Applied Mathematics**, vol. 57, pp. 327–346, 1997.

[8] W. Fitzgibbon, M. Langlais, and J. Morgan, "A mathematical model for indirectly transmitted diseases," **Mathematical Biosciences**, vol. 206, pp. 233–248, 2007.

[9] T. Caraco, S. Glavanakov, G. Chen, J. Flaherty, T. Ohsumi, and B. Szymanski, "Stage-structured infection transmission and a spatial epidemic: A model for lyme disease," **American Naturalist**, vol. 160, pp. 348–359, 2002.

[10] M. Lewis, S. Petrovskii, and P. JR, "Reaction–Diffusion Models: Single Species," in **The Mathematics Behind Biological Invasions**, pp. 69–105, Springer, 2016.

[11] Y. Lou and X. Zhao, "A reaction–diffusion malaria model with incubation period in the vector population," **Mathematical Biology**, vol. 62, pp. 543–568, 2011.

[12] R. Peng and X. Zhao, "A reaction–diffusion sis epidemic model in a time-periodic environment," **Nonlinearity**, vol. 25, no. 5, p. 1451, 2012.

[13] W. Wang and X. Zhao, "A nonlocal and time-delayed reaction–diffusion model of dengue transmission," **SIAM Journal of Applied Mathematics**, vol. 71, pp. 147–168, 2011.

[14] Y. Lou and X. Zhao, "Global dynamics of a reaction and diffusion model for lyme disease," **Journal of Mathematical Biology**, vol. 65, pp. 787–808, 2012.

[15] M. Keeling and C. Gilligan, "Metapopulation dynamics of bubonic plague," **Nature**, vol. 407, pp. 903–905, 2000.

[16] H. Gaff and E. Schaefer, "Metapopulation models in tick-borne disease transmission modelling," **Adv Exp Med Bio**, vol. 673, pp. 51–65, 2010.

[17] S. De Oliveira, J. Guimarães, G. Reckziegel, B. Costa, K. Araújo-Vilges, L. Fonseca, F. Pinna, S. Costa, E. Caldas, G. Gazeta, and R. Gurgel-Gonçalves, "An update on the epidemiological situation of spotted fever in brazil," **The Journal of Venomous Animals and Toxins Including Tropical Diseases**, vol. 22, pp. 1–8, 2016.

[18] J. F. Soares, H. S. Soares, A. M. Barbieri, and M. B. Labruna, "Experimental infection of the tick Amblyomma cajennense, Cayenne tick, with Rickettsia rickettsii, the agent of Rocky Mountain spotted fever," **Medical and Veterinary Entomology**, vol. 26, no. 2, pp. 139–151, 2012.

[19] F. S. Krawczak, F. A. Nieri-bastos, F. P. Nunes, J. Soares, and J. Moraes-filho, "Rickettsial infection in Amblyomma cajennense ticks and capybaras (Hydrochoerus hydrochaeris) in a Brazilian spotted fever-endemic area," **Parasites & Vectors**, vol. 7, pp. 1–7, 2014.

[20] C. E. Souza, J. Moraes-Filho, M. Ogrzewalska, F. C. Uchoa, M. C. Horta, S. S. L. Souza, R. C. M. Borba, and M. B. Labruna, "Experimental infection of capybaras Hydrochoerus hydrochaeris by Rickettsia rickettsii and evaluation of the transmission of the infection to ticks Amblyomma cajennense," **Veterinary Parasitology**, vol. 161, no. 1, pp. 116–121, 2009.

[21] M. B. Labruna, "Ecology of rickettsia in South America," **Annals of the New York Academy of Sciences**, vol. 1166, no. 1, pp. 156–166, 2009.

[22] M. B. Labruna, "Brazilian spotted fever: the role of capybaras," in **Capybara**, pp. 371–383, Springer New York, 2013.

[23] K. Ferraz, S. De Barros Ferraz, J. Moreira, H. Couto, and L. Verdade, "Capybara (Hydrochoerus hydrochaeris) distribution in agroecosystems: a cross-scale habitat analysis," **Journal of Biogeography**, vol. 34, no. 2, pp. 223–230, 2007.

[24] F. Del Fiol, F. Junqueira, C. Miranda, T. Maria, and B. Filho, "A febre maculosa no Brasil," **Revista Panamericana de Salud Pública**, vol. 27, no. 10, pp. 461–466, 2010.

[25] M. Rodrigues, T. Rego de Paula, L. Ferreira, E. Avila, L. Silva, and V. Souza, "Behavior of a group of capybaras in an urban area," **Acta Veterinaria Brasilica**, vol. 7, pp. 212–217, 2013.

[26] J. Krauer, "Landscape ecology of the capybara (hydrochoerus hydrochaeris) in the chaco region of paraguay," **Doctoral Thesis. University of Kansas, Manhattan.**, 2009.

[27] F. Vargas, S. Vargas, M. Moro, V. Silva, and C. Carrer, "Capybara (hydrochaeris hydrochaeris linnaeus, 1766) population monitoring in pirassununga, sp, brazil," **Ciencia Rural, Santa Maria**, vol. 37, pp. 1104–1108, 2007.

[28] K. Ferraz and L. Verdade, "Ecologia comportamental da capivara: bases biológicas para o manejo da espécie," **In: Mattos, W. R. S. [Ed.]. A Produção Animal na Visão dos Brasileiros. Sociedade Brasileira de Zootecnia, Piracicaba, SP, Brasil**, pp. 589–595, 2001.

[29] A. Almeida, M. Arzua, P. Trindade, and J. Silva, "Capybaras (hydrochoerus hydrochaeris, linnaeus, 1766) (mammalia: Rodentia) in green areas of curitiba, parana state, brazil," **Estudos de Biologia**, vol. 35, pp. 9–16, 2013.

[30] E. Herrera, "Growth and dispersal of capybaras (hydrochaeris hydrochaeris) in the llanos of venezuela," **Journal of Zoology**, vol. 228, pp. 307–316, 1992.

[31] E. Herrera, V. Salas, E. Congdon, M. Corriale, and T.-M. Z., "Capybara social structure and dispersal patterns: Variations on a theme," **Journal of Mammalogy**, vol. 92, pp. 12–20, 2011.

[32] E. Herrera and D. Macdonald, "Resource utilization and territoriality in group-living capybaras (hydrochoerus hydrochaeris)," **Journal of Animal Ecology**, vol. 58, pp. 667–679, 1989.

[33] M. Corriale, E. Muschetto, and E. Herrera, "Influence of group sizes and food resources in home-range sizes of capybaras from argentina," **Journal of Mammalogy**, vol. 94, pp. 19–28, 2013.

[34] G. Perea and P. Ruiz, "Organización social y hábitos territoriales del chigüiro.," **Undergraduate Thesis**, 1977.

[35] C. Alho and N. Rondon, "Rango de hogar y uso de hábitat de carpinchos en pastizales recién invadido en el chaco seco de paraguay," **Therya**, vol. 5, pp. 61–79, 2014.

[36] C. Alho and N. Rondon, "Habitat, population density and social structure of capybaras (hydrochoerus hydrochaeris) in the pantanal, brazil," **Revista Brasilera de Zoologia**, vol. 4, pp. 139–149, 1987.

[37] G. Schaller and P. Crawshaw, "Social organization in a capybara population," **Säugetierkundliche Mitteilungen**, vol. 29, pp. 3–16, 1981.

[38] L. Verdade and K. Ferraz, "Capybaras in an anthropogenic habitat in southeastern brazil," **Brazilian Journal of Biology**, vol. 66, pp. 371–378, 2006.

[39] G. Polo, M. B. Labruna, and F. Ferreira, "Satellite hyperspectral imagery to support tick-borne infectious diseases surveillance," **PLoS ONE**, p. e0119190, Nov. 2015.

[40] S. Nava, L. Beati, M. B. Labruna, A. G. Cáceres, A. J. Mangold, and A. A. Guglielmone, "Reassessment of the taxonomic status of amblyomma cajennense (fabricius, 1787) with the description of three new species, amblyomma tonelliae n. sp., amblyomma interandinum n. sp. and amblyomma patinoi n. sp., and reinstatement of amblyomma mixtum koch, 1844, and amblyomma sculptum berlese, 1888 (ixodida: Ixodidae)," **Ticks and Tick-borne Diseases**, vol. 5, no. 3, pp. 252 – 276, 2014.

[41] T. F. Martins, A. R. M. Barbieri, F. B. Costa, F. A. Terassini, L. M. A. Camargo, C. R. L. Peterka, R. de C. Pacheco, R. A. Dias, P. H. Nunes, A. Marcili, A. Scofield, A. K. Campos, M. C. Horta, A. G. A. Guilloux, H. R. Benatti, D. G. Ramirez, D. M.

Barros-Battesti, and M. B. Labruna, "Geographical distribution of amblyomma cajennense (sensu lato) ticks (parasitiformes: Ixodidae) in brazil, with description of the nymph of a. cajennense (sensu stricto)," **Parasites & Vectors**, vol. 9, no. 1, p. 186, 2016.

[42] M. Labruna, M. Amaku, J. Metzner, A. Pinter, and F. Ferreira, "Larval behavioral diapause regulates life cycle of Amblyomma cajennense (Acari: Ixodidae) in Southeast Brazil," **J Med Entomol**, vol. 40, p. 170–178, 2003.

[43] V. Sarango, "Manual para manejo de capibaras," **Programa para la conservación y manejo sostenible del patrimonio natural y cultural de la reserva de la biosfera Yasuni**, vol. 1, p. 1–39, 2011.

[44] J. Moreira, M. Alvarez, T. Tarifa, V. Pacheco, A. Taber, D. Tirira, E. Herrera, K. Ferraz, J. Aldana-Domínguez, and D. Macdonald, "Taxonomy, Natural History and Distribution of the Capybara," in **Capybara**, pp. 3–37, Springer New York, 2013.

[45] J. Ojasti, **Estudio biológico del chigüire o capibara**. Fondo Nacional de Investigaciones Agropecuarias, 1973.

[46] V. Sarango, "Manual para manejo de capibaras," **Programa para la conservación y manejo sostenible del patrimonio natural y cultural de la reserva de la biosfera Yasuni.**, vol. 1, pp. 1–39, 2011.

[47] J. Moreira, W. Helga, K. Ferraz, J. Aldana-Domínguez, L. Verdade, and D. Macdonald, "Taxonomy, Natural History and Distribution of the Capybara," in **Capybara**, pp. 147–167, Springer New York, 2013.

[48] M. Alvarez and F. Kravetz, "Reproductive performance of capybaras (Hydrochoerus hydrochaeris) in captivity under different management systems in Argentina," **Animal Research**, vol. 55, pp. 153–164, 2006.

[49] C. Chapman, "Reproductive Biology of Captive Capybaras," **Journal of Mammalogy**, vol. 72, pp. 206–208, 1991.

[50] "Instituto de Pesquisas Espaciais - INPE. CanaSat: monitoramento da cana-de-açúcar," 2013.

[51] D. Gillespie, "A general method for numerically simulating the stochastic time evolution of coupled chemical reactions," **Journal of Computational Physics**, vol. 22, p. 403–434, 1976.

[52] M. Pineda-Krch, "GillespieSSA: Implementing the Gillespie Stochastic Simulation Algorithm in R ," **Journal of Statistical Software**, vol. 25, 2008.

[53] A. Pinter, A. Franca, C. Souza, C. Sabbo, E. Mendes, F. Pereira, G. Katz, M. Labruna, M. Holcman, M. Alves, C. Horta, M. Mscheretti, R. Mayo, R. Angerami,

R. Brasil, R. Leite, S. Souza, S. Colombo, and O. V, "Febre Maculosa Brasileira," **BEPA Suplemento**, vol. 8, pp. 19–24, 2011.

[54] S. de Estado da Saúde, "Casos Confirmados Autóctones de FMB de residentes no estado de São Paulo segundo Município de Infecção e Ano de Início de Sintomas período de 2007 a 2016," 2016.

[55] S. Blower and D. H, " Sensitivity and uncertainty analysis of complex-models of disease transmission - an HIV model, as an example," **International Statistical Review**, vol. 62, pp. 229–243, 1994.

[56] S. Marino, I. Hogue, C. Ray, and K. DE, "A methodology for performing global uncertainty and sensitivity analysis In systems Biology," **Journal of Theoretical Biology**, vol. 254, pp. 178–196, 2008.

[57] J. Laguardia, C. Domingues, C. Carvalho, C. Lauerman, E. Macário, and R. Glatt, "Information system for notifiable diseases (sinan): challenges in developing a national health information system," **Epidemiologia e Serviços de Saúde**, vol. 13, pp. 135–146, 2004.

[58] INPE, "Instituto de Pesquisas Espaciais. CanaSat: monitoramento da cana-de-açúcar," **http://www.dsr.inpe.br/laf/canasat/en/)**, 2013.

[59] A. Rinaldi, "Ecologia de Capivaras (*Hydrochoerus hydrochaeris*, Linnaeus, 1766) em região alterada pela formação de um reservatório hidroeletrico. Ph.D. Thesis.," **Thesis, Universidade Federal do Paraná**, 2006.

[60] F. Jacomassa, "Atividade, uso de ambientes, comportamento e densidade de capivara *Hydrochoerus hydrochaeris* (Linnaeus, 1766) (Mammalia: Rodentia: Caviidae) no Pantanal do Miranda, MS," **Biodiversidade Pampeana**, vol. 88, pp. 46–49, 2010.

[61] V. Salas, E. Pannier, , C. Galindez-Silva, A. Gols-Ripoll, and E. Herrera, "Methods for capturing and marking wild capybaras in Venezuela," **Wildlife Society Bulletin**, vol. 32, pp. 202—-208, 2004.

[62] L. Guimaraes, F. Rodrigues, and M. Scotti, "Strategies for herbivory mitigation by capybaras *Hydrochoerus hydrochaeris* in a riparian forest under restoration in the Sao Francisco river basin Brazil," **Wildlife Biology**, vol. 20, p. 136–144, 2014.

[63] E. Tabacchi, L. Lambs, H. Guilloy, A. Planty-Tabacchi, E. Muller, and D. H, "Impacts of riparian vegetation on hydrological processes," **Hydrological Processes**, vol. 14, p. 2959–2976, 2000.

[64] N. Pollock and T. Beechie, "Does Riparian Forest Restoration Thinning Enhance Biodiversity? The Ecological Importance of Large Wood," **Journal of the American Water Resources Association**, vol. 50, p. 543–559, 2014.

[65] A. Bennett, D. Nimmo, and R. J, "Riparian vegetation has disproportionate benefits for landscape-scale conservation of woodland birds in highly modified environments," **Journal of Applied Ecology**, vol. 51, p. 541–523, 2014.

6. Current potential prediction distribution and potential response of *Amblyomma cajennense* (Fabricius, 1787) (Acari:Ixodidae) to climate and landscape changes in America

Abstract

The prediction of risk areas for the occurrence of disease outbreaks has become a major challenge for epidemiologists. Environmental predictors are increasingly used to decipher the potential presence of hosts and vectors important in the transmission of zoonotic diseases. In this study, the Maximum Entropy algorithm was used to estimate the current potential distribution of the *A. cajennense* (Fabricius, 1787), vector of different arboviruses and of the *Rickettsia rickettsii*, agent of the Rocky Mountain spotted fever, known n Brazil as the Brazilian spotted fever. We also estimated the future distribution of this tick vector, based on future bioclimatic conditions and its the potential response to landscape factors associated with climate change. In general, the variables that contributed in greater proportion to the current potential distribution of the different vectors studied were very diverse. Factors associated with few variations in seasonality and climatic conditions were especially related to *A. cajennense* s.s., those associated with humidity and precipitation to *A. mixtum*, high daytime and nighttime land temperatures to *A. sculptum* and those associated with specific conditions of the biome were linked to *A. tonelliae*. In response to changes in the landscape or climate, we found a potential disappearance of ticks from areas where they are currently reported. These changes in the geographical distribution of the ticks considered, with the exception of *A. mixtum*, would be mainly provoked by a higher incoming sunlight reflected, which is analogous to less vegetation, a lower leaf area index and a lowest net primary production. For *A. mixtum*, a higher vegetation index, higher leaf area index and higher net primary production are the most important variables. I all scenarios, predictions considering both bioclimatic and landscape variations presented a better or equal performance. This work will have an impact in the planning of future works associated to the epidemiology of these ticks and outlining strategies for the prevention of tick-borne infectious diseases in America.

6.1 Introduction

A major challenge for epidemiologist is to anticipate the responses of complex disease systems to climate change and anthropogenic impacts[1]. Ticks are important as vectors of a large number of pathogens, and tick-borne diseases set an emergent concern on human and animal health [1, 2, 3, 4, 5]. Due to its high sensitivity to humidity and temperature, ticks can variate their geographic distribution and abundance in response to climate change, which generates a shift in the geographical pattern of tick-borne diseases [6], particularly towards high latitudes and latitudes [4, 7].

Amblyomma cajennense (Fabricius, 1787) is one of the most important taxonomic groups of vectors in America [8, 9, 12]. Specifically, its distribution includes southern United States, Mexico, Central America, Caribbean and all countries of South America with the exception of Chile and Uruguay, where it feeds on a variety of vertebrate hosts [8].This tick is vector of different arboviruses [10, 11] and of the *Rickettsia rickettsii*, agent of the Rocky Mountain spotted fever [9]. A recent morphological work, separated this taxon in six species: *A. cajennense* sensu stricto (s.s.), *Amblyomma mixtum* Koch, 1844, *Amblyomma sculptum* Berlese, 1888, *Amblyomma interandinum* Beati, Nava and Caceres, 2014, *Amblyomma tonelliae* Nava, Beati and Labruna, 2014, and *Amblyomma patinoi* Labruna, Nava and Beati, 2014 [12]. Although, the current geographical distribution of *A. cajennense* (s.l.) was determined in Brazil [13], the potential geographical distribution of these species in the American continent is unknown.

Species distribution models have been used to predict species distributions across landscapes in space and time, according to environmental variables [14]. Diverse distribution models have been developed to predict potential effects of climate change on the geographical distribution of invertebrate species [14, 15, 16, 17, 18]. Some of these algorithms include generalized linear models (GLM), generalized additive models (GAM), boosted regression trees (BRT), bioclimatic (BIOCLIM), genetic algorithm for rule-set production (GARP) and maximum entropy modeling (MaxEnt) [14]. Comparisons of these algorithms have demonstrated that MaxEnt has a robust performance in terms of sample size, can fit complex functions between response and predictor variables for modeling presence-only data, and had showed a predictive performance consistently competitive when comparing with 16 of the highest performing algorithms [19]. The maximum entropy algorithm has also been widely applied to predict the potential distribution of different vector-borne infectious diseases around the world [20, 21, 22, 23, 24].

The choice of appropriate predictor variables is crucial to achieve a robust and reliable model for ticks and tick-borne pathogens [25]. Although variables associated with land and vegetation have a direct influence and a greater impact on ticks development

and distribution than macroclimate factors, several authors have used global temperature and rainfall variables to model ticks distribution [26, 27]. Consequently, to predict the geographical distribution of the taxon *Amblyomma cajennense* (Fabricius, 1787) (Acari: Ixodidae) in America, we employ the maximum entropy algorithm considering both climatic variables and factors associated with landscape. We model the current potential distribution of these ticks, the future distribution based on future climatic conditions of the year 2050, and the potential response to landscape changes, which are associated with climate change. This work will have an impact in the planning of future works associated to the epidemiology of these species and will have an impact outlining strategies for the prevention of tick-borne infectious diseases in America.

6.2 Materials and methods

Data and study area

Data related to the geographical distribution of the taxon *Amblyomma cajennense* (Fabricius, 1787) (Acari: Ixodidae) in America was obtained from previous surveys published [12, 13]. Although the taxon *A. cajennense* is conformed by six species [12], due to the small amount of data, we disregarded occurrences of *Amblyomma interandinum* and *Amblyomma patinoi*. In this way, our database was made up of 358 occurrences of the taxon *A. cajennense*, of which 58 were of *Amblyomma mixtum*, 188 of *Amblyomma sculptum*, 55 of *Amblyomma tomelliae* and 57 of *Amblyomma cajennense* s.s. Geographical distribution of the four species considered is shown in Figure 6.1.

Current and future climate variables

We used thirty three bioclimatic predictors obtained from the WorldClim database, which comprises a set of global climate layers with a spatial resolution of about 2.5 arc minute (roughly 5km). The predictors that were considered capture information about annual conditions, as well as seasonal mean climate conditions and intra-year seasonality: biome, altitude, precipitation of each month, annual mean temperature, mean diurnal range, isothermality, temperature seasonality, maximum temperature of the warmest month, minimum temperature of the coldest month, temperature annual range, mean temperature of the wettest, driest, warmest and coldest quarter, annual precipitation, precipitation of the wettest and driest month, precipitation seasonality, and precipitation of the wettest, driest, warmest and coldest quarter [28].

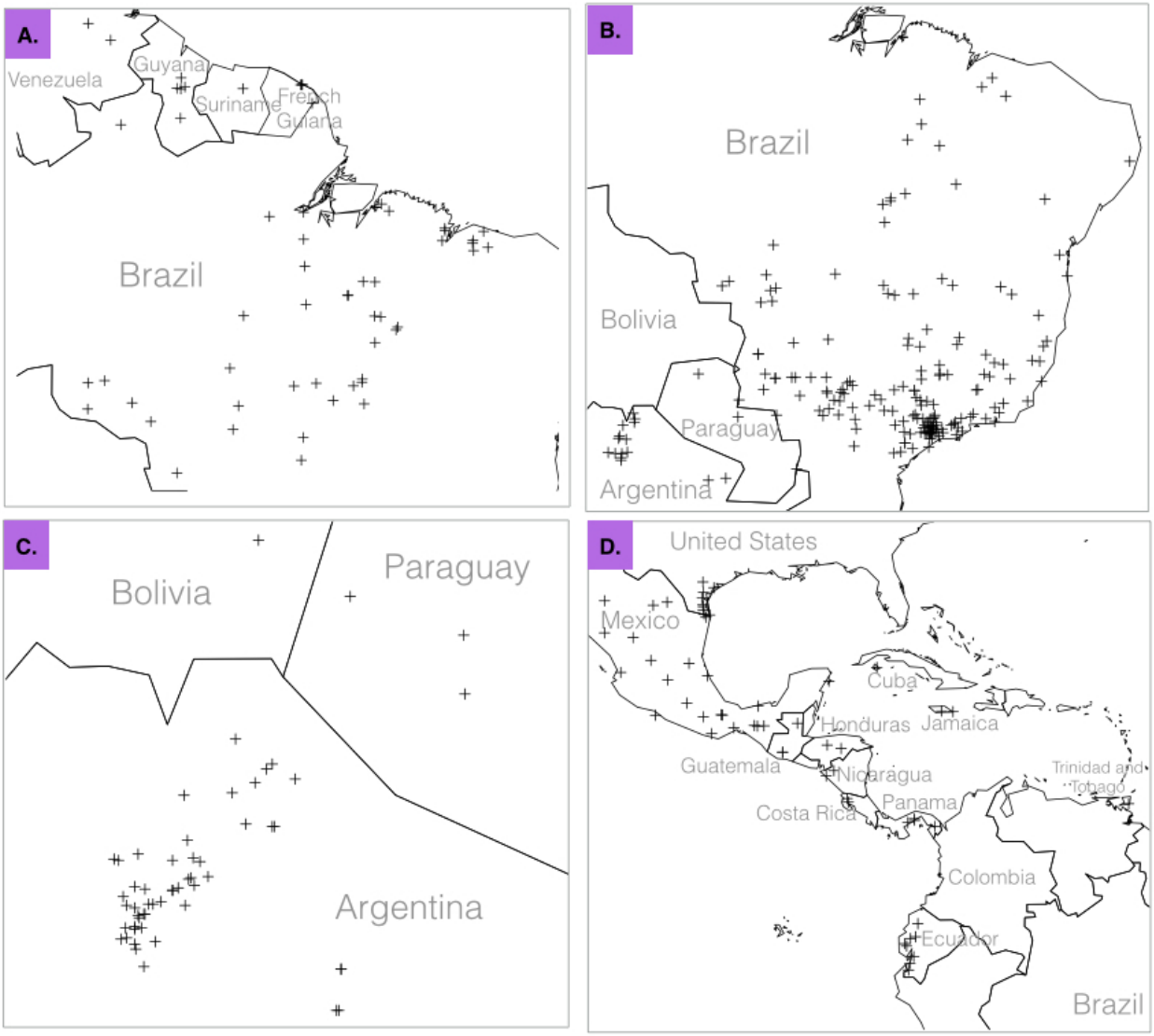

Figure 6.1 - Spatial distribution of **A.** *A. cajennense* s.s. **B.** *A. sculptum*. **C.** *A. tomelliae*. **D.** *A. mixtum*

.

Future bioclimatic predictors of these variables, with the exception of biome and altitude, were derived from the Coupled Model Intercomparison Project Phase 5 (CMIP5) for the year 2050.

Landscape variables

To obtained a more reliable model for the *A. cajennense* taxon in America, we considered seventy-three landscape variables, relevant to habitat suitability of ticks, from the global satellite imagery repository of the NASA Earth Observations (NEO)[29] . The predictors considered were: Monthly albedo, which is the ratio of reflected light to total incident sunlight for a given area of the land surface; monthly Normalized Difference

Vegetation Index (NDVI), collected by the Moderate Resolution Imaging Spectroradiometer (MODIS) aboard NASA's Terra satellite; MODIS land cover classification; monthly leaf area index, which describes the exchange of fluxes of energy, mass and momentum between the surface and the planetary boundary layer; monthly net primary productivity, the most fundamental measure of global change, representing where and how much carbon dioxide is taken in by vegetation during photosynthesis minus how much carbon dioxide is released when plants respire and, monthly nighttime and daytime land surface temperatures also obtained from MODIS [29].

As a predictor to climate change, we used fifty one anomalies measurements from 2017 compared to the average conditions during 2000 using thermal infrared measurements collected by the MODIS. In this way, the greatest historical changes of the selected variables would be presented geographically. The variables considered were: nighttime and daytime land surface temperature anomalies, NDVI, land cover, monthly net primary production, monthly albedo and monthly land area index changes.

Maximum entropy algorithm

We used the maximum entropy algorithm (MaxEnt), as implemented in the dismo package in the R language [30]. Maxent is based on a machine learning response designed to make predictions from presence-only data [30, 31]. From the region selected, this algorithm extracts a sample of background locations that it contrasts against the presence locations. By default, MaxEnt assumes that a particular species is equally likely to be in anywhere on the landscape, thus, every pixel has the same probability of being selected as background. This approach estimates the most uniform distribution (maximum entropy) of sampling points compared to background locations given the constraints derived from the data [31, 32]. Thus, the resultant output represents how much better the model fits the location data than would a uniform distribution[31, 32]. As entropy is a measure of how uninformative a given probability distribution is, a high entropy translates to high unpredictability. Thus, maximizing entropy is consistent with maximizing unpredictability, given the little information we may know about a species distribution.

To avoid overparametrization in the modeling procedure, we discarded highly correlated variables using Pearson test (r >0.6). The predictive power was evaluated through cross-validation. Through k-fold cross-validation, the original sample was randomly partitioned into five equal sized subsamples. A single subsample was retained as the validation data for testing the model, and the remaining subsamples were used as training data.

To assess the performance of the models, the area under the curve (AUC) was calculated from receiver operator characteristics (ROC) curves. The AUC represented the

probability that a randomly chosen presence location is ranked higher than a randomly chosen background point [32, 33]. In our case, AUC compares presences with background points [31].

6.3 Results and discussion

Amblyomma cajennense s.s.

The prediction of the current distribution of *A. cajennense* s.s, considering only bioclimatic factors (Fig 6.2A1), shows a potential presence of this tick in western and northeastern Brazil. It is possible to see some small areas with presence of this vector in Panamá, El Salvador, Honduras, north of Venezuela and Colombia. In addition, it is possible to observed that the presence of the tick is unlikely in the Colombian, Peruvian and Brazilian Amazon regions. The blioclim predictors that more contribute to this potential distribution are a precipitation less than 150 mm in the warmest quarter (35%), low temperature seasonality (30%), that is to say low temperature variation over a given year, annual precipitation greater than 5000 mm (20%) and precipitation in March less than 350 mm (14%).

Considering only landscape factors (Fig 6.2A2), prediction of the *A. cajennense* s.s distribution is restricted mainly to northeastern Brazil and south of Guyana. In addition, small and dispersed areas of potential distribution of this vector in Peru and in the Brazilian Amazon are also evident. Landscape factors that more contribute in the model are a high leaf area index in January (34%), constant NDVI in February and December (19%), low net primary production in January (17%), constant nighttime land temperature in May (12%) and constant sunlight reflection in March (5%).

On the other hand, when considered both bioclimatic and landscape factors, the more contributed variables are a low temperature seasonality (23%), high precipitation in the wettest quarter (21%), constant NDVI in February (14%) and low precipitation in September (11%). In this scenario potential areas with *A. cajennense* s.s are observed in Venezuela and Ecuador, and similarly to the findings of scenario Fig 6.2A1, the presence of the vector is unlikely inside the Amazon region (Fig 6.2A3). This prediction has a better performance (AUC=0.96) than those using only bioclimatic (AUC=0.86) or landscape factors (AUC=0.88) (Figure 6.4A).

Furthermore, a future shift in the *A. cajennense* s.s. distribution due to bioclimatic factors (Fig 6.3A1), can be generated by a higher precipitation of the wettest quarter (49%), an increase in the precipitation of the warmest quarter (37%) and a diminution in

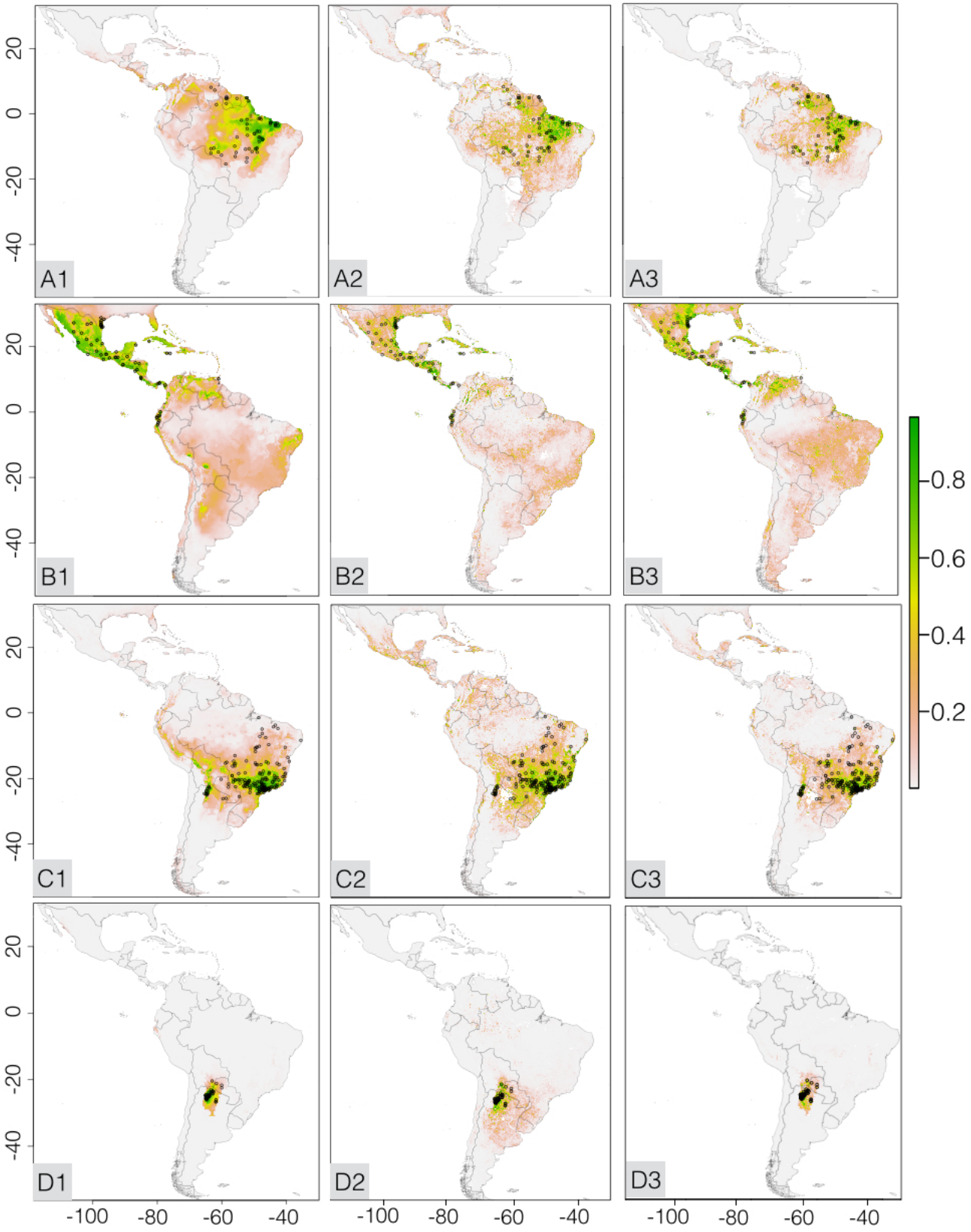

Figure 6.2 - Current potential distribution of **A)** *A. cajennense* s.s., **B)** *A. mixtum*, **C)** *A. sculptum* and **D)** *A. tonelliae* considering **1)** bioclimatic, **2)** landscape and **3)** bioclimatic and landscape variables

.

the precipitation of the driest quarter (9%). This change in distribution can be observed mainly in the north and northeast of Brazil, south of French Guiana, Suriname and Guyana, south of Ecuador, north of Colombia, west of Venezuela and south of Nicaragua, where the presence of the vector seems to be highly probable. Additionally, the presence of the vector in northern and central Brazil and northeastern Venezuela may be lower.

When considered variables associated with modification in the landscape, the probability to find the vector in South America is lower. The most important variables, whose historical transitions would have a greater impact on the geographical distribution of *A. cajennense* are an increase in the incoming light being reflected, which is associated with less vegetation in the region (18%), diminution of the leaf area index (11%), and a diminution of the NDVI (9%) (Fig 6.3A2). An increment in the presence of this vector seems to be more probable in the northeastern Brazil, in small areas of the north and southeastern Brazil, coast of Peru, Bolivia, Panama and Nicaragua.

The results of this scenarios coincide with previous works predicting *A. cajennense* in constant temperatures without a well-defined winter period and in sites with low NDVI variability [34]. The low prediction of the vector in Central America and the Caribbean observed in scenarios of Figures 6.2A1 6.2A2, 6.3A1 and 6.2A2, coincides with a low but positive suitability of this vector in the Caribbean and in Meso-American highlanDS [34].

In relation to the presence of the vector in the Amazon predicted by the consideration of landscape factors (Figures 6.2A2 6.2A3,6.3A2), although *A. cajennense* (s.s.) occurs generally in the Amazon biome [13], an extensive study in the Brazilian western Amazon concluded that this tick generally absent from areas with dense Amazon forest[35]. In addition, Martins et al. [13] suggested that this tick might not be adapted to the extremely humid rainforests of the Amazon.

Amblyomma mixtum

The prediction of *A. mixtum*, considering only bioclimatic factors (Fig 6.2B1) shows a widely distribution of this vector in North and Central America and the Caribbean. It is also predicted potential areas with *A. mixtum* in southern United States, Haiti, Venezuela, north and Pacific coast of Colombia, eastern Brazil, and in the center of Bolivia. The blioclim predictors that more contribute to the potential distribution of *A. mixtum* s.s are a precipitation near zero in February (49%), precipitation of the warmest quarter higher that 1500 mm (21%), a high temperature of the coldest quarter (18%) and a high variation in monthly precipitation over the course of the year (12%).

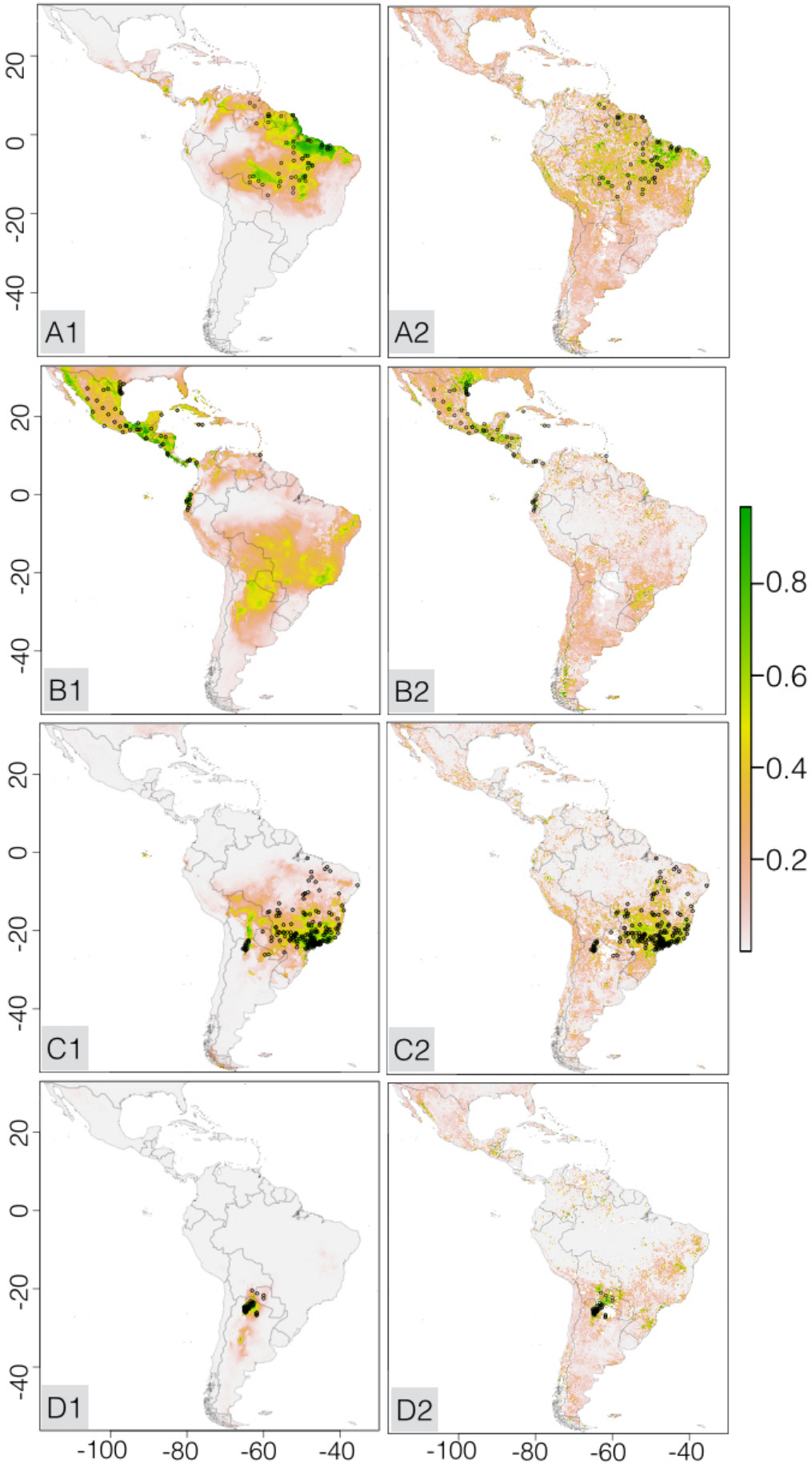

Figure 6.3 - Potential response of **A)** *A. cajennense* s.s., **B)** *A. mixtum*, **C)** *A. sculptum* and **D)** *A.tonelliae* to **1)** bioclimatic conditions of 2050 and **B)** landscape changes

.

Considering only landscape factors (Fig 6.2B2), there is a greater probability of finding this vector in Nicaragua, Caribbean islands and in the center of Colombia. Landscape factors that more contribute in the model are land cover (30%), high nighttime land temperature in May (15%), high incoming light being reflected in July (12%) and daytime land temperature in November near zero (10%).

Furthermore, when considered both bioclimatic and landscape factors (Fig 6.2B3), areas with potential presence of the tick can be seen in southern United States, Cuba, Nicaragua, Panamá, north of Colombia, north of Venezuela and small areas in Brazil. The more contributed variables in this scenario are land cover change (42%), high nighttime land temperature of May (21%), precipitation of the driest month near zero (14%) and daytime land temperature of August near zero (9%). This prediction has a better performance (AUC=0.92) than those using only bioclimatic (AUC=0.87) or landscape factors (AUC=0.90) (Figure 6.4B).

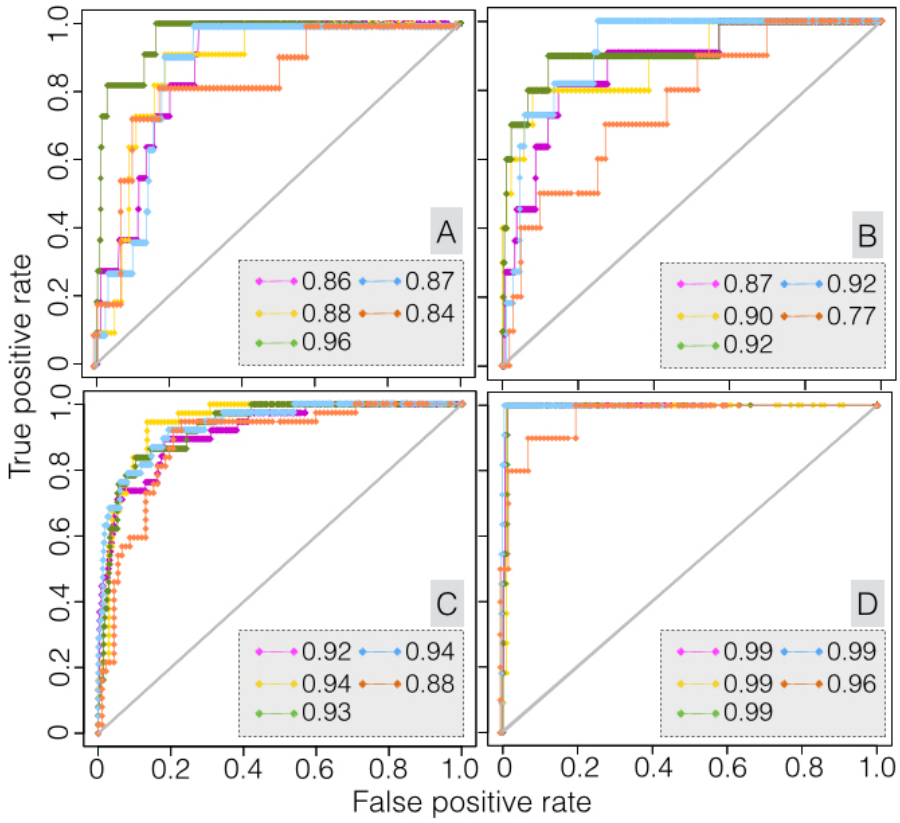

Figure 6.4 - ROC curves of **A)** *A. cajennense* s.s., **B)** *A. mixtum*, **C)** *A. sculptum* and **D)** *A. tonelliae* for the different scenarios considered. Magenta: bioclimatic factors; Gold: landscape factors; Green: bioclimatic and landscape factors; Blue: bioclimatic factors of 2050; Orange: changes in landscape conditions

On the one hand, a future shift in the *A. mixtum* distribution due to bioclimatic factors (Fig 6.3B1), can be associated to a higher precipitation in October (31%), lower precipitation of the driest month (28%), higher mean temperature of the coldest quar-

ter (21%) and higher precipitation of the warmest quarter (16%). An increment in the distribution of the vector can be observed mainly in Central, southeastern and northeastern Brazil, Paraguay, northern Argentina, Cuba and small areas of northern Colombia. Nonetheless, a diminution of the vector is probable in Mexico and Jamaica.

When considered variables associated with landscape, the most important variables, whose historical changes would have a greater impact on the advancement in the geographical distribution of *A. mixtum* are an increment NDVI (16%), increment in net primary production (14%) and increment in leaf area index (12%) (Fig 6.3B2). In this scenario, there is a general diminution in the presence of this vector, mainly in Mexico and Jamaica. However, it is probable an increment of the tick distribution in southern United States and southern Brazil. The performance of this prediction (AUC=0.77) was lower than that using future bioclimatic predictors of the year 2050 (AUC=0.92) (Figure 6.4B).

A. mixtum was previously associated with areas of dry and moist Meso-America and with large areas of suitability in the Caribbean [34]. All scenarios considering bioclimatic variables associate variables related to increase in precipitation with the potential geographical distribution of *A. mixtum* (Figures 6.2B1, 6.2B3, 6.3B1). This coincides with a previous finding in which a semi-desert arras were not predicted to be suitable for *A. mixtum*. It is possible to note that *A. mixtum* and *A. cajennense* have son similarity in the prediction off the geographical distribution in Central America and the Caribbean, as also noted previously [34].

Amblyomma sculptum

The prediction of *A. sculptum*, considering only bioclimatic factors (Fig 6.2C1) shows a current potential distribution of this vector in southern Brazil, northern Argentina, Bolivia and Peru. The blioclim predictors that more contribute to this potential distribution of *A. sculptum* are a high precipitation in February (26%), high mean temperature of the driest quarter (17%), precipitation of the warmest quarter higher than 1000 mm (16%), less precipitation in April (16%) and precipitation of July near zero (14%).

Considering landscape factors (Fig 6.2C2), the geographical predicted distribution includes Bolivia, Paraguay and small regions of southern Mexico, Guatemala, El Salvador, Honduras, Dominican Republic, Colombia, Ecuador and Peru. The landscape factors that more contribute in the potential distribution of the vector are high daytime land temperature of December (25%), high nighttime land temperature of July (20%) and August (14%) and high leaf area index of January (14%).

Furthermore, when considered both bioclimatic and landscape factors (Fig 6.2C3), a potential presence of the tick is restricted to the occurrence points. It is possible observed

small areas of potential presence of the vector in Bolivia and Ecuador. The variables that contribute more in this prediction are high precipitation of the warmest quarter (19%), high daytime land temperature in December (14%), low precipitation of wettest Month (11%) and high nighttime land temperature in August (10%). These three scenarios exhibit a similar performance (Figure 6.4C)

A future shift in the *A. sculptum* distribution due to bioclimatic factors (Fig 6.3C1), can be associated with a higher precipitation in February (35%), isothermality around 60%, which represents how large the day- to-night temperatures oscillate relative to the summer- to-winter (26%), lower precipitation in April (14%) and a higher annual mean temperature (14%). New areas with potential presence of this tick are Bolivia and the Galapagos Islands of Ecuador. Nonetheless, a diminution of the vector in Paraguay, northern and northeastern Brazil is possible.

When considered variables associated with land and vegetation, the geographical distribution of *A. sculptum* seems not to have many changes (Fig 6.3C2). Unlike the previous scenario, vector distribution seems likely in small areas of the northern Brazil. In addition, the vector could be less likely to be found in northern Argentina, northeastern Brazil and Paraguay. The most important variables, whose historical changes would have a greater impact on this new distribution are higher NDVI in July (26%), higher sunlight reflectance in May (25%) and higher net primary production in March(8%). The performance of this prediction (AUC=0.88) was lower than that using future bioclimatic predictors of the year 2050 (AUC=0.94) (Figure 6.4C).

Similarly to all scenarios, *A. sculptum* was previously predicted in the Atlantic forest and the Chaco in areas of Brazil and northern Argentina. The prediction areas suitable for the presence of this vector observed in scenarios of Figures 6.3C1 and 6.3C2, concentrated in southeastern Brazil in regions of Mata Atlantica biome, coincide with previous findings of *A. sculptum* in this bioma, which is the most degraded bioma of Brazil [13]. This degradation can be explained by the variables associated with the potential future distribution of the vector found in scenario of Figure 6.3C2 related to an increment of the sunlight reflectance, correlated with desert areas [29], and with the low net plant's primary production, which means decomposition or respiration overpowered carbon absorption, that is to say more carbon was released to the atmosphere than the plants took in [29]. The above may also explain the decrease in the probability of finding the vector in areas of northeastern Brazil. *A. sculptum* is not well adapted to the Caatinga biome, in the northeastern Brazil, where the semiarid climate is possibly the main limiting factor.

Amblyomma tonelliae

The prediction of *A. tonelliae*, considering only bioclimatic factors (Fig 6.2D1), shows a concentration of the vector in northern Argentina. The blioclim predictors that more contribute to this specific distribution of the vector are the amount of temperature variation over a given year (35%) and the biome (33%). Considering landscape factors (Fig 6.2D2), the predicted distribution includes the north of Argentina but additionally southern Bolivia. The landscape factors that more contribute in the potential presence of this vector are a low nighttime land temperature in May (50%) and high daytime land temperature in October (19%).

When considered bioclimatic and landscape factors (Fig 6.2D3), the presence of the vector is also concentrated in northern Argentina and southern Bolivia. The variables that contribute more in this distribution are the biome (49%) and low daytime land temperature of May (12%).

A future shift in the *A. tonelliae* distribution due to bioclimatic factors (Fig 6.3D1), can be associated mainly with changes in how large the day- to-night temperatures oscillate relative to the summer- to-winter (41%). New areas with potential presence of the tick can be seen in central Argentina. A diminution of the vector presence is possible in Paraguay and Bolivia. Contrary to the previous scenarios, when considered variables associated with land and vegetation, the geographical distribution of *A. tonelliae* seems to be wider (Fig 6.3D2). Small areas with probable presence of this tick can be seen in southern and northeastern Brazil, Venezuela, Colombia, Guatemala, Mexico and Honduras. The most influential variables, whose historical changes would have a greater impact on this new distribution are a increased sunlight reflectance, indicating lower vegetation in the regions (27%) lower leaf area index (15%) and a great diminution in the net primary production (13%).

The distribution of *A. tonelliae* is restricted to the small portion of the Forest salteña-tucamano oranense, in which the climate is warm and humid with dry winter season, intense summer precipitation and, in the highest part, snowfall in winter.

6.4 Conclusion

Our analyses of geographical distribution of *A. cajennense* ticks show that these species are predicted to have divergent patterns to environmental preferences, which can be detected via a set of environmental variables based on remotely sensed features of climate and vegetation. Nevertheless, it has to be contemplate that our models only

represent the potential distribution, whereas it might be difficult for *A cajennese* s.s. to migrate to those areas naturally because of their need for mammalian host to migrate long distances and the probable presence of natural barriers which may limit the dispersal ability.

Bibliography

[1] Dantas-Torres F. Climate change, biodiversity, ticks and tick-borne diseases: The butterfly effect. Int J Parasitol Parasites Wildl. 2015. 4(3):452-61

[2] Mwamuye, M, Kariuki M, Omondi E, Kabii D, Odongo J, Masiga D, Villinger J. Novel *Rickettsia* and emergent tick-borne pathogens: A molecular survey of ticks and tick-borne pathogens in Shimba Hills National Reserve, Kenya. Ticks and tick-borne diseases. 2017. 8(2): 208-218.

[3] Walter KS, Pepin K, Webb T, Gaff D. Invasion of two tick-borne diseases across New England: harnessing human surveillance data to capture underlying ecological invasion processes. Proceedings of the Royal Society. 2016. 283(1832): 0834

[4] Hai V. Almeras L, Socolovschi C, Raoult D, Parola P, Pages F. Monitoring human tick-borne disease risk and tick bite exposure in Europe: available tools and promising future methods. Ticks and tick-borne diseases. 2014. 5(6), 607-619.

[5] Fritz, CL. Emerging tick-borne diseases. Vet Clin North Am Small Anim Pract. 2009. 39(2):265-78

[6] Springer Y, Jarnevich CS, Barnett D, Monaghan J, Eisen R. Modeling the present and future geographic distribution of the Lone Star Tick, *Amblyomma americanum* (Ixodida: Ixodidae), in the continental United States. The Am Journal of tropical medicine and hygiene. 2015. 93(4): 875-890.

[7] Parmesan C, Yohe G A globally coherent fingerprint of climate change impacts across natural systems. Nature. 2003. 421:37–42.

[8] Estrada-Peña A, Guglielmone AA, Mangold AJ. The distribution and ecological preferences of the tick *Amblyomma cajennense* (Acari: Ixodidae), an ectoparasite of humans and other mammals in the Americas. Ann Trop Med Par. 2004;98:283–92

[9] Labruna MB. Ecology of rickettsia in South America.. Annals of the New York Academy of Sciences. 2009. 1166(1): 156-166.

[10] Belle E, King S, Griffiths B, Grant LS. Epidemiological investigation for arboviruses in Jamaica, West Indies. The American journal of tropical medicine and hygiene. 1980. 29(4): 667-675.

[11] Linthicum KJ, Logan T, Bailey CL, Gordon SW, Peters CJ, Monath P, Graham RR. Venezuelan equine encephalomyelitis virus infection in and transmission by the tick *Amblyomma cajennense* (Arachnida: Ixodidae). Journal of medical entomology. 1991. 28(3): 405-409.

[12] Nava S, Beati L, Labruna MB, Cáceres AG, Mangold AJ, Guglielmone AA. Reassessment of the taxonomic status of *Amblyomma cajennense* (Fabricius, 1787) with the description of three new species, Amblyomma tonelliae n. sp., *Amblyomma interandinum* n. sp. and *Amblyomma patinoi* n. sp., and reinstatement of *Amblyomma mixtum* Koch, 1844, and *Amblyomma sculptum* Berlese, 1888 (Ixodida: Ixodidae). Ticks Tick Borne Diseases. 2014. 5:252–76.

[13] Martins T, Barbieri A, Costa F, Terassini F, Camargo L, Peterka C, ..., Scofield A. Geographical distribution of *Amblyomma cajennense* (sensu lato) ticks (Parasitiformes: Ixodidae) in Brazil, with description of the nymph of *A. cajennense* (sensu stricto). Parasites & vectors. 2016. 9(1):186.

[14] Elith J, Leathwick JR. Species distribution models: ecological explanation and prediction across space and time. Annual review of ecology, evolution, and systematics. 2009. 40: 677-697.

[15] Fatima S, Atif S, Rasheed S, Zaidi F, Hussain E. Species Distribution Modelling of Aedes aegypti in two dengue-endemic regions of Pakistan.. Tropical Medicine & International Health. 2016. 21(3):427-436

[16] Wieland R, Kerkow A, Früh L, Kampen H, Walther D. Automated feature selection for a machine learning approach toward modeling a mosquito distribution. Ecological Modelling. 2017. 352: 108-112.

[17] Gomez M, Diotaiuti L, Gorla E. Distribution of pyrethroid resistant populations of *Triatoma infestans* in the Southern Cone of South America. PLoS Neglected Tropical Diseases. 2016. 10(3): e0004561.

[18] Raghavan R, Goodin D, Hanzlicek G, Zolnerowich G, Dryden M, Anderson G, Ganta R. Maximum entropy-based ecological niche model and bio-climatic determinants of Lone Star Tick (*Amblyomma americanum*) niche. Vector-Borne and Zoonotic Diseases. 2016. 16(3): 205-211.

[19] Elith J, Graham CH, Anderson RP, Dudík M, Ferrier S, Guisan A, ..., Li, J. Novel methods improve prediction of species' distributions from occurrence data. Ecography. 2006. 29(2): 129-151.

[20] Rose H, Wall R. Modelling the impact of climate change on spatial patterns of disease risk: sheep blowfly strike by *Lucilia sericata* in Great Britain. International journal for parasitology. 2011. 41(7): 739-746.

[21] Fischer D, Thomas S, Beierkuhnlein C. Modelling climatic suitability and dispersal for disease vectors: the example of a phlebotomine sandfly in Europe. Procedia Environmental Sciences. 2011. 7: 164-169.

[22] Mischler P, Kearney M, McCarroll JC, Scholte R, Vounatsou , Malone JB. Environmental and socio-economic risk modelling for Chagas disease in Bolivia. Geospatial health. 2012. 6(3): 59-66.

[23] Machado-Machado EA. Empirical mapping of suitability to dengue fever in Mexico using species distribution modeling. Applied Geography. 2012. 33: 82-93.

[24] Zhang L, Hou XX, Liu HX, Liu W, Wan KL, Hao Q. Prediction of potential geographic distribution of Lyme disease in Qinghai province with Maximum Entropy model. Zhonghua liuxingbingxue zazhi. 2016. 37(1): 94-97.

[25] Williams HW, Cross D, Crump H, Drost C, Thomas C. Climate suitability for European ticks: assessing species distribution models against null models and projection under AR5 climate. Parasites & vectors. 2015. 8(1): 440.

[26] Estrada-Peña A, Venzal JM. Climate niches of tick species in the Mediterranean region: modeling of occurrence data, distributional constraints, and impact of climate change. J Med Entomol. 2007. 44(6):1130–8.

[27] Porretta D, Mastrantonio V, Amendolia S, Gaiarsa S, Epis S, Genchi C, ..., Urbanelli S. Effects of global changes on the climatic niche of the tick Ixodes ricinus inferred by species distribution modelling.. Parasites Vectors. 2013. 6(1):271.

[28] O'Donnell MS, Ignizio DA. Bioclimatic predictors for supporting ecological applications in the conterminous United States: U.S.. Geological Survey Data Series. 2012. 691:10

[29] National Aeronautics and Space Administration. NASA Earth Observations. 2017. (NEO) (https://neo.sci.gsfc.nasa.gov).

[30] Hijmans R, Phillips S, Leathwick J, Elith J. dismo: Species Distribution Modeling.. R package version 1.1-4. 2017. https://CRAN.R-project.org/package=dismo

[31] Merow C, Smith MJ, Silander JA. A practical guide to MaxEnt for modeling species' distributions: what it does, and why inputs and settings matter. Ecography. 2013. 36:1058–1069.

[32] Baldwin R Use of Maximum Entropy Modeling in Wildlife Research. Entropy. 2009. 11:854-866

[33] Merow C, Smith MJ, Silander JA. A practical guide to MaxEnt for modeling species' distributions: what it does, and why inputs and settings matter. Ecography. 2013. 36:1058–1069.

[34] Estrada-Peña A, Tarragona E, Vesco U, de Meneghi D, Mastropaolo M, Mangold AJ, Guglielmone AA, Nava S. Divergent environmental preferences and areas of sympatry of tick species in the *Amblyomma cajennense* complex (Ixodidae). International Journal for Parasitology. 2014. 44(14):1081–1089.

[35] Labruna MB, Camargo LM, Terrassini FA, Ferreira F, Schumaker TTS, Camargo EP. Ticks (Acari: Ixodidae) from the state of Rondônia, western Amazon Brazil. Syst Appl Acarol. 2005;10:17–32.

7. Conclusions

In this thesis, we have addressed a fundamental issue: the prevention of human cases of BSF, the most lethal tick-born infection, whose dynamics involves not only humans, hosts and ticks, but also environmental and anthropogenic conditions. Specifically, our work was focused on four main aspects related to the prevention of BSF: *i* the modeling and the understanding of the effect of each kind of individual involved in the BSF transmission. This also includes the effects of the rates associated with inter- and intra-species transmissions, births, and deaths; *ii* the most important parameters defining the basic reproduction number, R_0, of this infection; *iii* the spatial relation between human cases of BSF and the change in the food source pattern of amplifiers host (capybaras); *iv* the meta-population model describing the host mobility effect on the BSF transmission; *v* the possible expansion of ticks due to the change of climate and landscape conditions.

We used interdisciplinary methods to understand these theoretical aspects. For instance, mathematical models to describe the dynamics, computational simulations of Markov processes, treatment of satellite imagery and maximum entropy modeling of species. In this way, we have constructed a simple description, but not obvious, that explains BSF dissemination. We found that only one capybara with one attached tick is enough to trigger the infection in a population of susceptible animals. This makes evident that the capybara's migration play an important role in the BSF dissemination, and also that the R_0 for this diseases is greater than 1, which was confirmed by means of the next generation matrix method. For instance, we found a $R_0 = 1.7$ in a population with only one infected capybara. Accordingly, if the migration of capybaras can be modeled by the pattern of host food sources, risk areas for human BSF can be predicted through the change of this food pattern. Surprisingly, using the human cases distribution we formulated a host-mobility model which confirms that regions with a high density of sugarcane have a higher BSF dissemination velocity. Finally, although the mobility of infected ticks is limited by the host movement, it is possible a higher probability of tick expansion and a consequent BSF dissemination due to climate and landscape changes. We found that the capybaras birth rate is correlated with the increase of infected individuals. Consequently, we propose two ways to regulate this migration: the control of the capybaras birth rate and the delimitation of capybaras movement through natural barriers.

The results of this thesis besides being beneficial in the planning of public health policies related to the prevention of BSF can open a path to further mathematical and computational studies focused on the dynamics and prevention of other vector-borne infectious diseases.